Synthesis of Carboxy-pyrrole and indole Ru-Complexes and Conversion of Coordination from k^2-(O,O) to k^2-(N,O)

Aida Rezapourakbari

Relator: Prof. Silvia Bordoni

Co-Relator: Dr. Giacomo Drius

OCTOBER 2024

University of Bologna, Low Carbon Technologies and Sustainable Chemistry

Table of Contents

Abstract

Organometallic compounds are playing an increasingly important role in medicinal chemistry due to their unique features, such as their ability to interact with biological molecules, showing different reactivity, and tunable electronic structures. These compounds are utilized for a variety functions in medicinal chemistry, including use as anticancer, antibacterial, antiviral, and anti-inflammatory agents, in targeted drug delivery, imaging, and enzyme inhibition or modulation.

Indole and pyrrole derivatives are particularly important ligands when coordinated to ruthenium. Their coordination helps fine-tuning of the stability, electronic properties, and biological activity of the Ruthenium complexes, a crucial aspect in designing new metal-based anticancer drugs and catalysts.

Solvent ligands, such as water, alcohols, acetonitrile, and dimethyl sulfoxide (DMSO), also play a key role when coordinated to Ruthenium complexes. They can significantly influence stability, reactivity, and overall characteristics of the complexes. Solvent addition contributes to stabilization, prompts to ligand exchange and electronic tuning, increasing solubility features.

In this context, indole and pyrrole-2-carboxylic acid are first coordinated to $[Ru(H)_2(CO)(PPh_3)_3]$, followed by a subsequent coordination of acetonitrile molecule for both complexes. Interestingly, a change in the coordination site of pyrrole and indole-2-carboxylic acid is observed, shifting the coordination from k^2-(O,O) to k^2-(N,O), upon acetonitrile incorporation. In the second step, these solvent-complexes react with organic ligands as the 4-picoline and 4-aminopyridine, leading to the displacement of acetonitrile. Additionally, the biologically compatible DMSO is coordinated in exchanging the acetonitrile-solvento coordination to enhance the solubility of the obtained complexes.

Introduction

- **The role of organometallic complexes in Medicinal Chemistry**

Cancer is a leading cause of death worldwide. Current cancer treatments include surgery, radiotherapy, and cytotoxic agents, despite their known side effects and the issue of developing resistance. However, for most types of metastatic cancer, there is no curative therapy available, highlighting the urgent need for the discovery and development of new effective chemotherapeutic agents.[1] Organometallic complexes are one of those chemotherapeutic agents.

Organometallic complexes are extensively used in various medical fields due to their physicochemical properties, making them viable direct drug candidates. Their suitability and empower as drug candidates are founded on their structural diversity in coordinating different organic ligands, the redox properties exhibited by the central metal, the ease of ligand exchange, and catalytic properties.[2] Organometallic complexes can catalyze specific reactions *in situ*, meaning they can activate or modify drug molecules at precise locations within the body. This targeted activation can reduce side effects and increase the drug's effectiveness by ensuring that the active form of the drug is generated only where needed, for example organometallic complexes can catalyze hydrogenation of intracellular biomolecules.[3] There are multiple properties of these complexes which makes them suitable to be applied for drug synthesizing. Furthermore, we discuss in detail the specificity of these metal complexes and their chemistry, which implies synthesis and characterization procedures.

The application of metals in medicine differs by thermodynamic and kinetic behaviors depending of their nature towards distinct biological environments. One of the key features required is that complexes must remain stable within cells to become active against tumoral tissues and leave intact the healthy ones. Before reaching their target sites, metal complexes can be altered by ligand substitution or redox reactions.

The process may be monitored during *in vitro* tests and transformations within cell culture media.[4] Beside the metal center itself, the ligands coordinated to the metal also play a remarkable role in the biological activity of the complex. Organic ligands as simple amino acids and their derivatives, or biocompatible organic fragments anchored on metal center constitute organometallic scaffolds, which could be components of a drug or a prodrug themselves.

- **The importance of aromatic rings in organometallic complexes**

One of the essential structural elements in medicinal chemistry are aromatic ring systems, which serve as the core building blocks for the majority of drugs available on the market today.[5] The ring systems are able to increase the metabolic stability, the polarity or the lipophilicity of the related complexes. Modern medicinal chemists recognize the importance of rings due to their significant impact on molecular properties like electronic distribution, three-dimensional structure, and scaffold rigidity.[6]

Properties like hydrophobicity and polarity are crucial for a molecule's bioavailability and the activity within organisms. The electronic characteristics of the scaffold are key points influencing molecule reactivity, which affects its metabolic stability and toxicity.[7] So the ligands are crucial factors as well as the metal nature for reaching the desired efficiency and function of the global organometallic system in the biological compartments.

One of the most applied scaffolds coordinated to metal is five or six-membered aromatic rings most of the times containing a heteroatom such as nitrogen, for example pyrrole, phenyl or pyridine rings. Six-membered aromatic rings with carboxylic groups are found in natural products and endogenous ligands, making them a common selection for medicinal chemistry in designing new chemical active compounds.[8] It is worth noting that coordinated ligands containing a ring member are abundant and significant along medicines based on metal complexes.

- **Different metals choice in medicinal chemistry**

Chemists have the ability to utilize elements with tuned characteristics from across the entire periodic table to synthesize metal complexes.[9] A significant number of drugs are metal-based, and considerable efforts are being made to develop new ones, which generally very often guarantee more thermodynamic robustness and kinetic half-time life. Here, we provide a brief overview of the various metal-based complexes, categorized by type of metal.

  - **Platinium-based drugs**

Various Pt-containing compounds are used as drugs, primarily as chemotherapeutic agents. Platinum compounds began to be used clinically as anticancer agents with the approval of *cis*-platin (called cisplatin) in 1978.[10] Platinum-based anti-cancer drugs, such as cisplatin, carboplatin, and oxaliplatin (Fig.1), are widely used in clinical settings due to their significant therapeutic effects and well-defined mechanisms of action.[11]

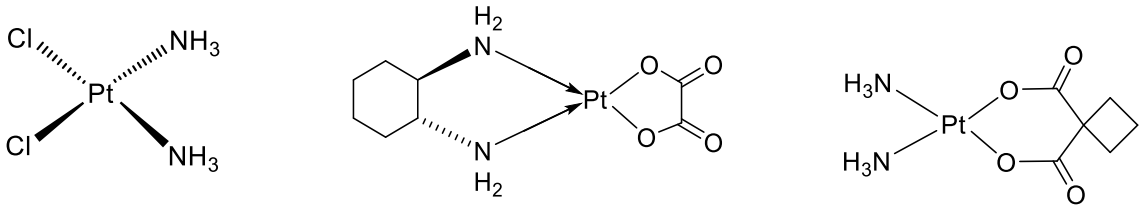

Cisplatin Oxaliplatin Carboplatin

Fig.1. The chemical structures of cisplatin, carboplatin, and oxaliplatin which are utilized in clinical treatments for tumor diseases.[12]

Cisplatin, carboplatin, and oxaliplatin share physicochemical and pharmacological properties, especially their ability to form DNA adducts. Oxaliplatin exhibits some resistance mechanisms distinct from those of cisplatin and carboplatin. While carboplatin can be seen analogues of cisplatin, it exhibits significantly different pharmacokinetic properties, side effects, and intrinsic activity. Therefore, choosing between these two species can be done rationally based on patient characteristics.[13]

Compared to cisplatin, oxaliplatin requires a lower intracellular concentration and fewer DNA-Pt adducts to achieve its cytotoxic effects. Resistance to oxaliplatin is mediated by similar mechanisms as cisplatin, including reduced drug accumulation and decreased DNA-Pt adduct formation.[14]

Cisplatin induces cytotoxicity by interfering with transcription and/or DNA replication mechanisms, depending on the cell type and concentration. Additionally, it damages tumors by inducing apoptosis through the activation of various signal transduction pathways, such as calcium signaling, death receptor signaling, and mitochondrial pathway activation.[15]

However, the side effects of platinum drugs, such as lack of selectivity, high systemic toxicity, and drug resistance, significantly limit their clinical use.[16] Other common side effects include ototoxicity, neurotoxicity, gastrointestinal toxicity, hematological toxicity, cardiotoxicity, hepatotoxicity, and severe hearing loss. These adverse effects decrease patients quality of life and often require reducing drug dosage or discontinuing use, thereby compromising the treatment effectiveness.[17,18]

- **Gold-based drugs**

There are many advantages that make gold-based compounds interesting candidates to be used as anticancer treatment. Historically, the medicinal use of gold complexes began when it was observed that the potassium salts of dicyanoaurate(I), initially suggested by Robert Koch for tuberculosis treatment, actually demonstrated anti-inflammatory properties.[19] Besides these, gold compounds exhibit acute toxicity to cells, including those cancer cell lines that have demonstrated *in vitro* to be

resistant to platinum. A significant obstacle to FDA approval of Au(I)- and Au(III)-based compounds for cancer treatment is their limited solubility and chemical stability in physiological conditions. This limitation not only decreases their cytotoxic effectiveness but also leads to the undesirable buildup of heavy metals in vital organs.[20] Easy reduction of Au(III) to Au(I) and Au(0) is responsible for fast ligand exchange, but, on the other hand, the release of either the free ligands or the metal site can lead to loss of activity and potential side effects.[21] What becomes crucial then, is to develop the drugs stability in the biological environments. One of these improvements is the application of gold-based nanomedicines, in which a nanoparticle is utilized as carrier to deliver the gold-based complex to untouched cancer cells.

There are numerous gold-based anticancer complexes, but for this discussion, we will focus on three specific types as examples for the following discussion.

1. *Auranofin and analogues*

Auranofin is a lipophilic organogold compound approved by the FDA for the treatment of rheumatoid arthritis. It possesses anti-inflammatory and potential antineoplastic properties. Gold-containing drugs like Auranofin are recognized for their anti-inflammatory effects, and the triethyl phosphine derivative can decrease cytokine production, while enhancing cell-mediated immunity.[22] Auranofin is a monomeric compound with the general formula R_3PAuSR, where the triethyl phosphine group (R_3P) stabilizes the gold-thiol complex (AuSR) and imparts lipophilic properties. The main reason for stabilization exerted by phosphine groups is that phosphine ligands (auranofin) are typically less labile than thiolate ligands and undergo slow aquation that exhibit strong stability. (Fig.2) [23]

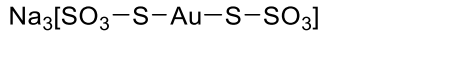

auro-bis(thiosulfate)

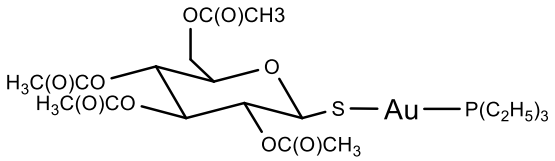

auranofin

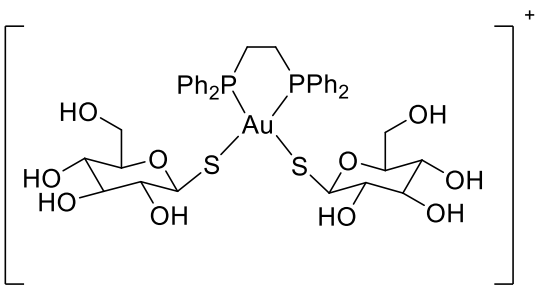

μ-(1,2-bis(diphenylphosphino)ethane)-bis((1-thio-D-glucopyranosato-S)gold ^{I})

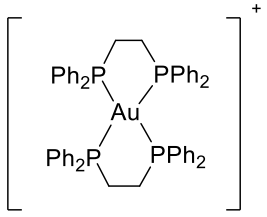

(1,2-bis(diphenylphosphino)ethane)gold ^{I})

Fig.2. Gold ^{I} Complexes with thiolate and phosphine ligands.

2. Gold ^{III} porphyrins

A series of gold ^{III} tetraarylporphyrins (Fig.3) are stable against demetallation under physiological conditions in the presence of glutathione and are significantly stronger than cisplatin in killing human cancer cells.[24] The most successful example is a cyclometallated gold ^{III} complex, for example bipyridyl gold ^{III} Compounds.[25]

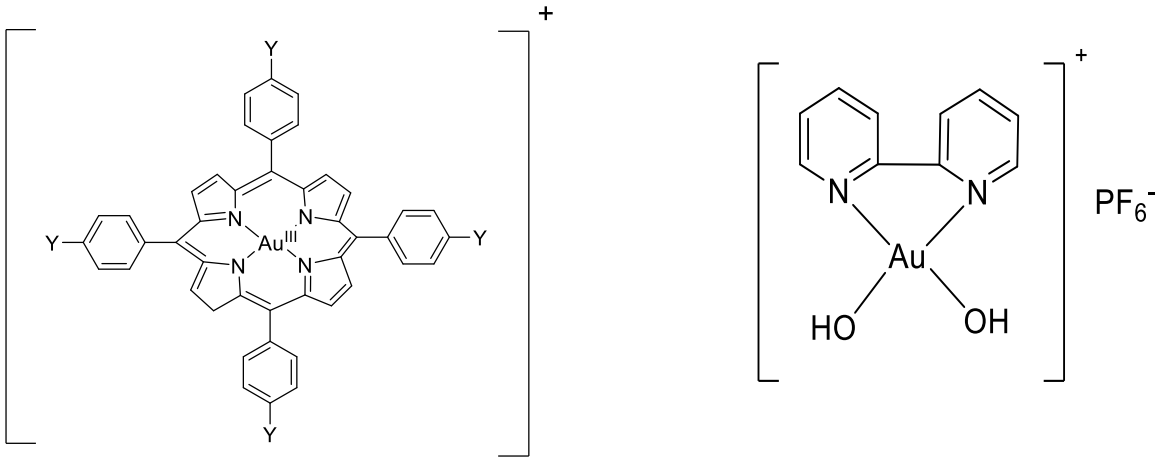

gold^{III} tetraarylporphyrins [Au(bipy)$(OH)_2$][PF_6]

Fig.3. gold^{III} tetraarylporphyrins[26] and bipyridyl gold^{III}Compounds[27]

3. Gold ^{III} dithiocarbamates

Sulfur-containing compounds are significant because they are similar to sulfur-containing amino acids as cysteine and methionine. Consequently, they play a role in cellular uptake, deactivation, and binding processes. Ronconi and Fregona groups have synthesized several Au ^{III} dithiocarbamato derivatives of the form [Au ^{III} X_2(dtc)] (where X = Cl, Br and dtc represents various dithiocarbamato ligands) to closely mimic the key features of cisplatin, but less toxicity and larger activity.[28] In Fig.4 some of those Gold ^{III} dithiocarbamates have shown.

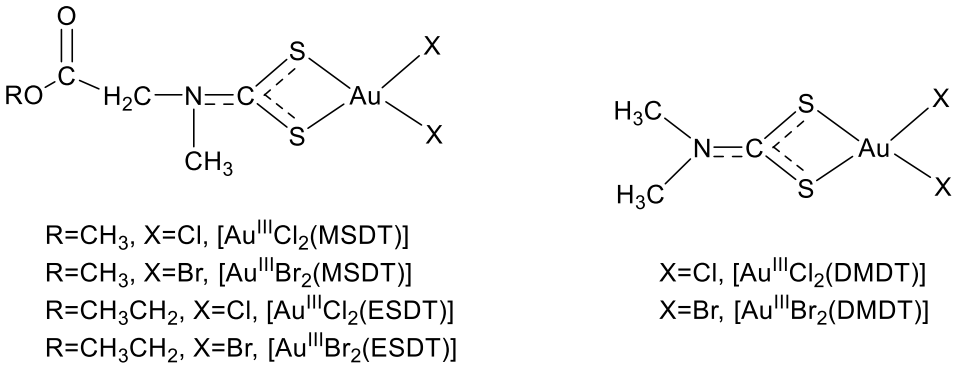

Fig.4.Selected Au(III)-dithiocarbamato derivatives include: X = Cl or Br; DMDT = N,N-dimethyldithiocarbamate ($(CH_3)_2NCSS$-); MSDT = methylsarcosinedithiocarbamate ($CH_3O(O)CCH_2N(CH_3)CSS$-); and ESDT = ethylsarcosinedithiocarbamate ($CH_3CH_2O(O)CCH_2N(CH_3)CSS$-).[29]

- **Ruthenium-based drugs**

Ruthenium complexes exhibit multiple targets and mechanisms for antitumor properties. Among the metal-based compounds studied, Ruthenium complexes have demonstrated exceptional antitumor activity.[30] Various Ruthenium complexes designed to replicate and improve the action of platinum complexes, exhibiting either *in vitro* or *in vivo* antitumor efficacy. Based on the type of the ligands coordinated to Ruthenium complexes can be categorized into distinct groups.[31]

1. *Ruthenium Chloro-ammino derivatives*

The group of Clarke and colleagues pioneering in the investigation of chloro-ammino derivatives with the general formula $[Ru(NH_3)_{6-x}Cl_x]Y^+$.[32] These compounds are mimicking cisplatin structure.(Fig.5)

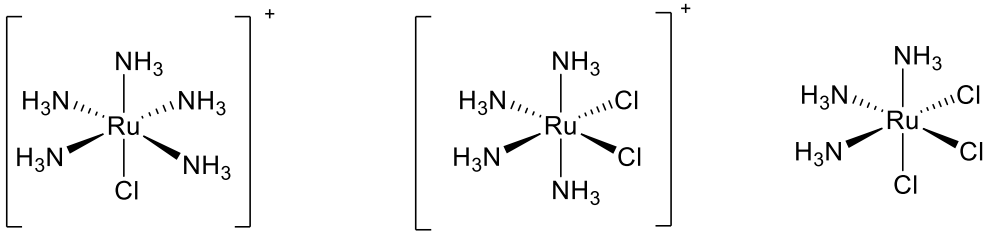

Fig.5. Chloro-ammino derivatives.

2. Ruthenium Dimethyl-sulfoxide complexes

The solubility of Ruthenium complexes can be highly improved by substituting the ligands by dimethyl sulfoxide (DMSO) molecules. As DMSO can be replaced by water ligands in aqueous environments, such as biological systems, where water molecules are abundant. In Fig. 6, an example of the exchange of DMSO and chloride ligands with water is illustrated. When two chloride ligands are in the *cis* position, the exchange of water ligands occurs at a faster rate. [33]

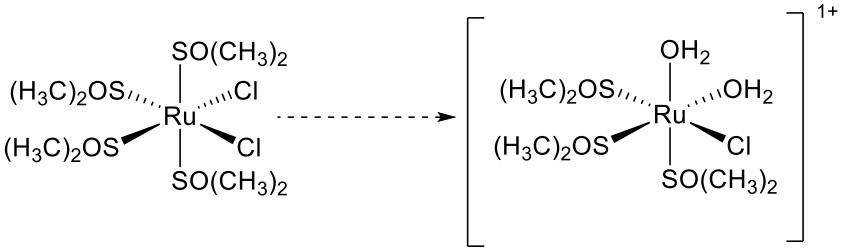

Fig.6. Dimethyl-sulfoxide complexes. *cis*-[$Ru^{II}(DMSO)_4Cl_2$] and the corresponding aqua species.

3. Ruthenium complexes with both chloride and heterocyclic ligands

Ru^{II} complexes of the type *cis*-[$Ru^{II}(L)_2Cl_2$] (where L is a bidentate heteroaromatic ligand) have been synthesized and are currently investigated for their antitumor effectiveness recognition, owing to their similarity in action with cisplatin.[34](Fig.7)

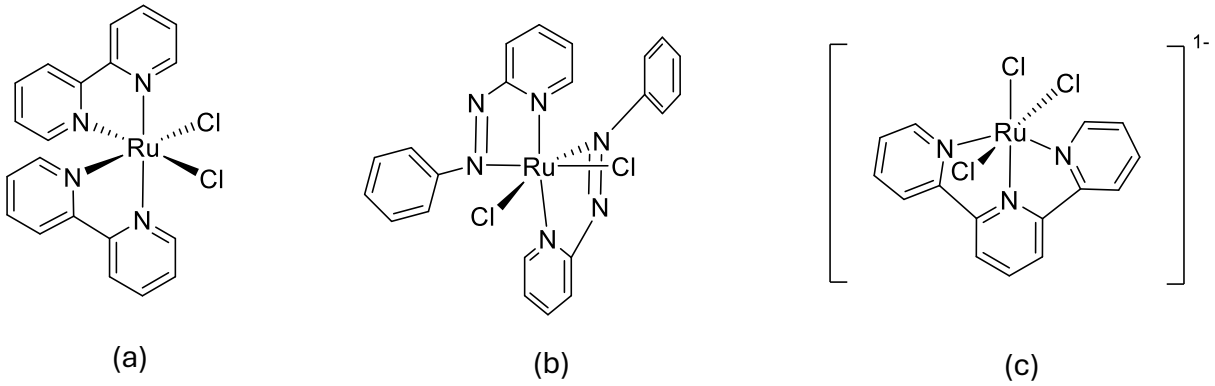

Fig.7. Complexes with chlorides and heterocyclic ligands. (a) *cis*-[$Ru^{II}(bpy)_2Cl_2$], (b) *cis*-[$Ru^{II}(azpy)_2Cl_2$], (c) *mer*-[$Ru^{II}(terpy)Cl_3$]$^-$

4. Ruthenium arene complexes

Ruthenium arene complexes exhibit strong selectivity in recognizing nucleic acid bases, with the properties of the coordinated arene significantly impacting the kinetics of their binding. Haimei and his group found that organometallic Ruthenium(II) complexes of the type [(η^6-arene)Ru(en)(X)] (X is Cl^- or H_2O and arene can be Biphenyl (Bip), p-cymene (Cym), Benzene (Ben), Tetrahydro anthracene (THA), Dihydroanthracene) by applying a stereospecific hydrogen bonding can enable the selective recognition of specific DNA sites, while the role of arene-purine hydrophobic interactions in affecting the kinetics of DNA binding is also considered. In this way they are cytotoxic to cancer cells.(Fig.8)[35]

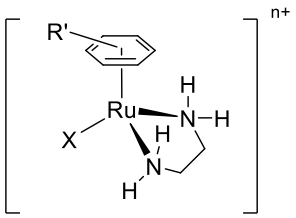

X=Cl^-, H_2O
R'=Biphenyl (Bip), p-cymene (Cym), Benzene (Ben),
Tetrahydro antheracene (THA), Dihydro anthracene (DHA)

Fig.8. Arene complexes.

Why Ruthenium?

The development of metal-based anticancer drugs has traditionally concentrated on cytotoxic platinum compounds,[36] notably, many Ru-compounds are considered less toxic than Pt-based drugs, and some of them showed higher selectivity towards cancer cells.[37] Ruthenium is situated in the middle of the second row of transition metals and belongs to the same group of Iron exhibiting properties between early and late transition metals.[38] The higher selectivity of Ruthenium to cancer cells is devoted to Iron mimicking phenomena in biological environment.[39] The overexpression of transferrin receptors on cancer cells, due to their increased iron demand, can effectively deliver Ru complexes to these cells.[40]

Ruthenium (Ru) complexes have attracted much attention for many other reasons.[41] Organometallic complexes are typically considered unstable in air or moist conditions. However, a range of bioactive Ruthenium complexes has been developed remaining stable in aqueous and alcoholic solutions and exhibit to be less sensitive to oxygen and sulfur[42], hence Ru complexes demonstrate prominent bioactivity and bioavailability.[43] The rapid expansion of Ru-based anticancer agents is primarily

attributed to the unique ability of Ru-core to accommodate multiple oxidation states, allowing for versatile electron-transfer pathways. Both Ru(II) and Ru(III) oxidation states support six-coordinated octahedral configurations, where the additional axial ligands help fine-tuning on the steric and electronic properties.[44] Significant factors include relative weakness of certain metal-ligand bonds and eventually thermodynamic and kinetic stability of Ru(III) complexes compared to Ru(II) complexes, as ligand exchange directly influences kinetics of the activity.[45]

- **Ru-Based Anticancer Agents that successfully entered Clinical Trials**

Numerous Ru-based anticancer agents have been developed, but none of them have yet been approved for clinical use as anticancer drug. There are some Ruthenium complexes that successfully entered clinical trials. Here we will discuss them in detail.

- **NAMI-A**

NAMI-A {$H_2Im[trans\text{-}RuCl_4(DMSO)HIm]$, or imidazolium-trans-DMSO-imidazole-tetrachlororuthenate} (Fig.9) has been the first Ruthenium-based compound showing antimetastatic activity in preclinical studies.[46]

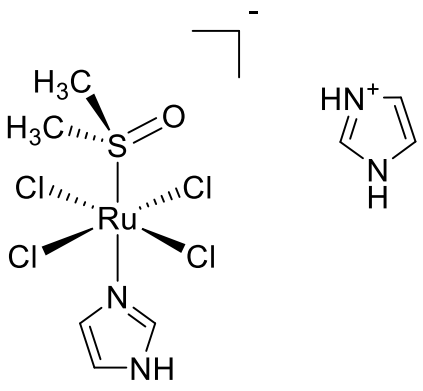

Fig.9. Chemical structure of NAMI-A. Molecular weight=458.18 g/mol. Molecular formula:$C_8H_{15}C_{l4}N_4ORu(III)S$.

NAMI-A is a Ruthenium compound that obtained by replacing Na^+ with ImH^+. NAMI-A turns out to be capable both in preventing formation of metastasis and inhibiting cell growth. These features made

NAMI-A an ideal candidate for clinical testing.[47] The mechanism of action of NAMI-A is to thicken the capsule close to the primary tumor with the extracellular matrix around tumor blood vessels. This behavior helps to avoid the tumor cells from infiltrating adjacent tissues and blood vessels.[48,49]

Recently, NAMI-A has been found to inhibit matrix metalloproteinases, inducing antiangiogenic effects.[50] Additionally, NAMI-A forms covalent bonds with DNA, suggesting its cytotoxicity to be directly corelated to DNA interaction.[51]

While NAMI-A is stable in solid form, it undergoes pH-dependent aquation processes in solution.[52] At physiological pH and 37 °C (in a phosphate buffer with 0.9% NaCl), NAMI-A undergoes a stepwise dissociation of two chloride ions within minutes. This process, which includes the gradual release of the DMSO-S ligand, ultimately results in the formation of uncharacterized dark green polyoxo species. However, at room temperature and slightly acidic pH (3–5), aquation processes are nearly completely inhibited, by observing a slow dissociation of DMSO occurring approximately at 2% per hour. These conditions are selected for administering NAMI-A to patients via slow infusion. Due to the presence of the moderate π-acceptor DMSO-S, NAMI-A has a relatively high reduction potential (E° +235 mV vs. NHE).[53,54]

- **KP1019**

Indazolium trans-[tetrachlorobis(1H-indazole)ruthenate(III)] is a further Ruthenium anticancer drug which has reached clinical trial. NAMI-A demonstrated a significant efficacy in preventing the formation of metastases[55,56], while KP1019 showed activity against a wide range of preclinical tumor models, including colorectal carcinomas and various primary explanted human tumors.[57] Here structure of KP1019 is presented.[58] (Fig.10)

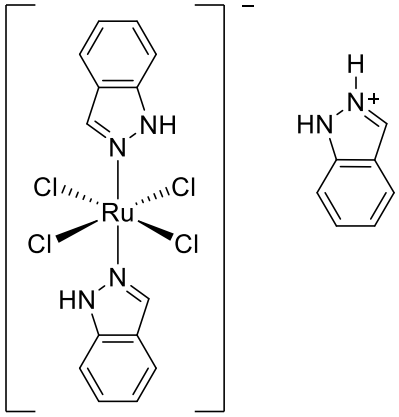

Fig.10. Structure of KP1019.

- **Complexes of Ruthenium(II) with different solvato ligands**

The coordination of solvent can offer several advantages:

- Enhanced stability: The coordination of solvent molecules, such as water or acetonitrile, to a metal center can stabilize the complex by completing coordination sphere, thus preventing undesirable reactions associated with the under-coordinated and electron0deficient metal center. It also facilitates ligand exchange. Solvent molecules are often labile and can be easily displaced by other ligands, promoting them as useful transition states or intermediates for synthesizing further compound to targeted applications.
- Enhance solubility: This is crucial point in reactions where solubility significantly impacts reaction rate or conversion. Solvent coordination can alter the electronic environment of metal center, thus fine-tuning to enhance the reactivity. Depending on the nature of solvent and metal, solvent molecule is able to donate electron density or withdraw it.
- Increased reactivity: The geometry of metal complex can be highly influenced by the coordinating solvent molecules, promoting reactivity and inducing catalytic activity, or interaction to biological targets in medicinal chemistry.[59,60] For example in 1988, *cis*- and *trans*- $Ru(DMSO)_4Cl_2$ were synthesized and tested their activity as anti-tumor agents.[61,62] In 1995 has been used by N Farrell and colleagues to prepare heterodinuclear Pt–Ru compounds crosslinked by 1,4-diaminobutane.[63](Fig.11).

cis-$Ru(DMSO)_4Cl_2$ *trans*-$Ru(DMSO)_4Cl_2$ [{*cis*,fac-$RuCl_2$-$(DMSO)_3$}($NH_2(CH_2)_4NH_2$){cis-

Fig.11. Ru-DMSO solvato complexes.

Herein we described the synthesized Ruthenium complexes to undergo attempts for coordinating MeCN or DMSO to afford the related solvato-species. Ruthenium complexes with monodentate or labile ligands provide excellent starting materials for entry into synthetic Ruthenium chemistry. The solubility of solvato-complexes is markedly increased.[64,65,66,67]

The lability of the Ru-coordinated acetonitrile ligands offers several advantages, for example this lability allows for the synthesis of complexes with less labile ligands, using acetonitrile complexes as the starting materials.[68]

- **Pyrroles in medicinal chemistry**

The varied structures and biological properties of natural products make them ideal candidates for discovering novel compounds for treating human diseases. Among them 5-membered nitrogen-containing aromatic heterocycles are recently playing a significant role in the medicinal chemistry research.[69]

Pyrroles with 5-membered nitrogen containing heterocyclic compound are recognized as biologically active scaffolds with a broad spectrum of activities and are present in a variety of natural products. Common natural molecules containing pyrrole rings include bile pigments like bilirubin, porphyrins of heme, porphyrinogens, chlorophyll, and Vitamin B12.[70] Marketed drugs containing pyrrole ring systems display a variety of biological activities, including anticancer, antibacterial, anti-inflammatory, antimalarial, and antipsychotic properties, among others.[71] The prevalence of N- heterocycles in biologically active compounds is due to the stability and efficiency as well as the ability to binding DNA through hydrogen-interactions.[72]

- **Indoles in medicinal chemistry**

Indole has become highly popular as pharmacophore in various pharmacological contexts. The intriguing molecular structure captured the attention of organic and medicine chemists, in motivating to develop derivatives with therapeutic potential. Chemically, the heterocyclic ring system is composed by a fused six-membered benzene ring with a five-membered pyrrole ring.[73] The electrophilicity of the indole nucleus is well-documented in the literature, enabling facile synthesis of various indole derivatives through nucleophilic addition and cycloaddition reactions.[74] This advantage enhances its potential for further synthetic modification. Indole-derived phytoconstituents and bacterial metabolites are produced through biosynthesis, involving coupling of tryptophan with other amino acids.[75]
The indole nucleus is a planar, bicyclic molecule with 10 π-electrons (8 π-electrons from double bonds and 2 π-electrons from nitrogen lone pair), making it aromatic according to Huckel's rule. It behaves as

weak base, prone to protonation only in the presence of strong acids. The highest electron density is found at the third C-position of the ring, making it the most reactive site for electrophilic substitution. Additionally, the slightly acidic nature of the NH group makes it prone to N-substitution reactions under basic conditions.[76]

Indole is often preferred over pyrrole in medicinal chemistry due to its unique structural and chemical properties, which make it preferred for drug design and development. Here are summarized some key reasons:

- **Biological Significance:**

Natural Presence: Indole constitutes is a key component in many essential biological molecules, as amino acid tryptophan and the neurotransmitter serotonin, as well as various plant-derived compounds. Because indole is so common in nature, it tends to interact well with many biological systems, which is a big plus when developing new medicines.[77]

Receptor Interaction: The indole structure plays a crucial role in how drugs interact with certain receptors in the body. For instance, indole derivatives are well-known for their ability to bind to serotonin receptors, making them especially valuable in creating drugs for mental health and neurological issues.[78]

- **Structural Flexibility:**

Aromatic Stability: Indole's chemical structure includes a stable aromatic ring, because it is a planar, heteroaromatic molecule with ten π-electrons that circulate throughout its structure. Chemically, indole is only weakly basic because the lone pair of electrons on the nitrogen atom is delocalized into the π-electron system, allowing it to move freely across the ring. As a result, the nitrogen lone pair is not readily available for protonation. Instead, protonation occurs at the C-3 position, as this location allows the molecule to retain aromaticity, making it more thermodynamically stable. This balance contributes to indole, ability to be reactive enough for chemical applications while remaining stable enough to finalize effectively its function in the body.[79] So, the fused benzene ring provides it an edge over pyrrole, often resulting in drugs with better performance in the body.

- **Chemical Behavior:**

Targeted Reactivity: Indole is particularly reactive at a specific spot on its structure, allowing the 3-position for precise chemical modifications.[80] This predictability is important in medicinal chemistry because it helps in fine-tuning drug properties, inducing its development more controlled and efficient.

- **Safety Profile:**

Lower Risk of Toxicity: Indole compounds typically have a lower risk of causing toxic side effects compared to pyrrole-based drugs. Pyrrole can sometimes break down into harmful byproducts, which limits its use in drug development. In contrast, indole's breakdown products are generally more robust and therefore safer.[81]

- **π-extended Aromaticity**

π-Extended aromaticity refers to the delocalization of π-electrons across a larger conjugated system, often spanning multiple fused aromatic rings. This extended conjugation enhances the stability, electron delocalization, and unique chemical properties of such molecules. π-extended aromatic compounds, like polycyclic aromatic hydrocarbons (PAHs) and certain organometallic complexes. These compounds often show strong interactions with biomolecules, which can influence their biological activity, including their potential use in drug development and molecular recognition.[82]The positioning of nitrogen atoms within ligand structure and the nature of the metal moiety appear to influence the electronic behavior and aromaticity of the π-extended structures in both ground and excited states. Structural, electronic, and magnetic aromaticity indices were employed to assess the aromaticity of both free and coordinated ligands. The metal fragment significantly impacts the aromatic character of the ligands, with aromaticity or antiaromaticity depending on the electron-withdrawing properties of the ligand-metal systems. The observed electronic distribution on aromatic ligand controls the modulation of π-stacking potential.[83]

When Indole or Pyrrole is coordinated to Ruthenium, a π-extended aromaticity occurs interacting with central Ruthenium site helping the global stability of the complex.

Fig.12.a)Carboxypyrrole and b)Carboxyindole Coordinated to Ruthenium

Aim of this work

The main goal of this work is:

- The comparison between the synthesis and characterization of the homoleptic dihapto-pyrrole-Ru derivatives
- Conversion to k^2-(N,O) heteroleptic acetonitrile species with the analogous behavior monitored by the extended indole carboxy- derivatives
- Altering the metal skeleton by coordinative solvent incorporation as DMSO to study future medicinal features as antibacterial or anticancer activity.

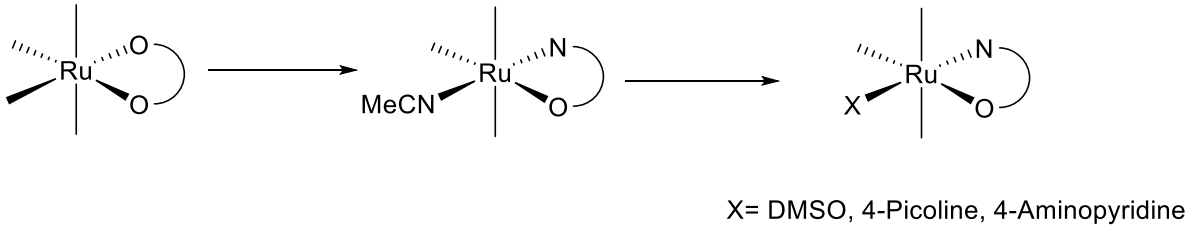

Fig.13. Conversion of ligand coordination from homoleptic (O,O) to heteroleptic (N,O) in Ruthenium Complexes.

Results and Discussion

- **Characterization of Complex 2 [RuH(CO)(PPh_3)$_2$(K^2(O,O)-Carboxypyrrole)]**

Complex **2** was synthesized by refluxing Complex **1** and Pyrrole-2-carboxylic acid in toluene under Argon atmosphere. Here the characterization of Complex **2** is as followed:

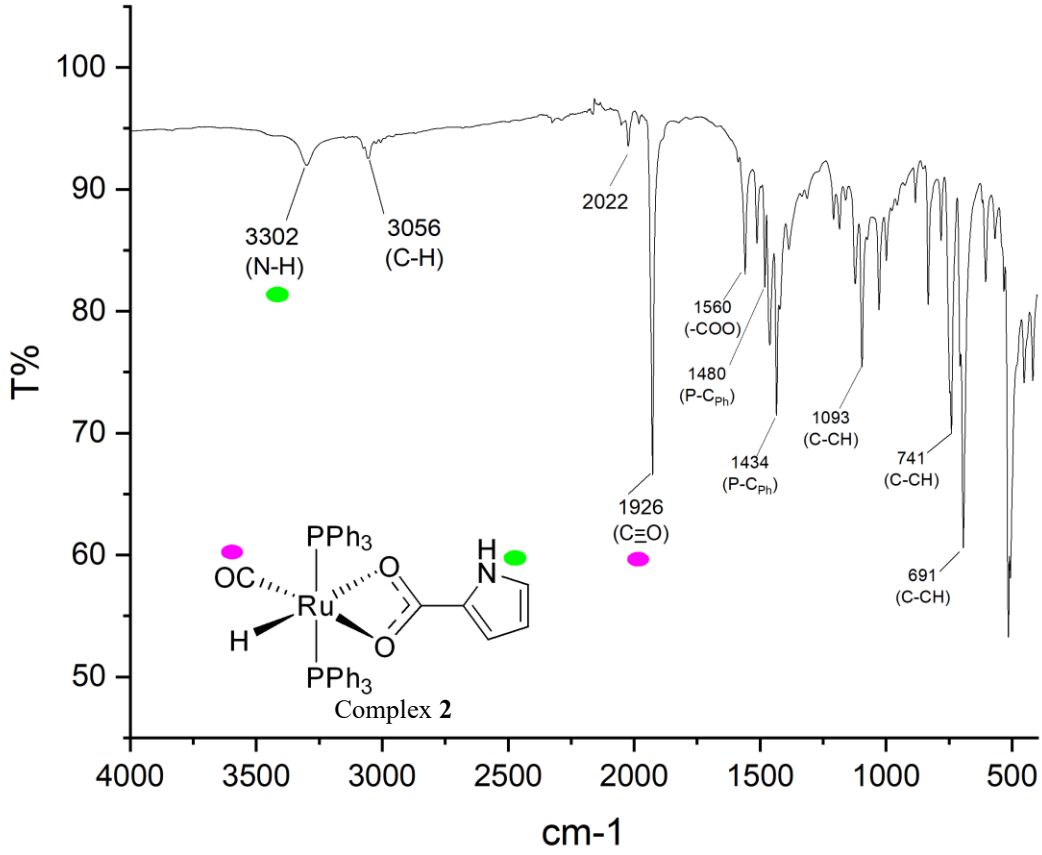

Complex **2**

IR of complex 2: As indicated by the spectrum, the N-H stretch of the pyrrole coordinated to Ruthenium is marked in green, and the CO peak has shifted from 1940 cm^{-1} to 1926 cm^{-1}.

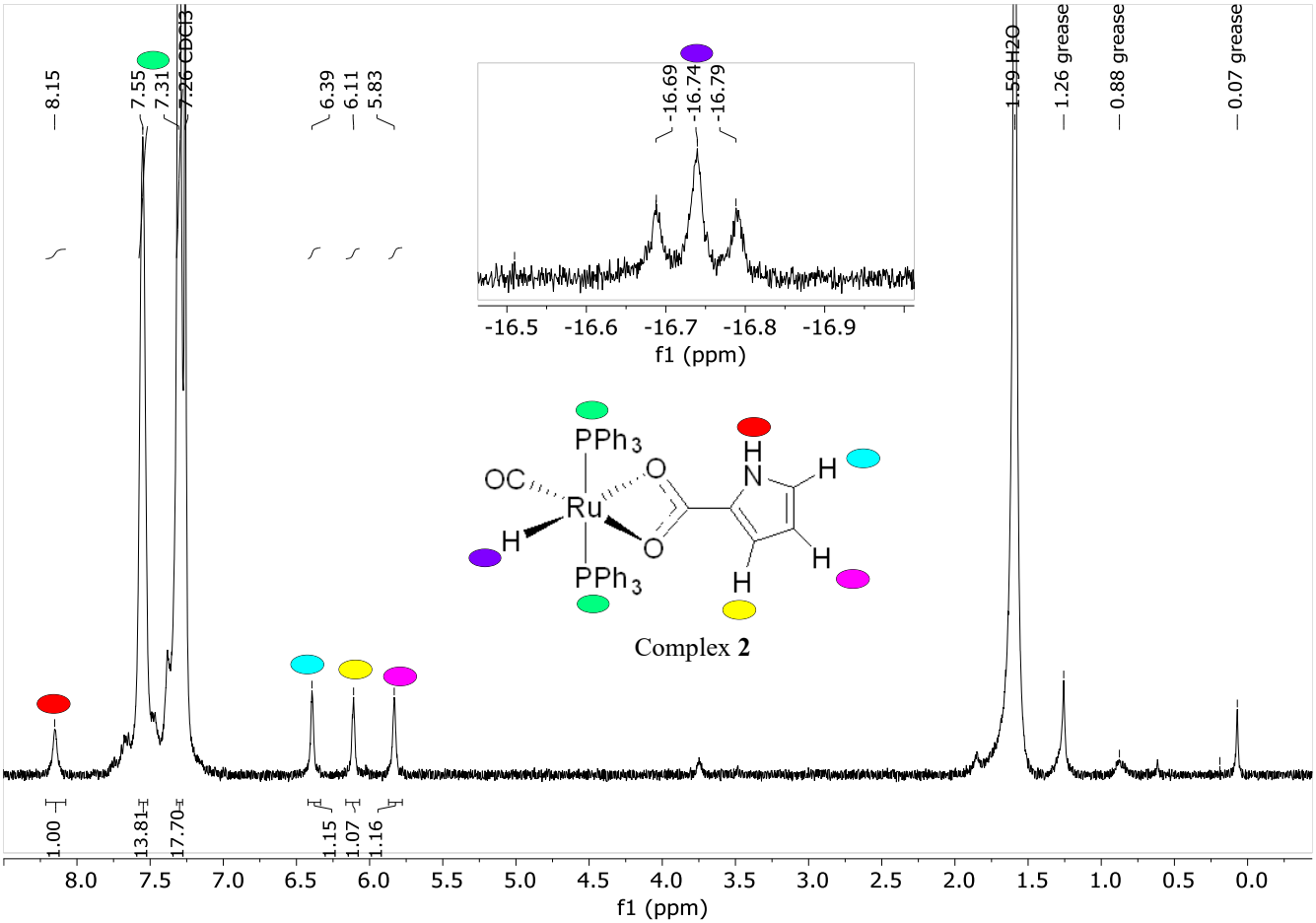

Complex **2**

^{1}H-NMR of Complex 2: When Pyrrole-2-carboxylic acid coordinates to complex **1**, four distinct types of hydrogens are observed in the H-NMR spectrum. The hydride ligand directly bound to Ruthenium appears around -16 ppm, which is due to the proximity to the plethora of electron density about the metal site. The peak appears as a triplet because it is coupled with two equivalent phosphorus atoms in *trans*-positions.

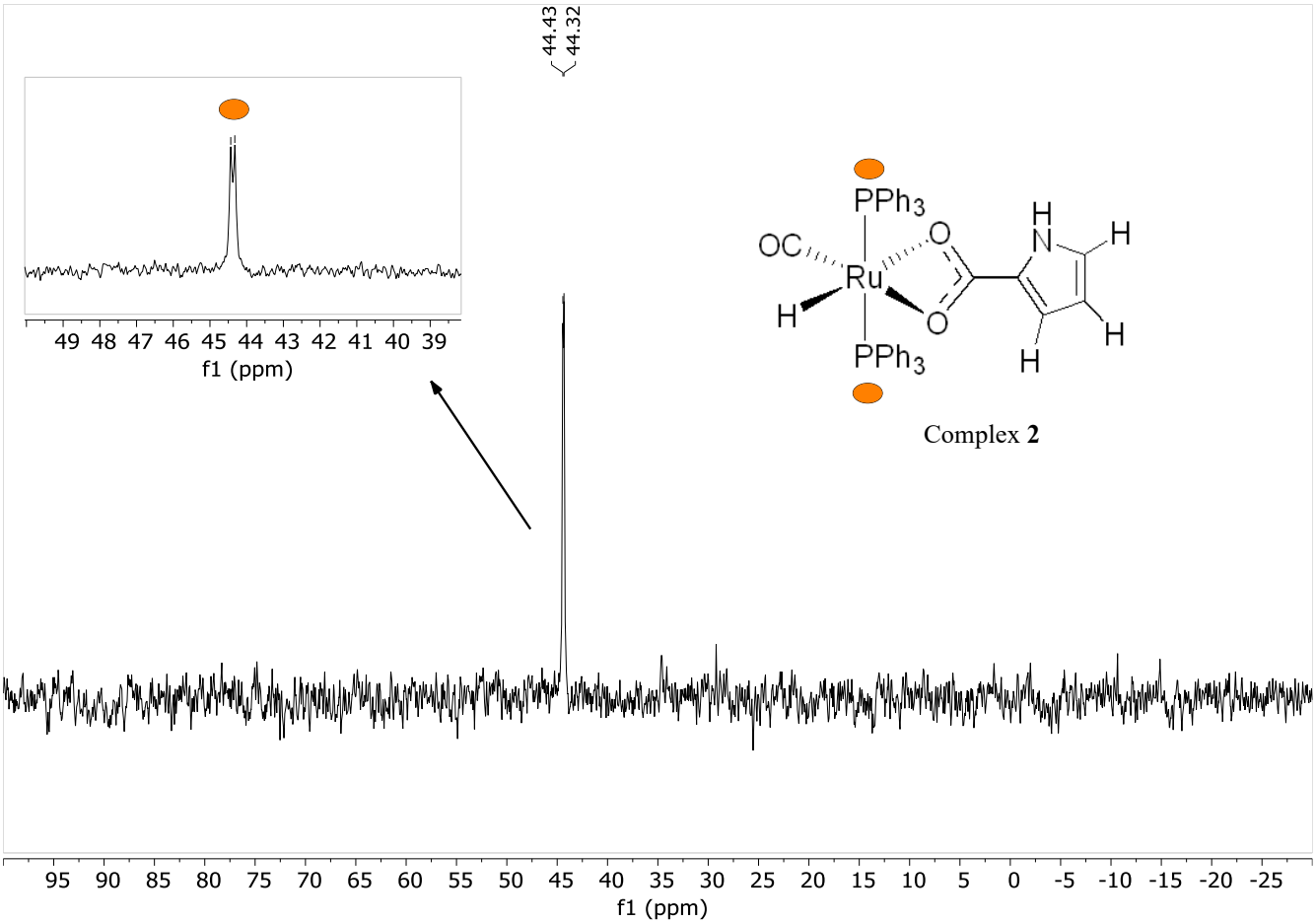

Complex **2**

^{31}P-NMR of complex 2: The doublet peak is observed at 44 ppm. Since the two phosphorus groups have the same chemical environment, only a single peak is observed in the ^{31}P-NMR spectrum. The peak appears as a doublet due to coupling with the hydride ligand bound to Ruthenium.

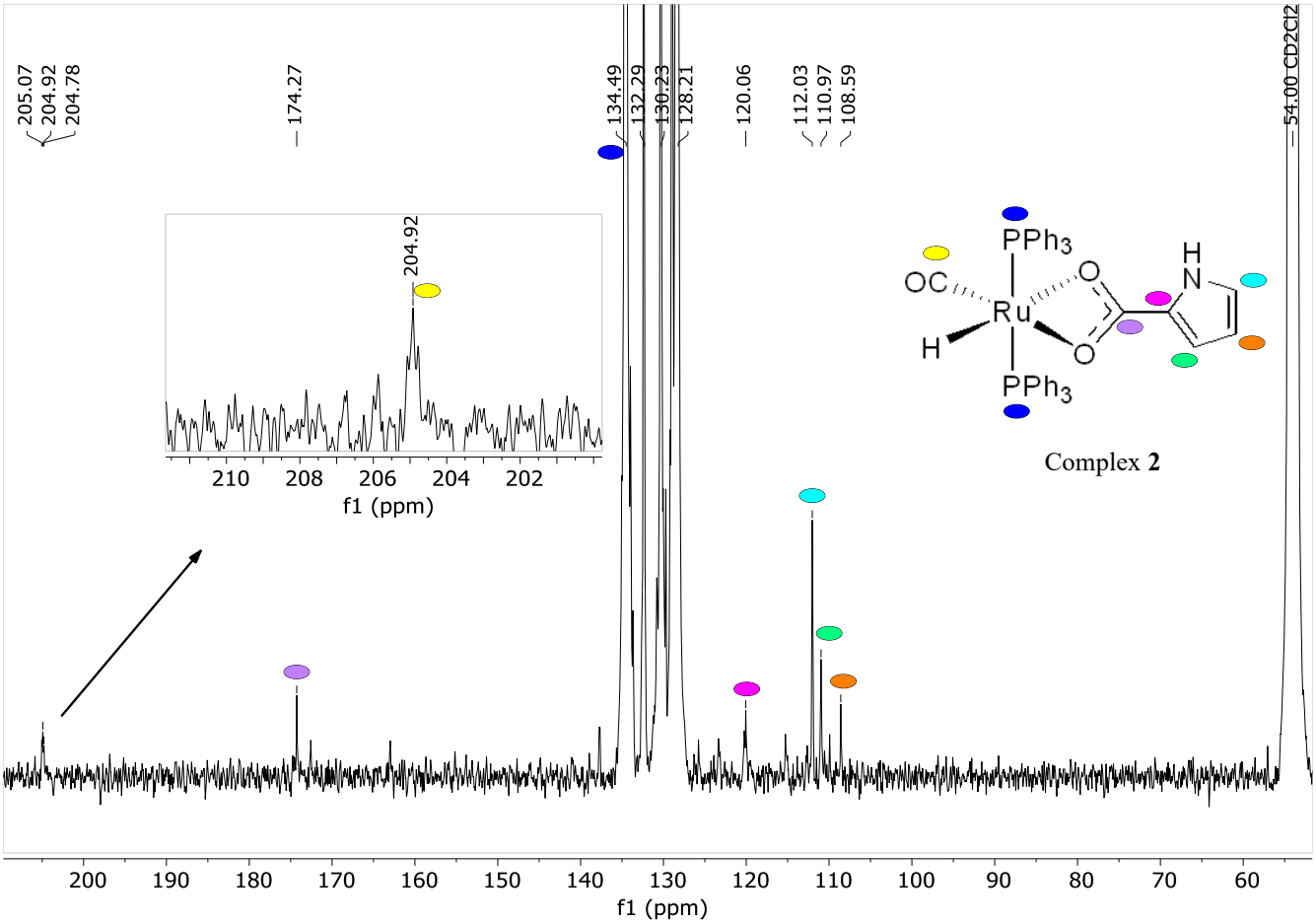

^{13}C-NMR of complex 2: The Pyrrole-2-carboxylate coordinated to Ruthenium contains five distinct types of carbons, which are identified in this spectrum. The carbon of the C≡O group appears around 205 ppm as a triplet, due to coupling with two phosphorus atoms. A deshielded carbon signal at 174.27 ppm, corresponds to the carboxylate group. The C-atoms of phenyl rings from the triphenylphosphine ligands, highlighted in dark blue, are multiplets due to the coupling to the two P atoms.

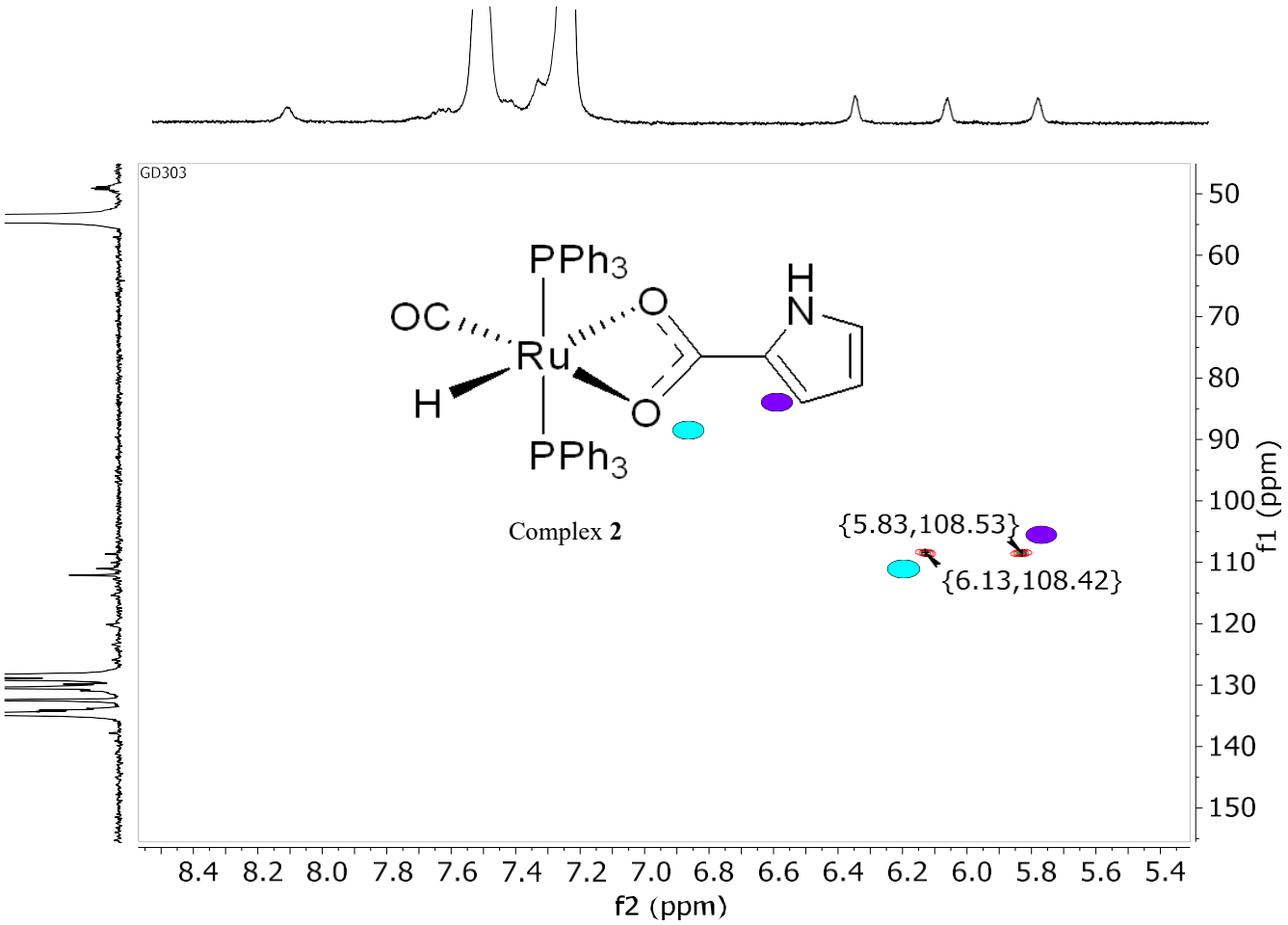

Heterocorrelated NMR spectrum {^{13}C,^{1}H} HSQC of complex 2: In this spectrum, only two peaks are visible, corresponding to the carbons that are directly bonded to hydrogen atoms. These are the only two peaks we can be undoubtedly assign.

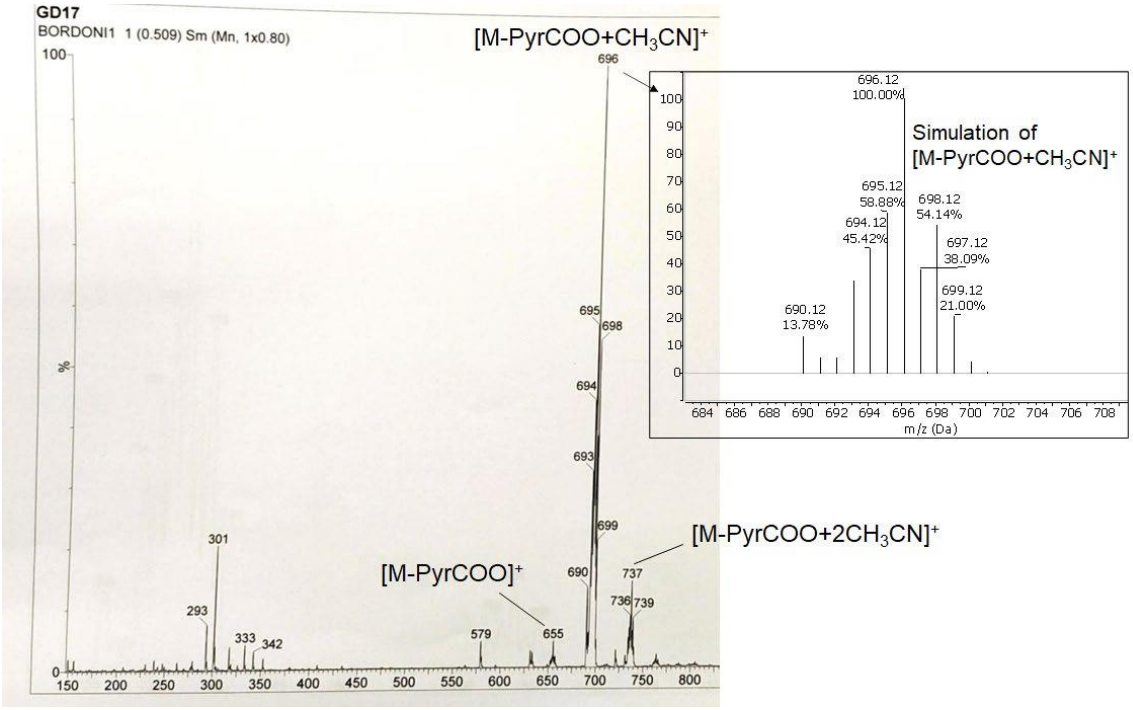
GD17
BORDONI1 1 (0.509) Sm (Mn, 1x0.80)
[M-PyrCOO+CH3CN]+
Simulation of
[M-PyrCOO+CH3CN]+
[M-PyrCOO]+
[M-PyrCOO+2CH3CN]+
%
m/z (Da)

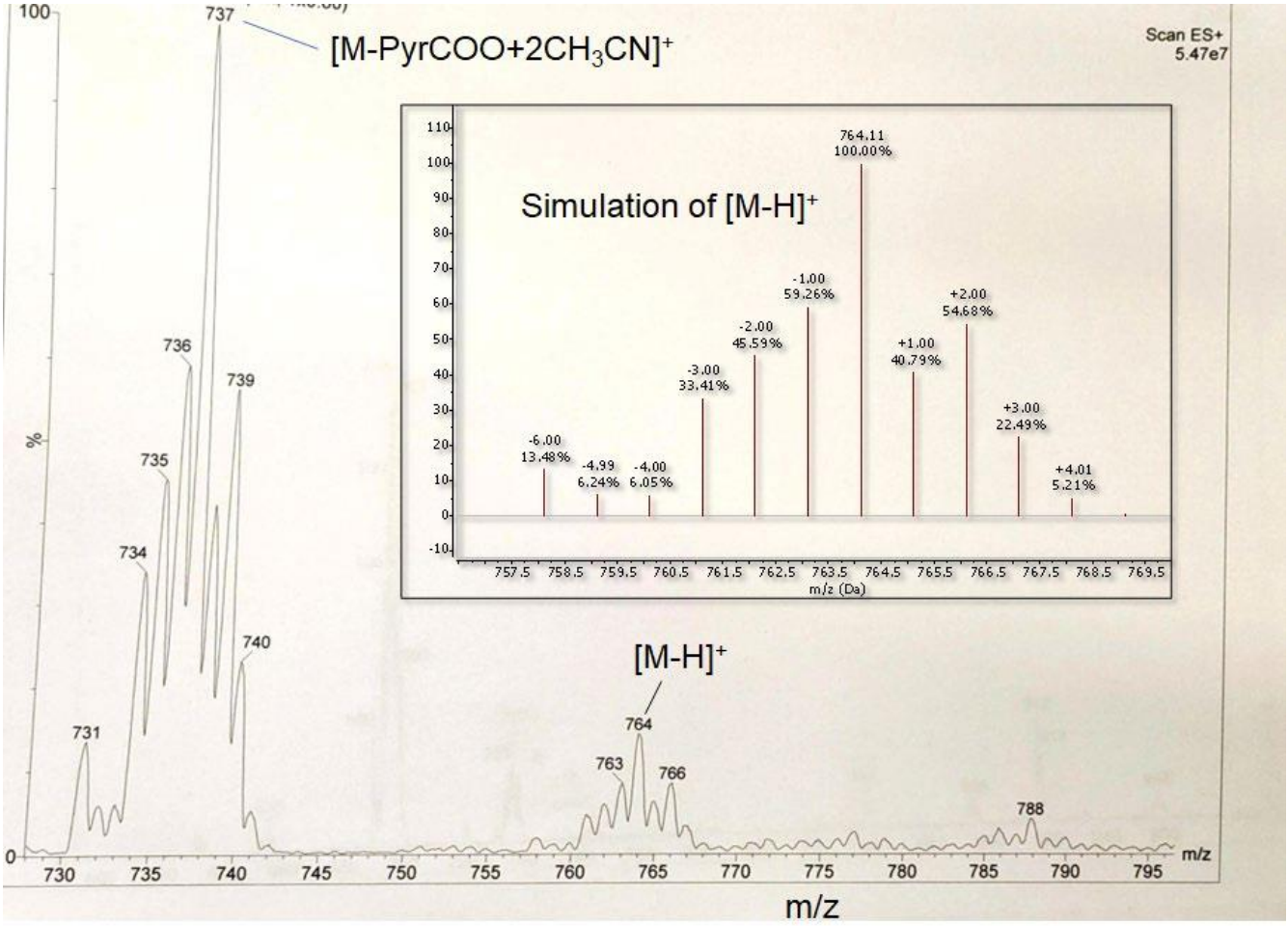
[M-PyrCOO+2CH3CN]+
Scan ES+
5.47e7
Simulation of [M-H]+
764.11
100.00%
-1.00
59.26%
-2.00
45.59%
-3.00
33.41%
+2.00
54.68%
+1.00
40.79%
+3.00
22.49%
+4.01
5.21%
-6.00
13.48%
-4.99
6.24%
-4.00
6.05%
m/z (Da)
[M-H]+
m/z

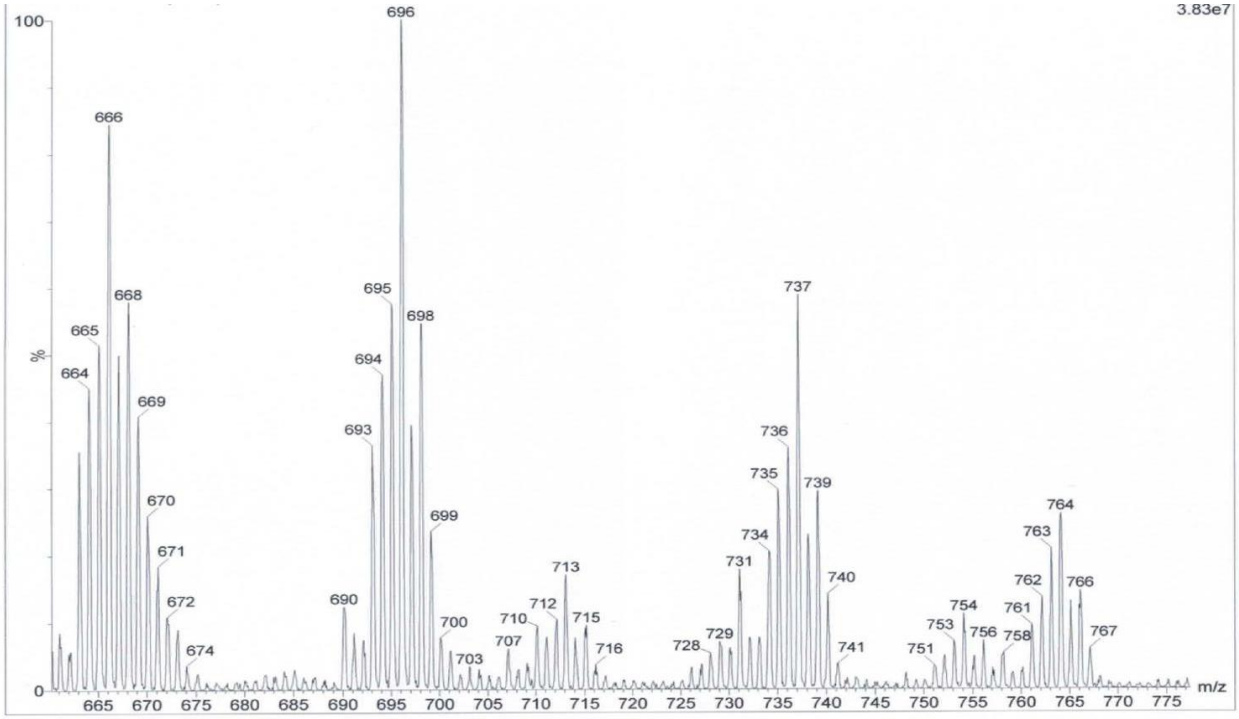
3.83e7
m/z

ESI-Mass of complex 2: [M] =765 (m/z), $[M-H]^+$ =764 (m/z), $[M-L+2CH_3CN]^+$ =737 (m/z), [M-L+ MeCN]$^+$ =696 (m/z), $[M-L]^+$ =655 (m/z).

The mass spectrum exhibits the expected signals corresponding to the loss of either the hydride or pyrrole-2carboxylate ligand, with peaks at $[M-H]^+$=764 (m/z) and $[M-L]^+$=655 (m/z). Peaks at 696 and 737 (m/z) are attributed to subsequent incorporation of acetonitrile (MeCN). Significant fragmentation is observed, notably above the molecular peak, corresponding to Pyrrole-2-carboxylate ligand loss (696) and further acetonitrile incorporation (737).

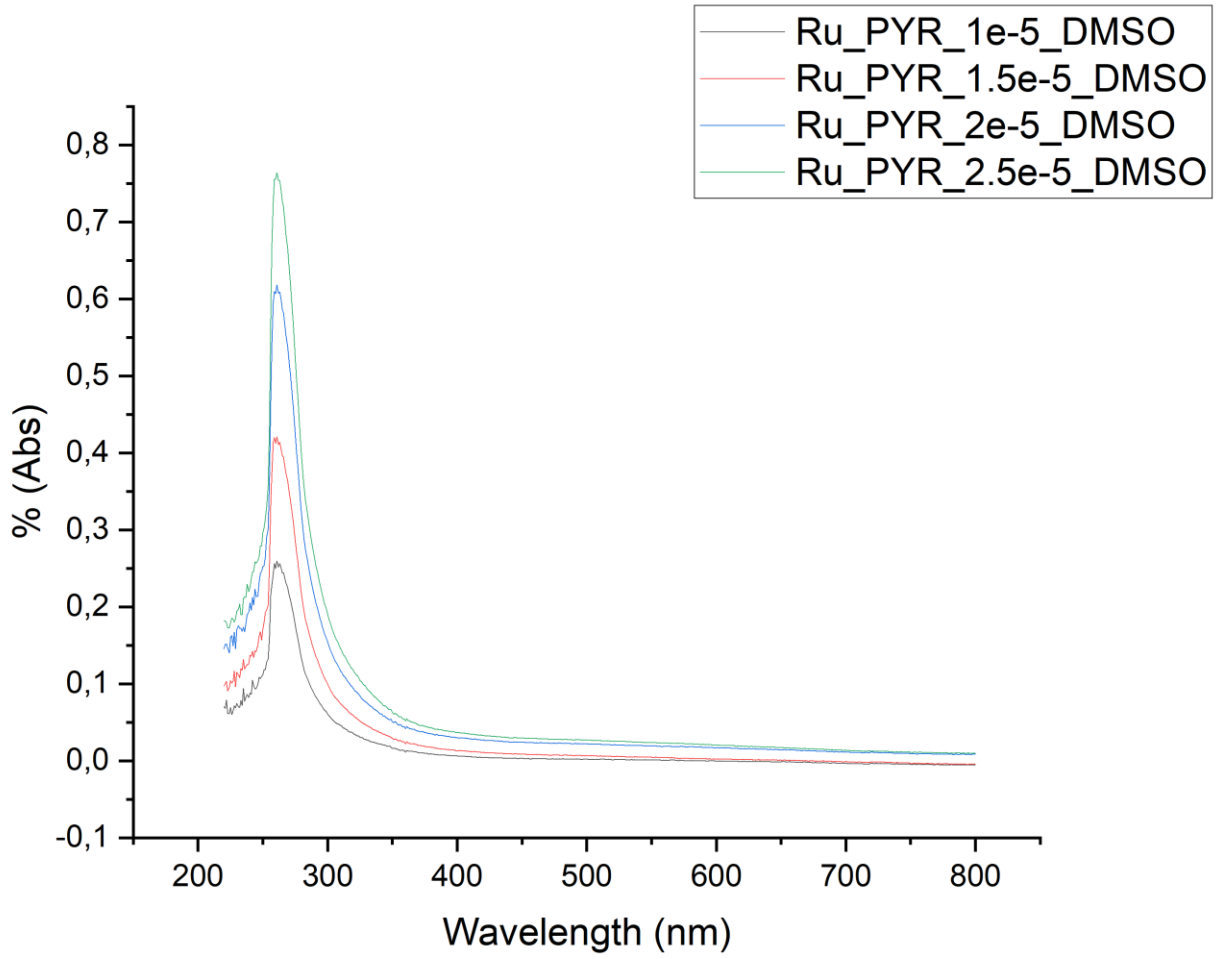

UV-Vis of complex 2: λ_{max}=260nm , Ɛ=17060

The absorption peak at 260 nm observed in the UV-Vis spectrum of complex **2** is attributed to a ligand-centered transition. Four acquisitions were made at different concentrations of the complex to obtain the molar extinction coefficient (Ɛ) value according to the Lambert Beer law.

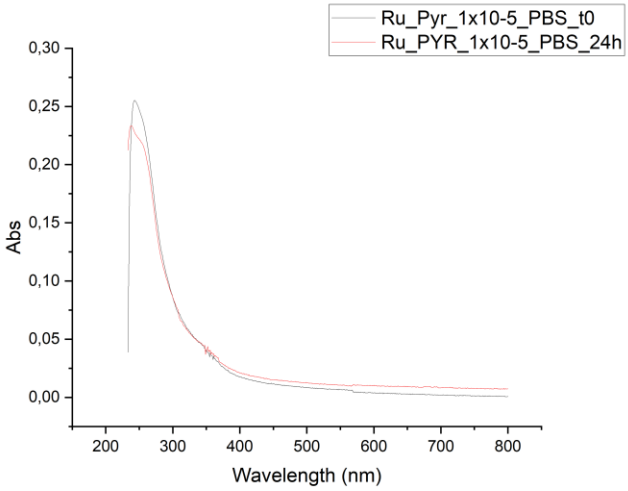

Stability of Complex 2 in PBS after 24 hours at 37 ˚C: To provide qualitative insight into the stability of complexes at physiological pH in solution phase, their UV–Vis spectra were recorded in phosphate buffer solution (PBS-5% DMSO) over a period of time of 24 h.

The spectra of the complexes show no wavelength shifts, indicating that their structural stability was maintained throughout the experiment.

- **Characterization of Complex 3 [Ru(NCMe)(CO)(PPh_3)$_2$(K^2(N,O)-Carboxypyrrole)]**

Complex **3** was synthesized by refluxing Complex **2** in Acetonitrile under Argon atmosphere.

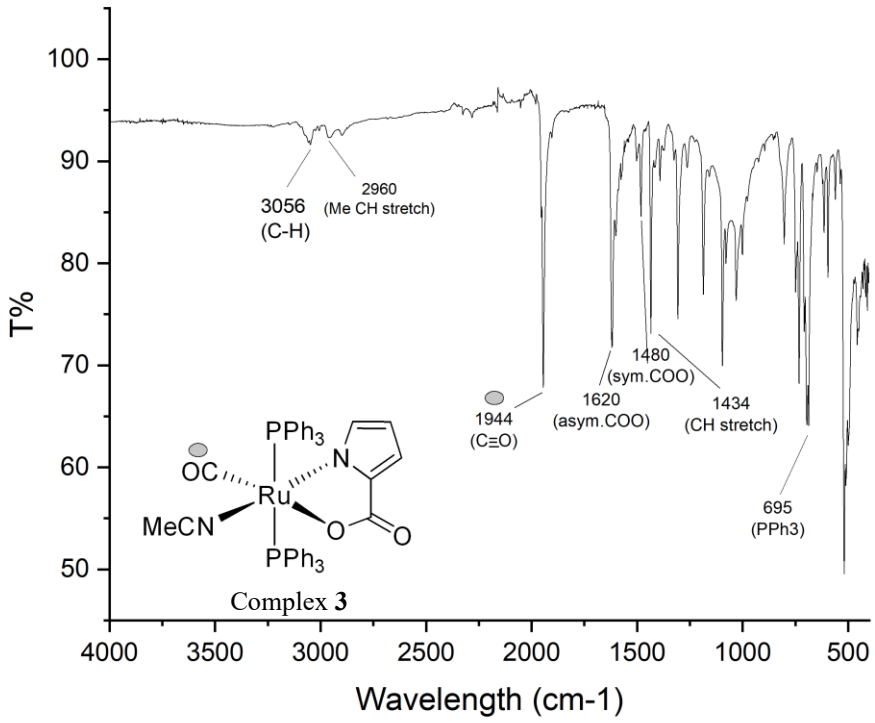

IR of complex 3: As shown in the spectrum, in comparison to the IR spectrum of Complex 2, the peak related to N-H stretch of the pyrrole is not visible because the pyrrole ring N is coordinated to Ruthenium directly, and the CO peak has shifted from 1926 cm^{-1} to 1944 cm^{-1}.

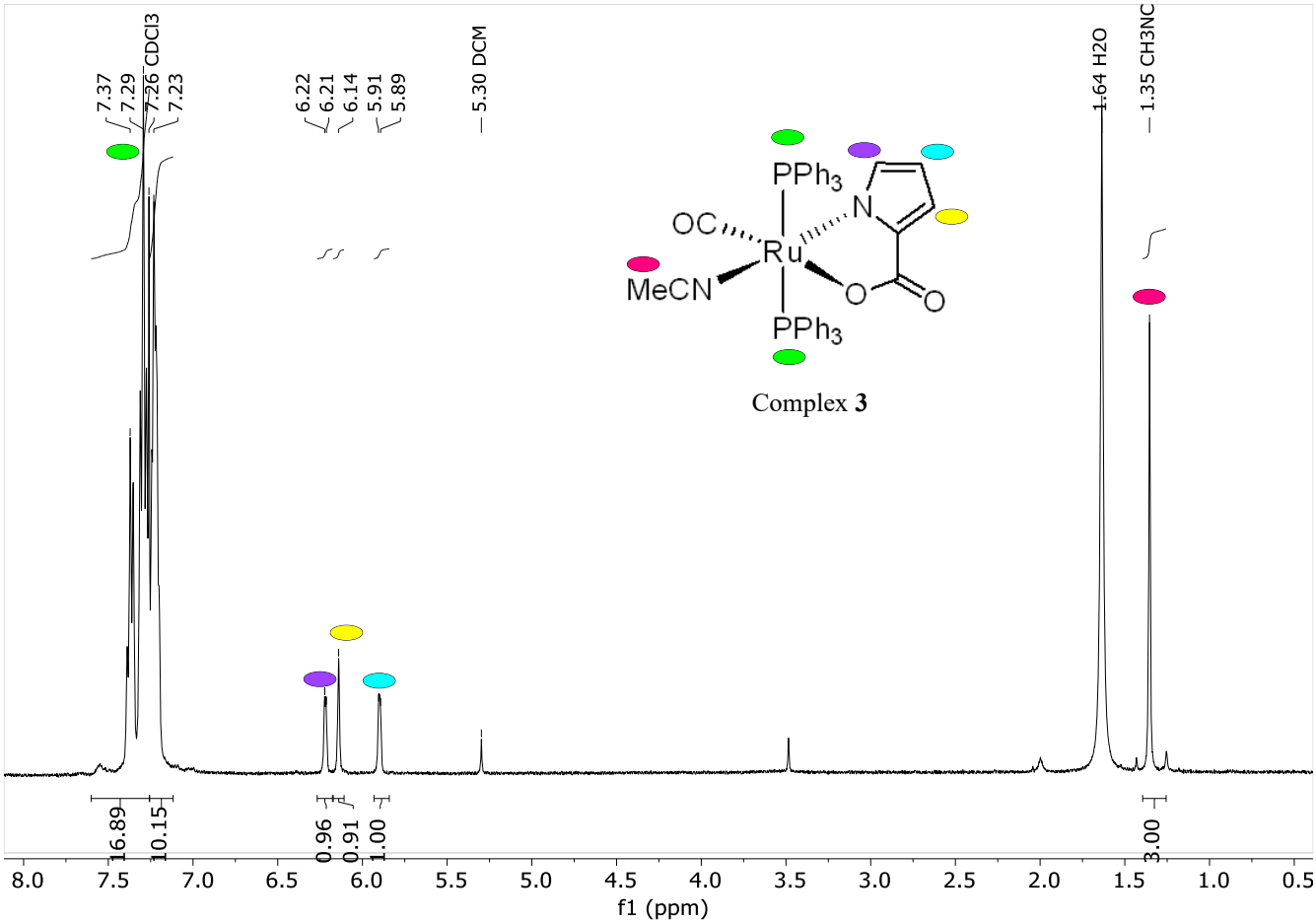

Complex **3**

^{1}H-NMR of Complex 3: In this spectrum, three distinct hydrogens from Pyrrole-2-carboxylic acid coordinated to Ruthenium are visible, along with a peak at 1.35 ppm, integrating to 3, which is assigned to the three hydrogens of the methyl group in acetonitrile. A comparison with the ^{1}H-NMR spectrum of complex **2** reveals that the peak corresponding to the hydride (around -16.74 ppm) is not visible, indicating that the hydride has been successfully replaced by acetonitrile in the coordination process.

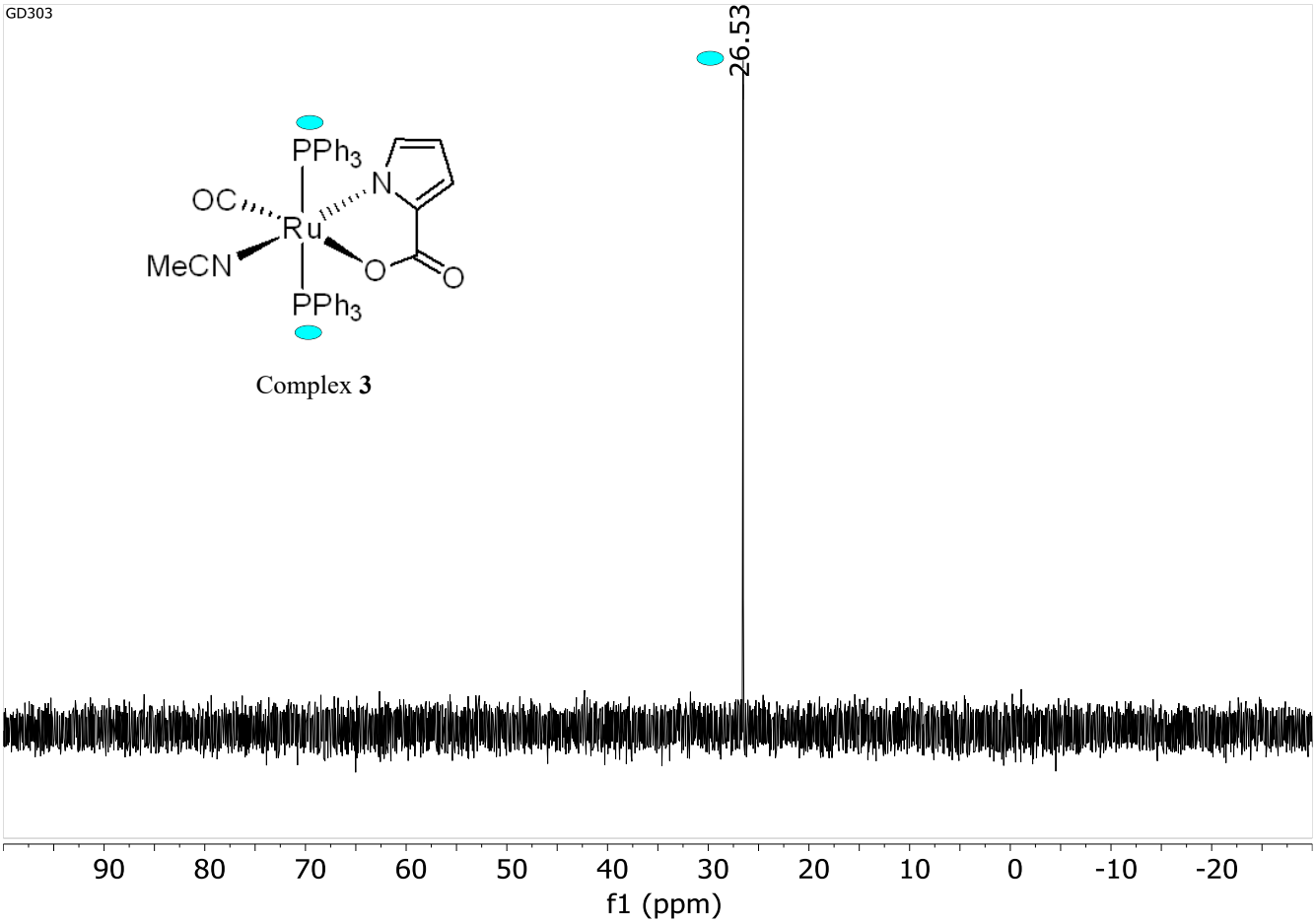

Complex **3**

^{31}P-NMR of complex 3: In this spectrum, a singlet peak is observed at 26.53 ppm, indicating perfect decoupling due to the absence of a hydride coordinated to Ruthenium. The two phosphorus atoms share the same chemical environment, as the other ligands coordinated to Ruthenium are in the same plane.

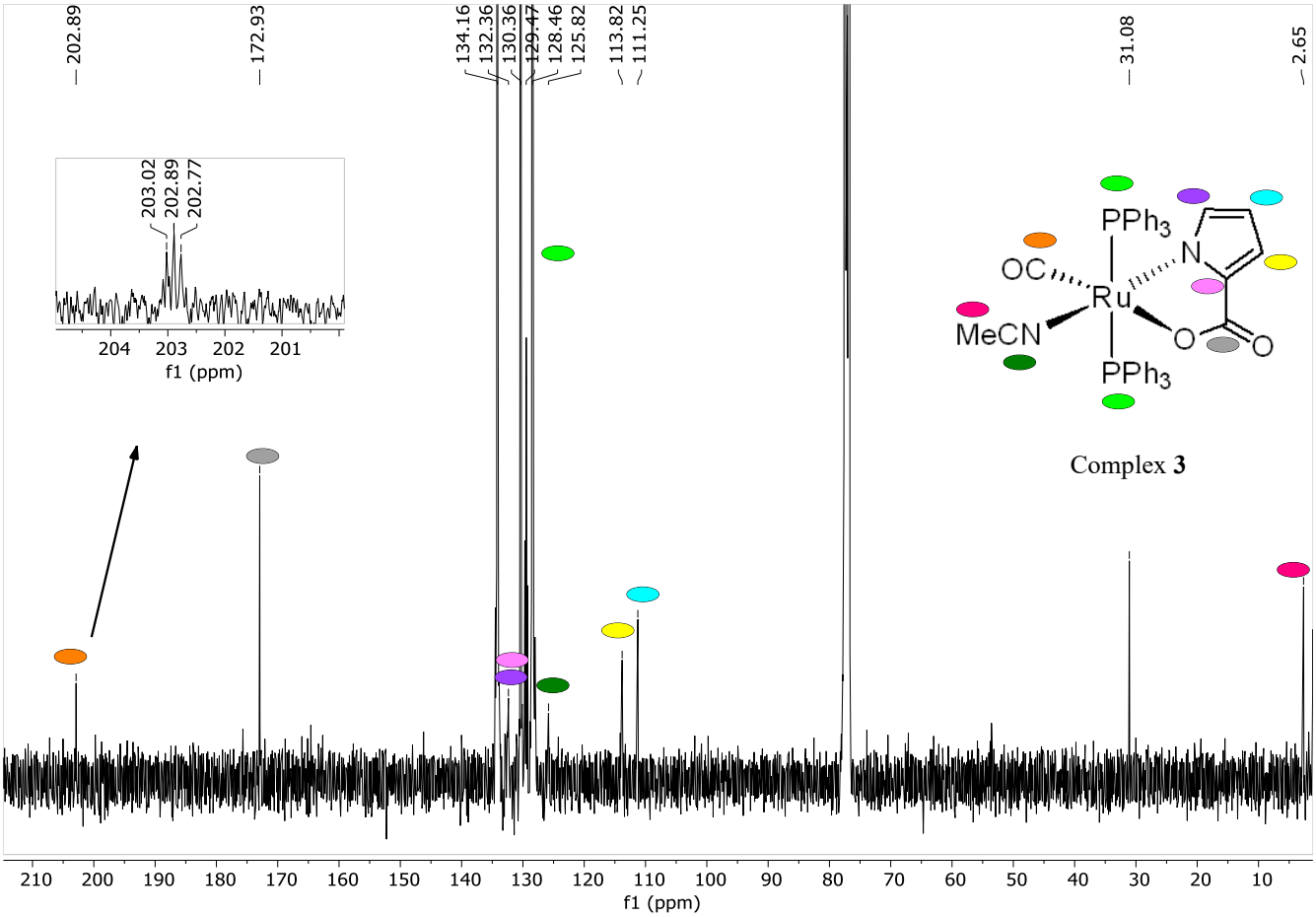

^{13}C-NMR of complex 3: As shown in the spectrum, the carbon of the methyl group appears downfield at 2.65 ppm. The other aliphatic carbon, associated with the CN group, is observed at 128.46 ppm. A triplet peak appears at the most upfield position, corresponding to the C≡O group, which is coupled with two phosphorus atoms. In the pyrrole ring, the carbons farther from the nitrogen appear more upfield compared to those closer to the nitrogen. The carbon signal of the carboxylate group is more deshielded, but less than the C≡O signal.

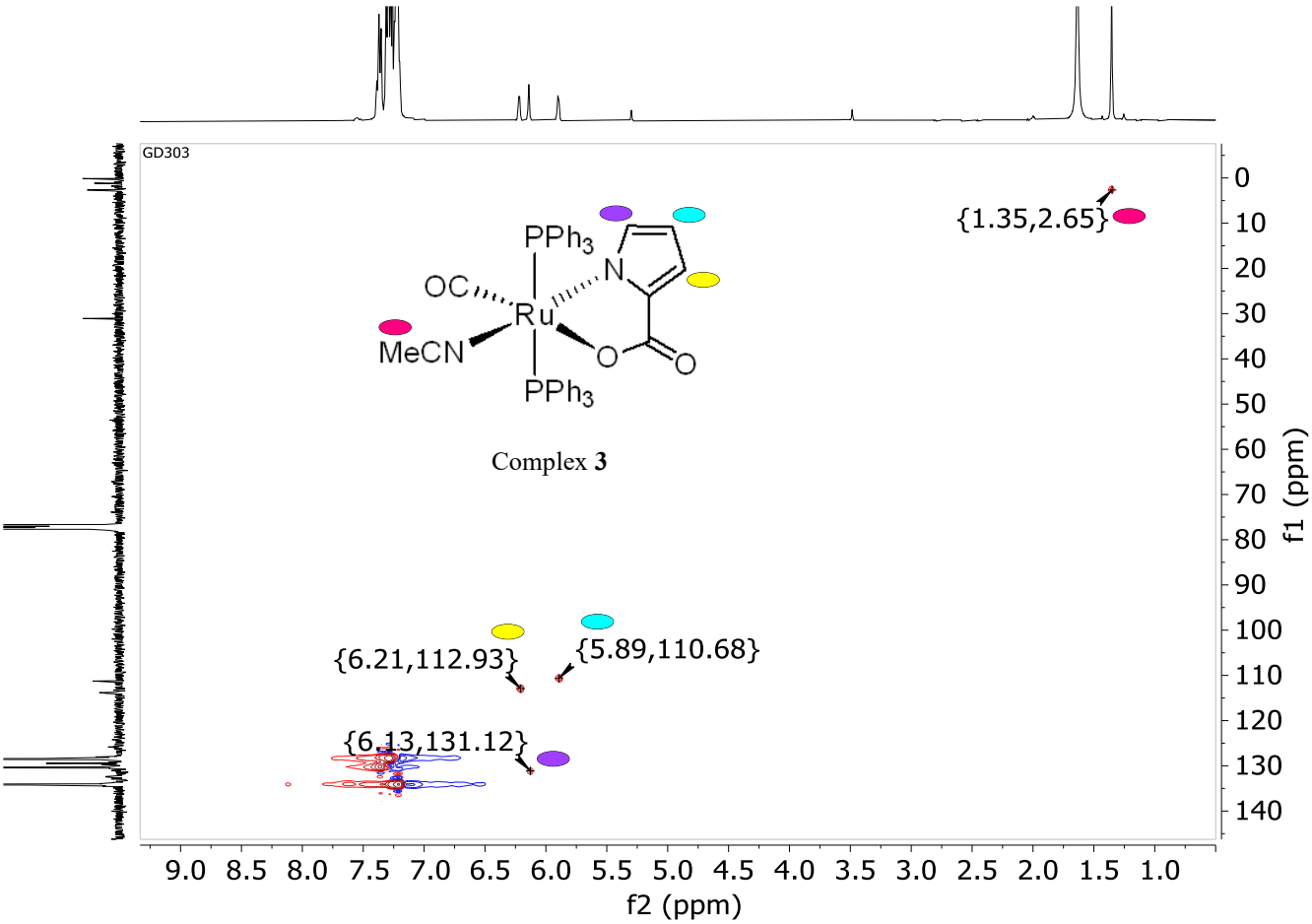

Complex **3**

Heterocorrelated NMR spectrum {^{13}C,^{1}H} HSQC of complex 3: In this spectrum, four signals are visible, corresponding to the carbons that are directly bonded to hydrogen atoms. They are assigned by the way of their attachment.

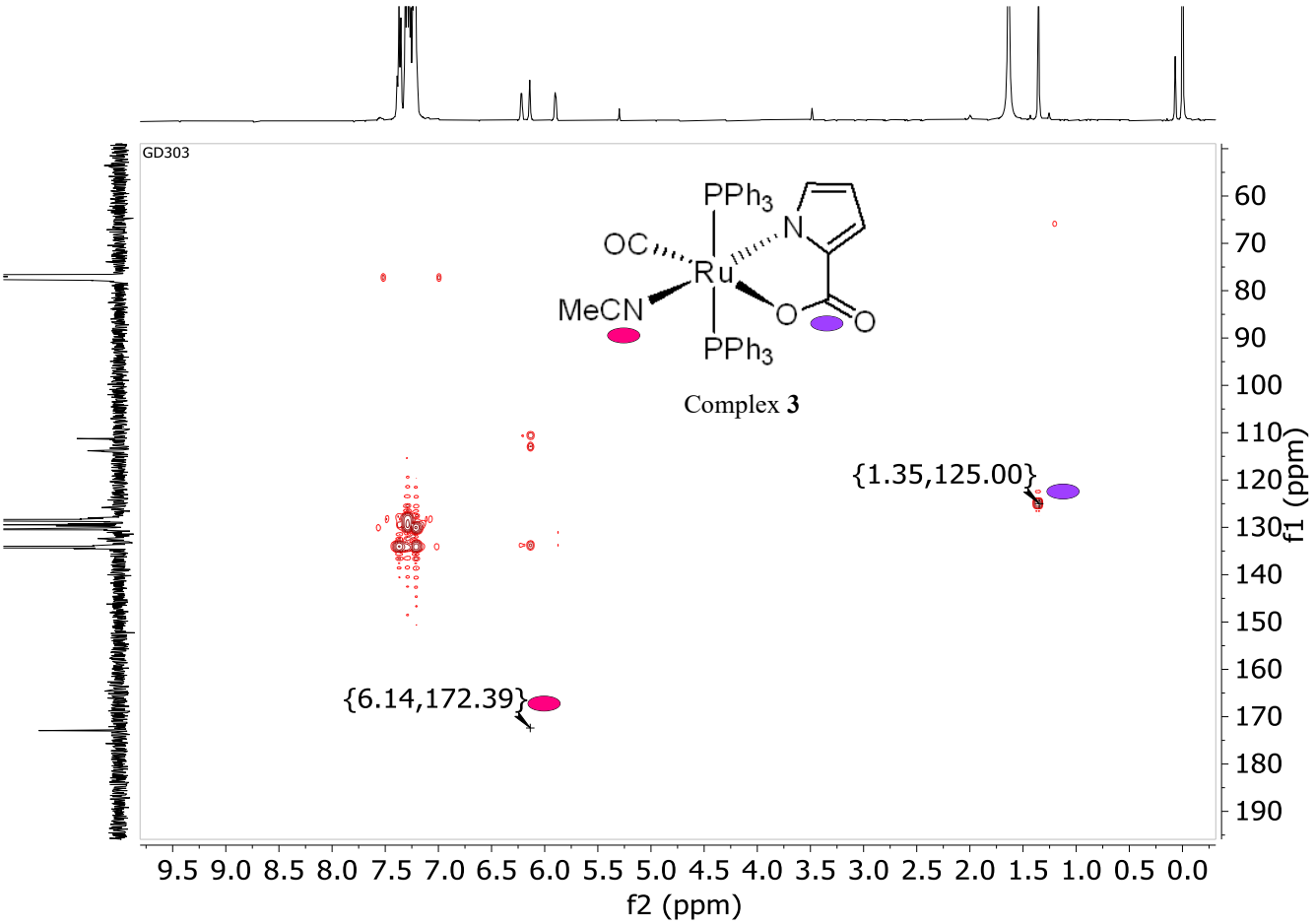

Complex **3**

Heterocorrelated NMR spectrum {^{13}C,^{1}H} HMBC of complex 3: In this spectrum, the positions of two peaks corresponding to quaternary carbons are observed. The peak that appears upfield is associated with the C≡N group, marked in red, while the downfield peak in violet corresponds to the carboxylate carbon.

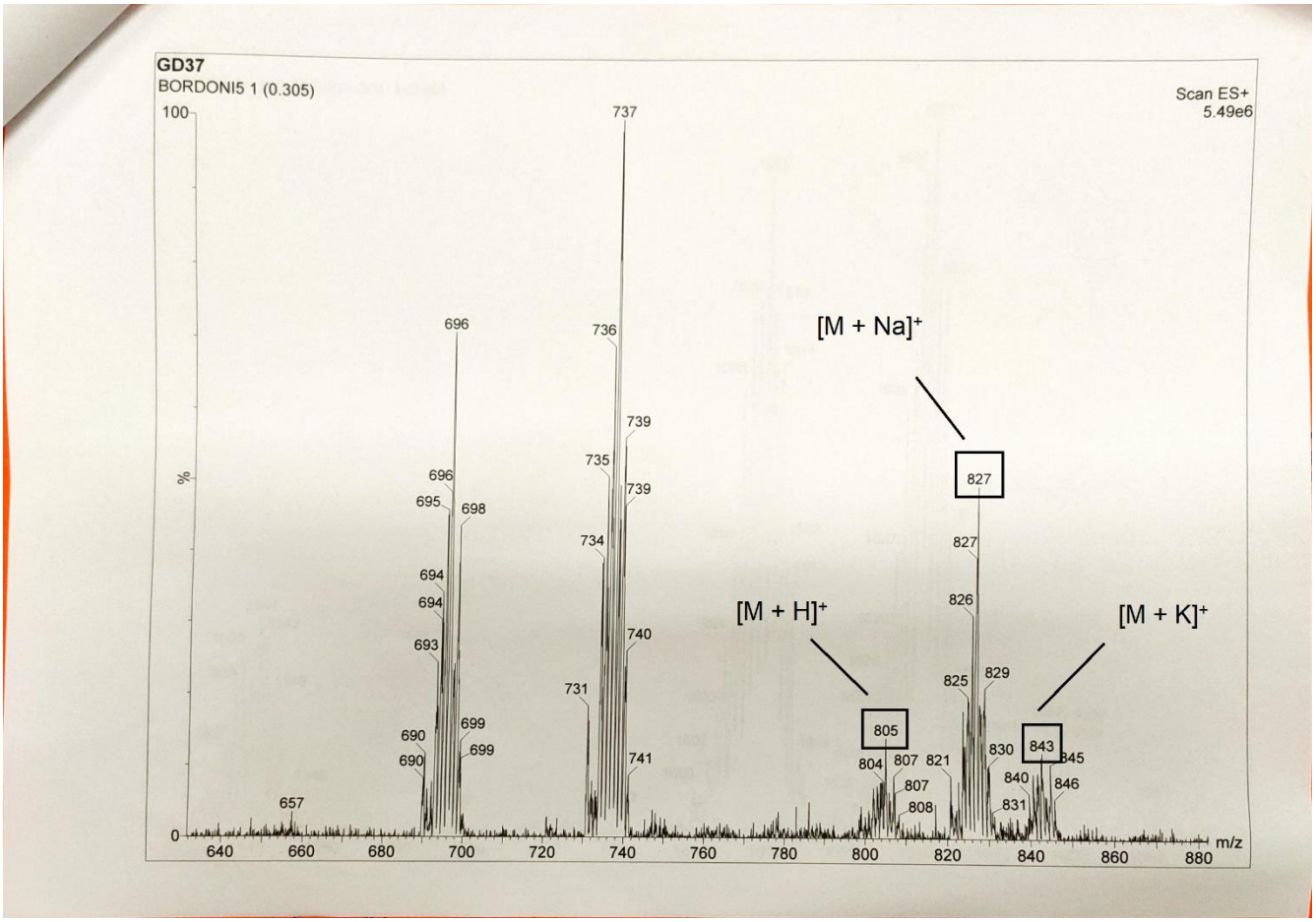
GD37
BORDONI5 1 (0.305)
Scan ES+
5.49e6
100
%
0
[M + Na]+
[M + H]+
[M + K]+
737
696
736
739
735
739
696
695
698
734
827
827
694
694
826
693
740
731
825
829
805
843
690
699
690
699
741
804
807
821
830
807
840
846
808
831
657
640
660
680
700
720
740
760
780
800
820
840
860
880
m/z

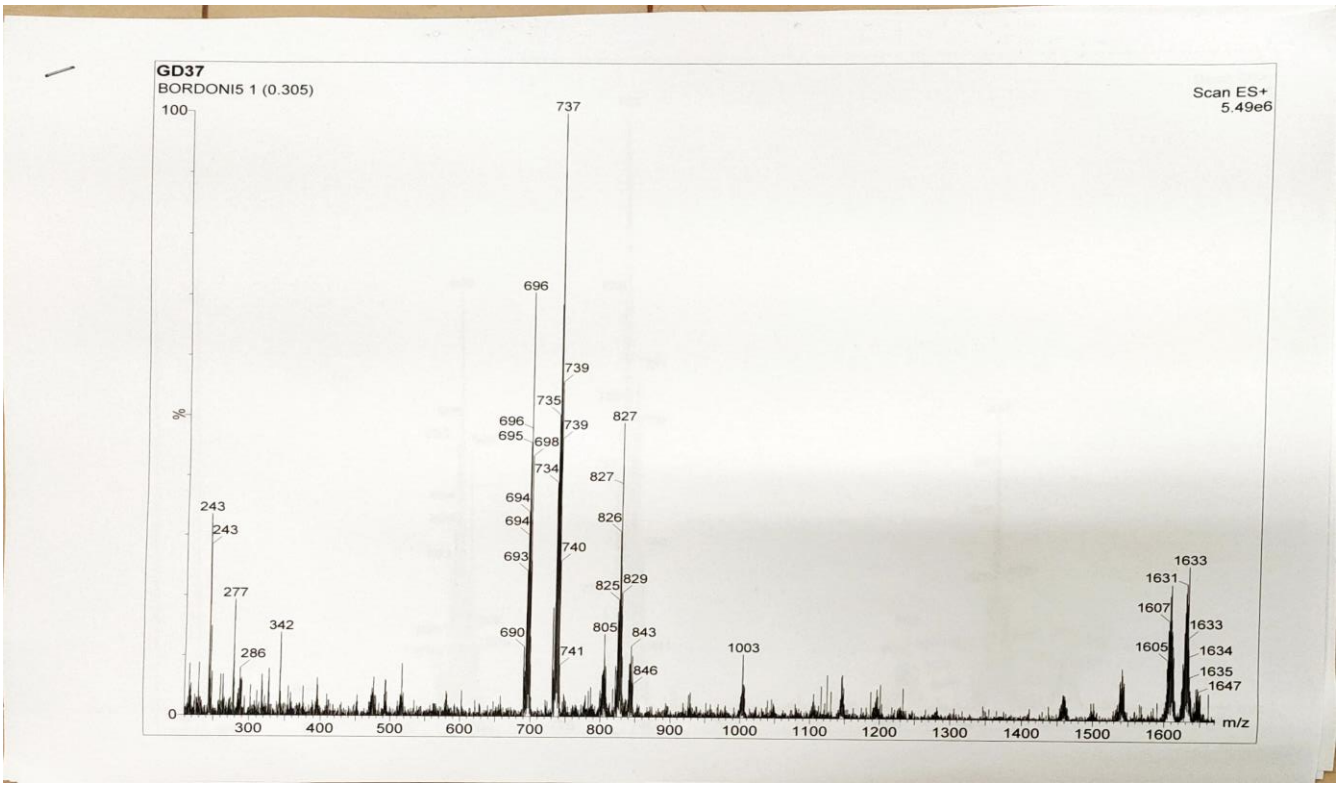
GD37
BORDONI5 1 (0.305)
Scan ES+
5.49e6
100
%
0
737
696
739
735
696
695
739
827
698
734
827
694
826
694
693
740
825
829
243
243
277
342
286
690
805
843
741
846
1003
1633
1631
1607
1633
1605
1634
1635
1647
300
400
500
600
700
800
900
1000
1100
1200
1300
1400
1500
1600
m/z

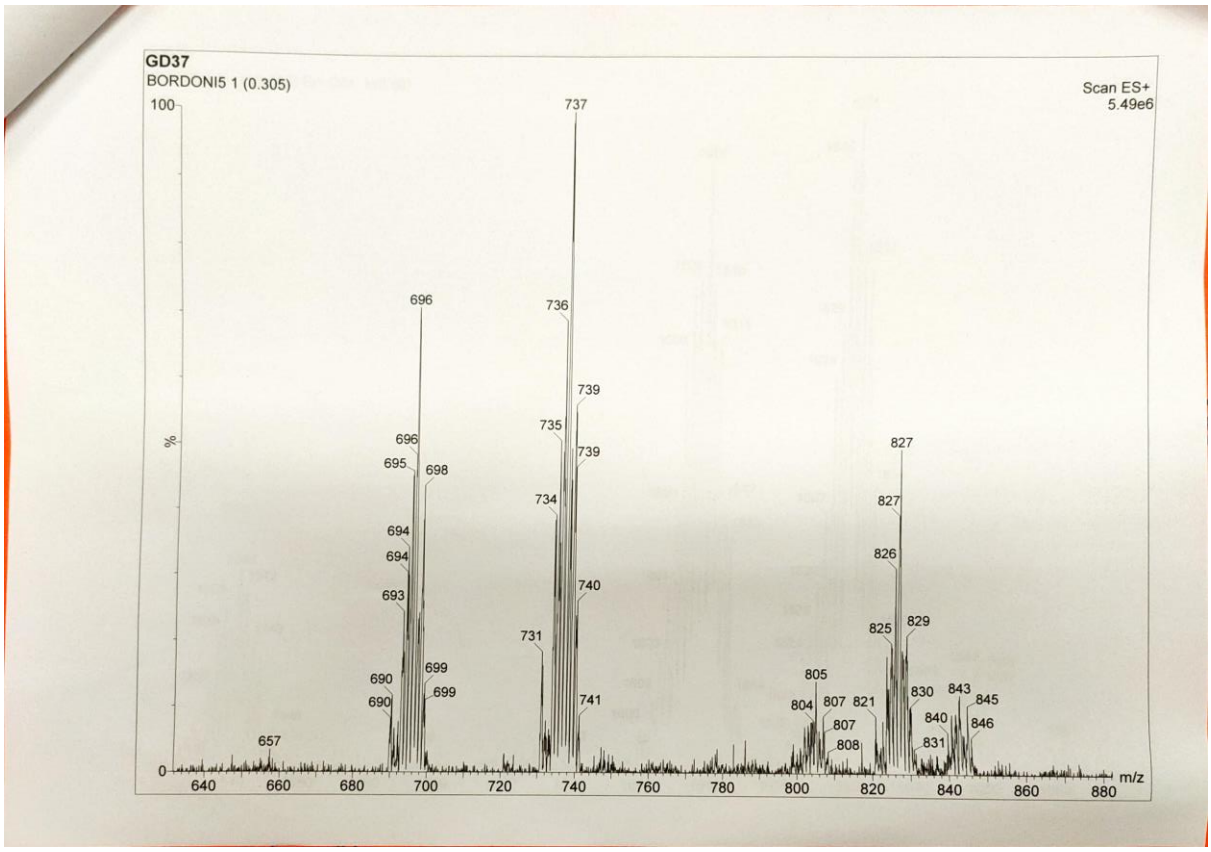
GD37
BORDONI5 1 (0.305)
Scan ES+
5.49e6
100
%
0
737
696
736
739
735
739
696
695
698
734
827
827
694
694
826
693
740
825
829
731
699
805
690
699
804
807
821
830
843
845
690
741
807
840
846
657
808
831
640
660
680
700
720
740
760
780
800
820
840
860
880
m/z

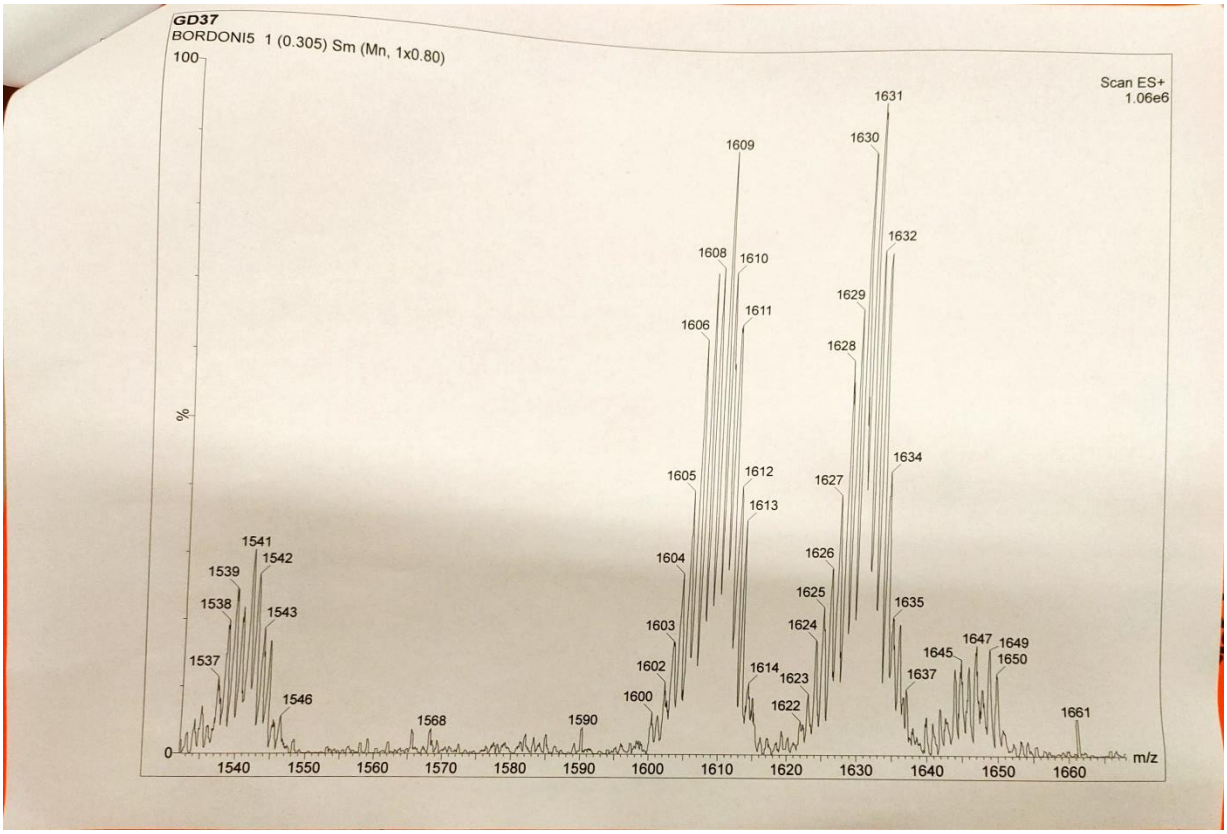
GD37
BORDONI5 1 (0.305) Sm (Mn, 1x0.80)
Scan ES+
1.06e6
100
%
0
1631
1609
1630
1608
1610
1632
1606
1611
1629
1628
1605
1612
1634
1627
1613
1604
1626
1625
1635
1603
1624
1647
1645
1649
1650
1602
1614
1623
1637
1600
1622
1661
1541
1542
1539
1538
1543
1537
1546
1568
1590
1540
1550
1560
1570
1580
1590
1600
1610
1620
1630
1640
1650
1660
m/z

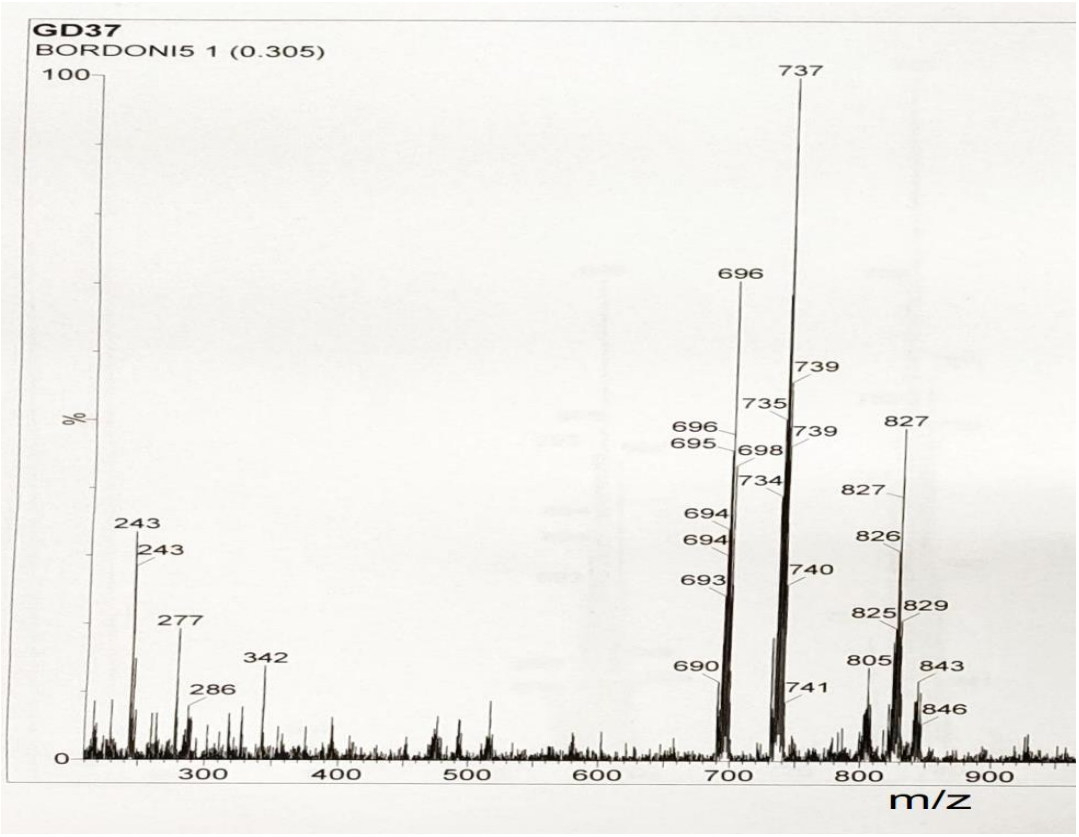

ESI-Mass of complex 3: [M]=804 (m/z), $[M+H]^+$ =805(m/z), $[M+Na]^+$ =827(m/z), $[M+K]^+$ =843(m/z), $[M-L+2CH_3CN]^+$ =737 (m/z), $[M-L+ CH_3CN]^+$ =696 (m/z), $[M-L]^+$ =655 (m/z).

The mass spectrum shows the expected signals for the loss of the pyrrole-2-carboxylate ligand, with a peak at m/z 655 $[M–L]^+$. Peaks at m/z 696 and 737 are linked to the subsequent incorporation of acetonitrile (MeCN). Additionally, three prominent peaks appear at m/z 805 $[M + H]^+$, 827 $[M + Na]^+$, and 843 $[M + K]^+$ for the solvent complex **3**.

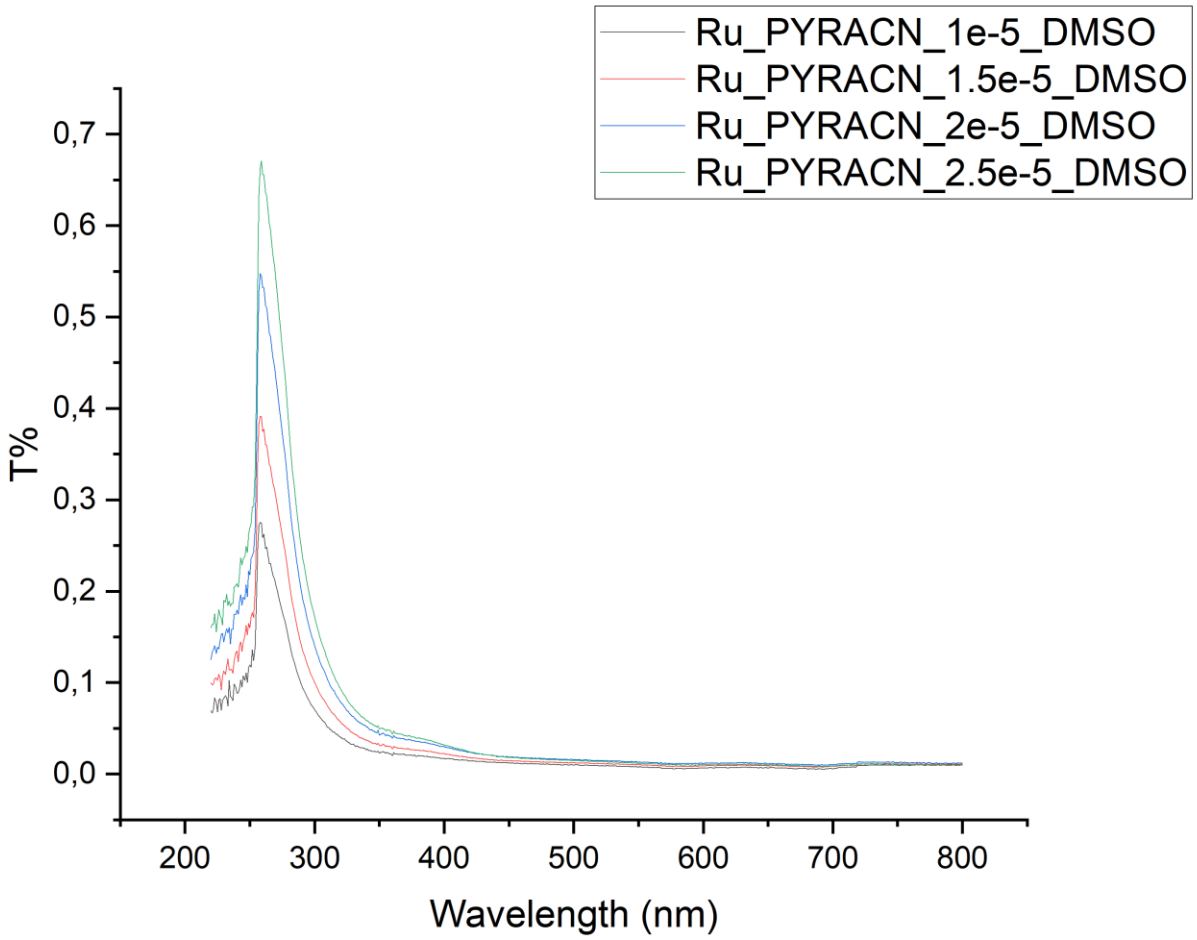

UV-Vis of complex 3: λ_{max}=259nm , Ɛ=13380

The absorption peak at 259 nm in this UV-Vis spectrum of complex **3** is assigned to a ligand-centered transition. To determine the molar extinction coefficient (Ɛ), four measurements were taken at different concentrations of the complex in DMSO, following the Lambert-Beer law.

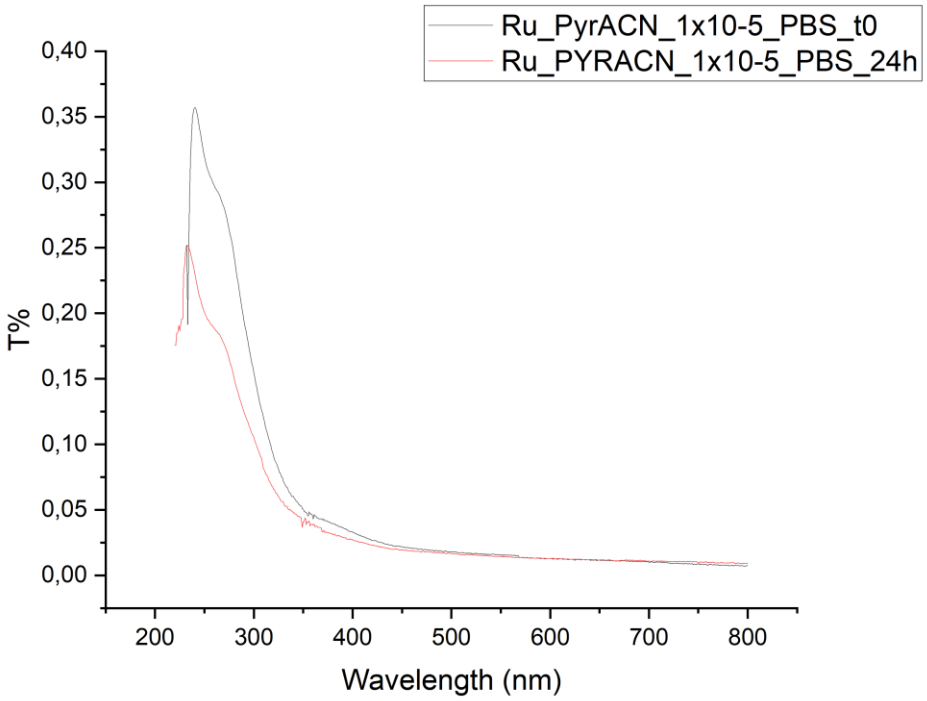

Stability of complex 3 for 24 h in PBS at 37 ˚C: To gain qualitative insight into the stability of the complexes at physiological pH in solution, their UV–Vis spectra were recorded in a phosphate buffer solution (PBS-5% DMSO) over a 24-hour period. The spectra revealed no shifts in wavelength, suggesting that the complexes maintained their structural stability throughout the experiment. Even if the bands have not shifted, a decrease in the intensity of the bands can be observed after 24 hours. This is an indication of a lower concentration of the complex in the solution, which can be caused by the precipitation of part of the complex over time.

- **Characterization of Complex 4 [Ru(4-picoline)(CO)(PPh_3)$_2$(K^2(N,O)-Carboxypyrrole)] and Complex 8 [Ru(4-Picoline)(CO)(PPh_3)$_2$(K^2(N,O)-Carboxyindole)]**

Complex **4** was synthesized by refluxing Complex **3** and 4-picoline in toluene under Argon atmosphere. Complex **8** was synthesized by adding 4-picoline to Complex **7** and refluxing them in 1,4-Dioxane.

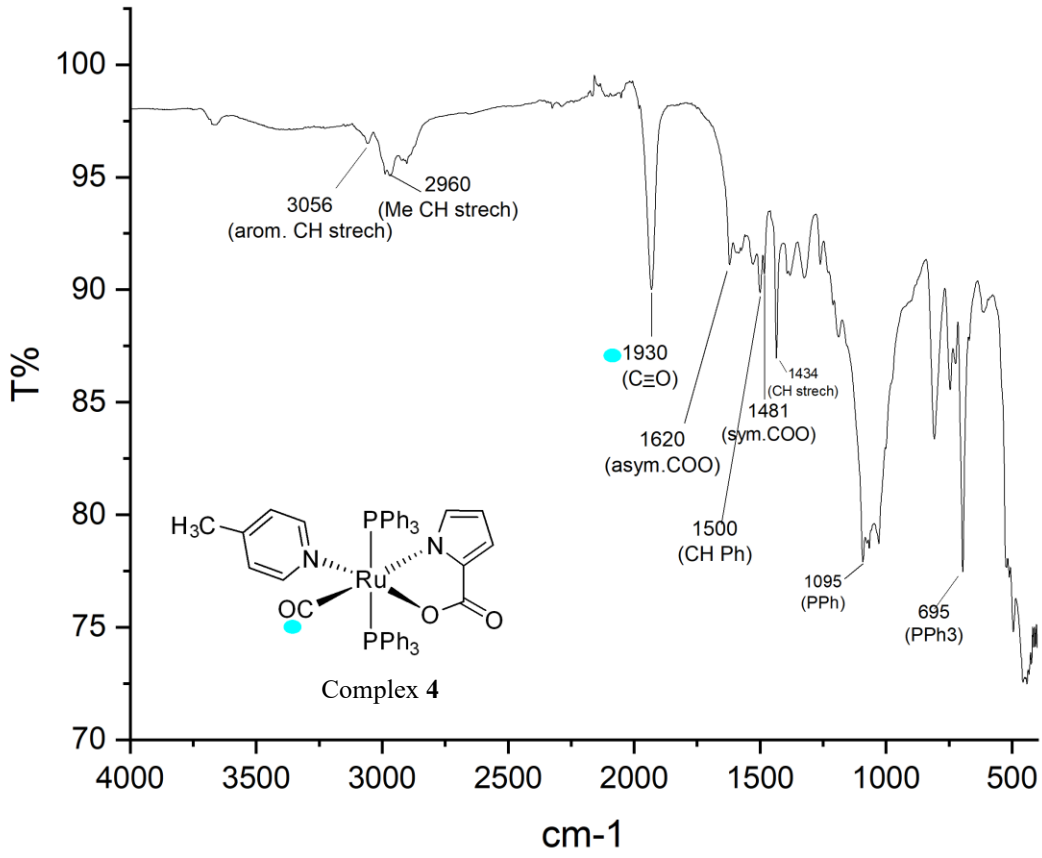

Complex **4**

IR of Complex 4: The spectrum displays a sharp CO peak at 1930 cm^{-1}, indicating a significant shift compared to the CO peak of the reactant (complex **3**) at 1944 cm^{-1}.

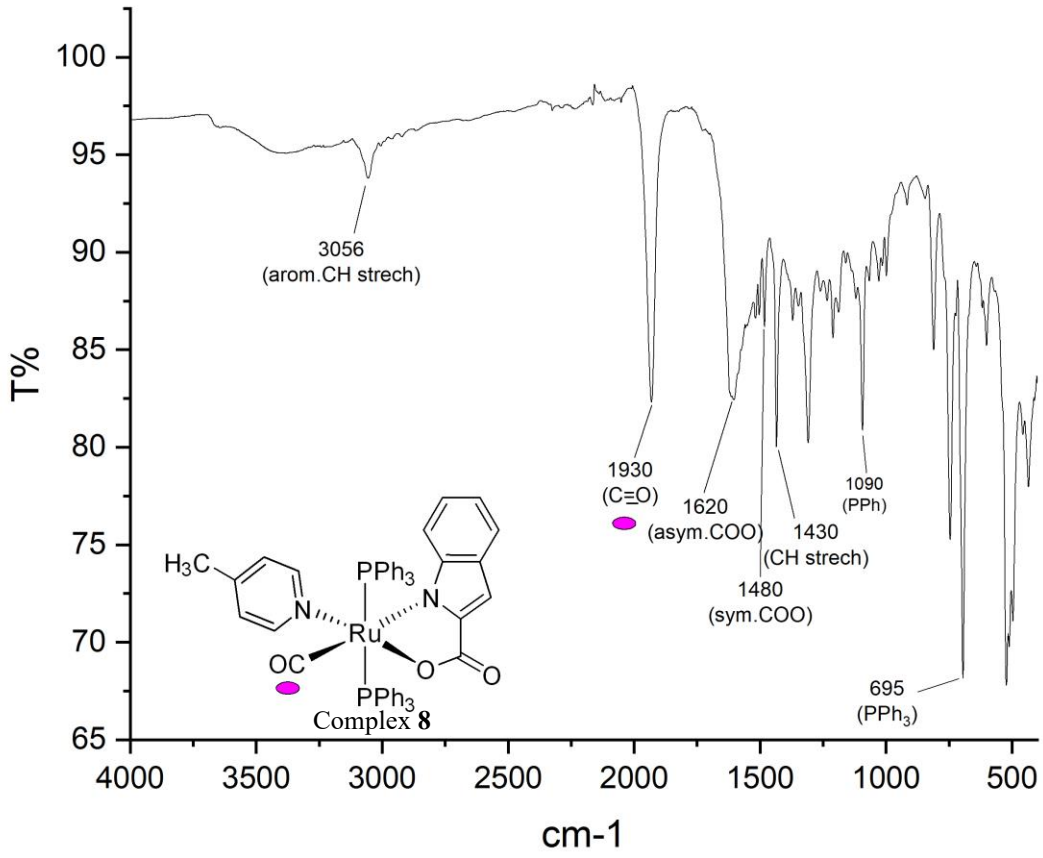

IR of Complex 8: The spectrum displays a sharp CO peak at 1930 cm^{-1}, indicating a significant shift compared to the CO peak of the reactant (complex **7**) at 1944 cm^{-1}.

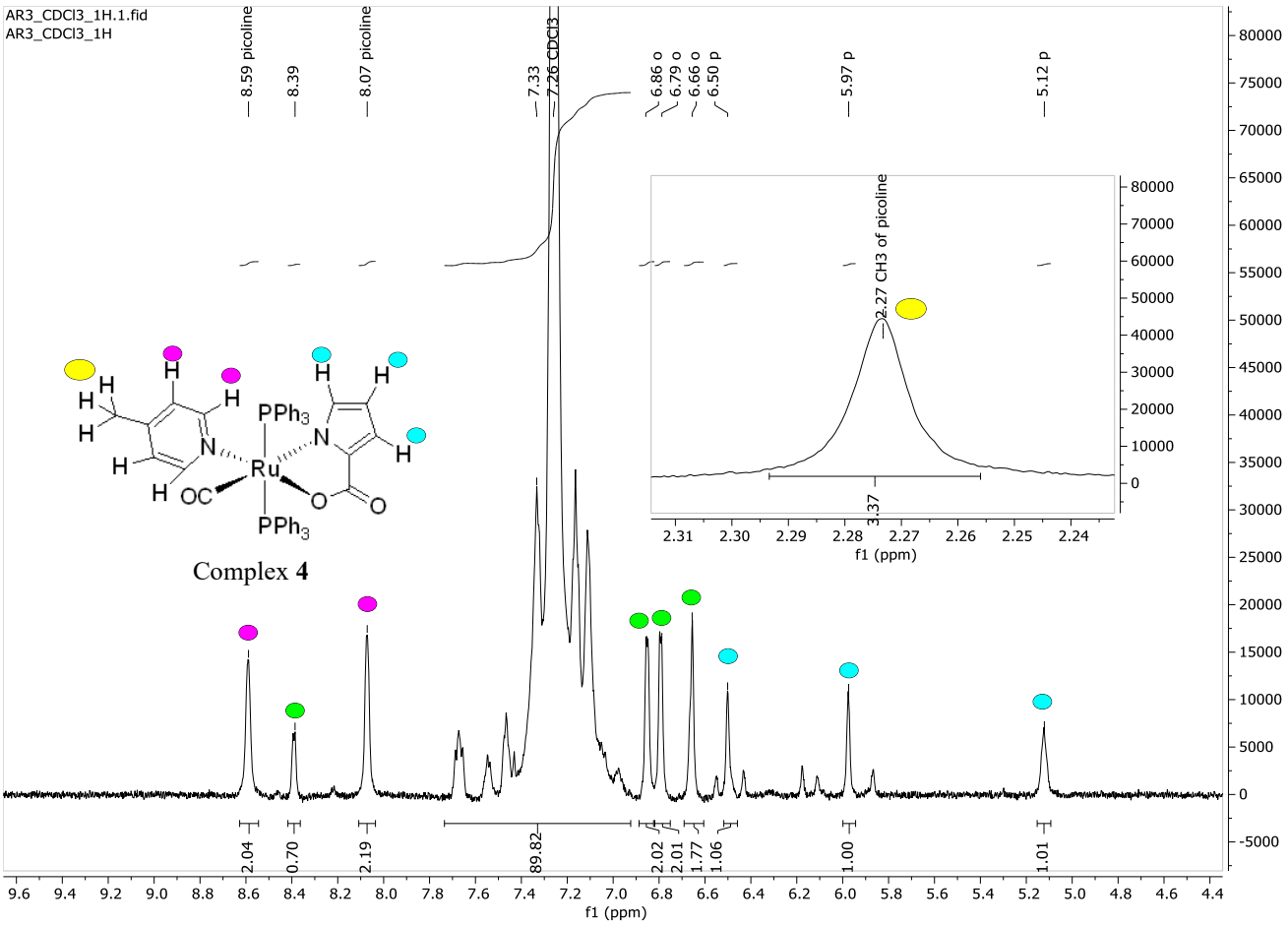

^{1}H-NMR of Complex 4: As indicated in the spectrum, the product peaks are highlighted in blue and pink. However, the spectrum also reveals the presence of an additional complex alongside the product, with its peaks marked in red. The signals integrating 89.82 corresponds to the triphenylphosphines of all species of the mixture. This value is higher compared to previous complexes, which show integration of 30. The increase is likely due to the presence of another, unidentified complex. The four broad singlets highlighted with green color are related to the Pyrrole moiety of a side product formed during the reaction. The peak at 8.39 ppm may refer to NH moiety of the pyrrole in by-product.

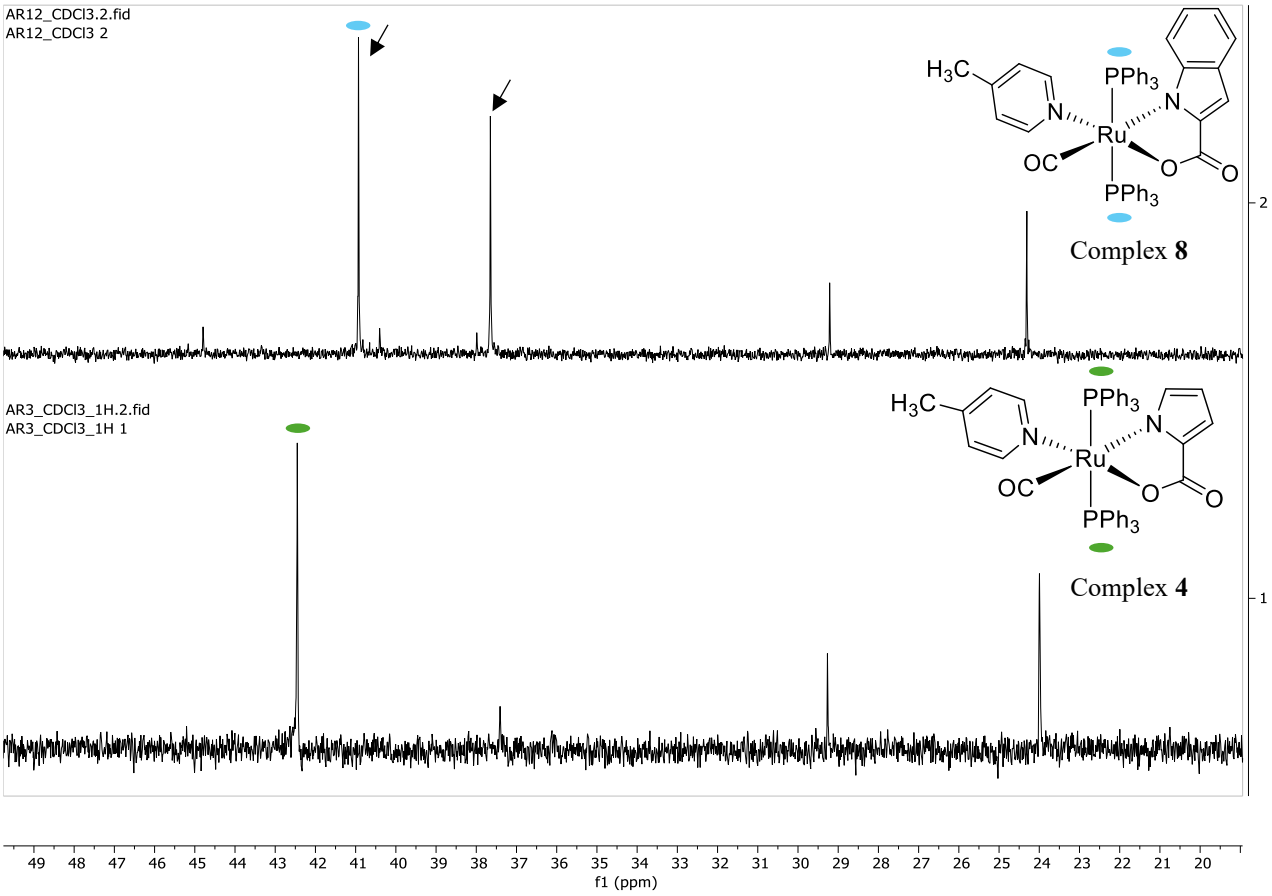

^{31}P-NMR of Complex 4 and 8: In the spectrum of Complex **4**, (bottom spectrum), the presence of four phosphorus-containing compounds is revealed, with two being the major ones. The more intense peak at 42.31 ppm corresponds to the main product where picoline is successfully coordinated, and the other at 23.86 ppm refers to a Ruthenium-Pyrrole derivative, but the structure is still unknown. The peak at 29.12 ppm is attributed to triphenyl phosphide oxide. Under varying reaction conditions, the product with indole shows chemical shifts that are similar but slightly different from those of the product with pyrrole. Like spectrum of complex **4**, the indole Complex **8** (upper spectrum) shows the presence of a four-compound mixture which the product peak is observed at 42.63 ppm. In this spectrum, the intensity of two peaks on the left, marked by arrows, are approximately the same, so it is not straightforward to properly assign the signals of the H-NMR spectrum for complex **8**.

- **Characterization of Complex 6 [RuH(CO)(PPh_3)$_2$(K^2(O,O)-Carboxyindole)]**

Complex **6** is synthesized by dissolving Complex **1** and Indole-2-carboxylic acid in Toluene under Argon atmosphere.

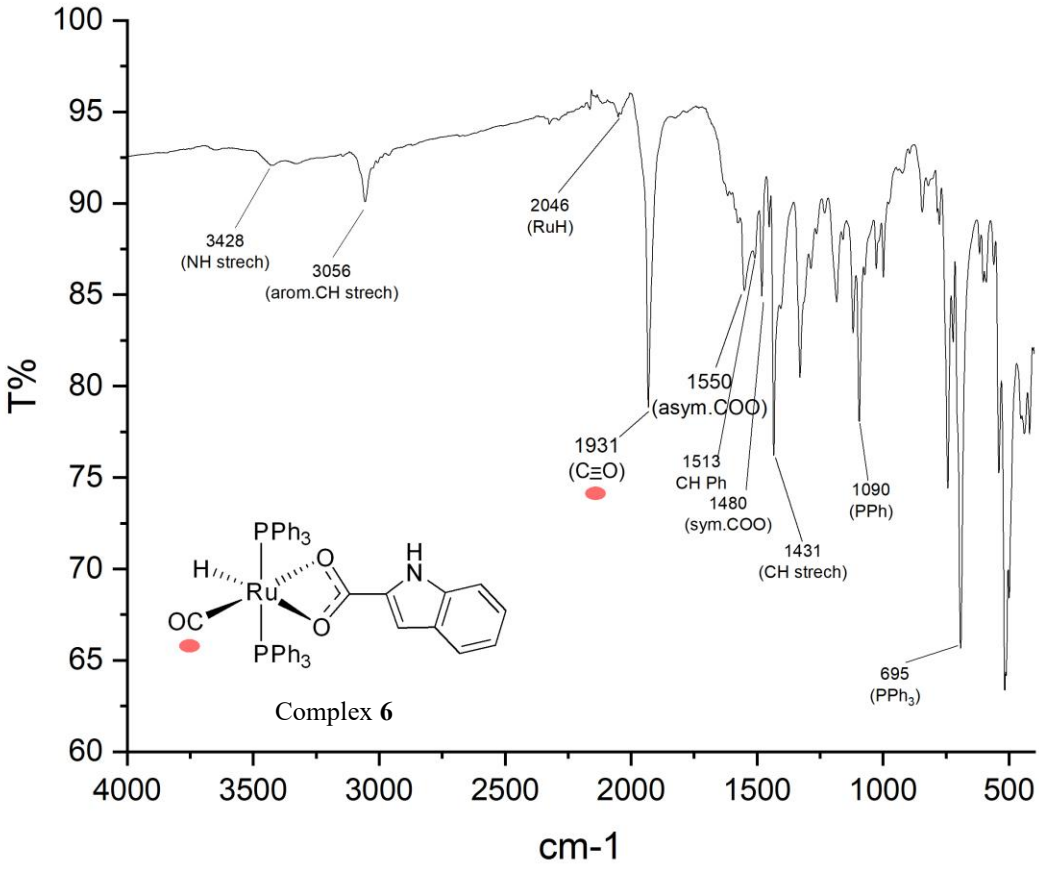

Complex **6**

IR of Complex 6: As shown in the spectrum, the N-H stretch of the indole coordinated to Ruthenium is marked in orange, and the CO peak has shifted from 1940 cm^{-1} to 1931 cm^{-1}.

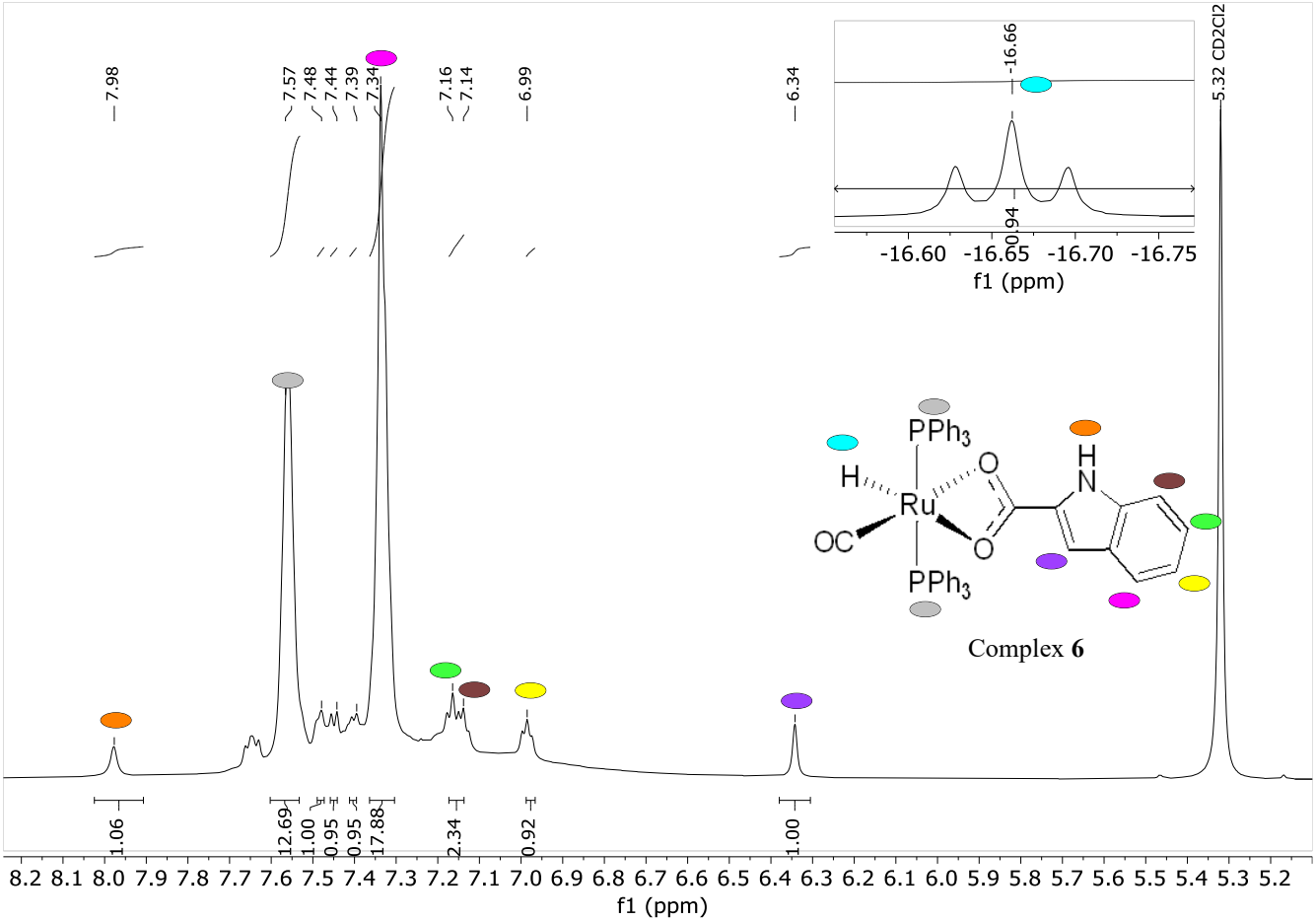

Complex **6**

^{1}H-NMR of Complex 6: This spectrum illustrates the six distinct proton signals of indole-2-carboxylate coordinated to Ruthenium, with their assignments based on nearby atoms. The hydride ligand directly attached to Ruthenium appears in the upfield region as a triplet due to coupling with two phosphorus atoms. The hydrogen bonded to the nitrogen of the indole appears downfield, as the more electronegative nitrogen causes the hydrogen to be more deshielded.

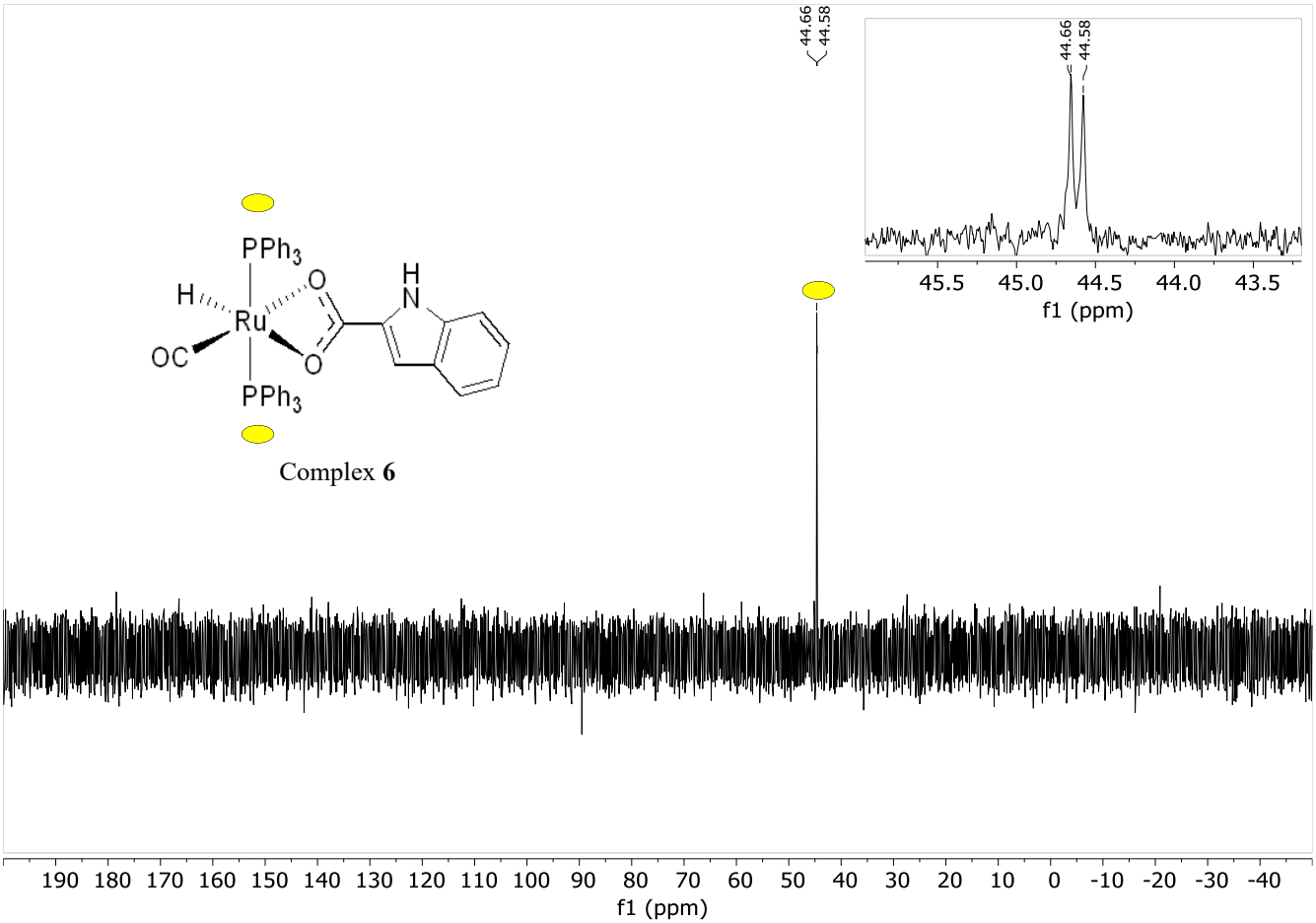

^{31}P-NMR of complex 6: In the spectrum, a doublet peak is observed for the two phosphorus atoms, which share the same chemical environment. The reason it appears as a doublet is due to coupling with the hydride coordinated to the Ruthenium.

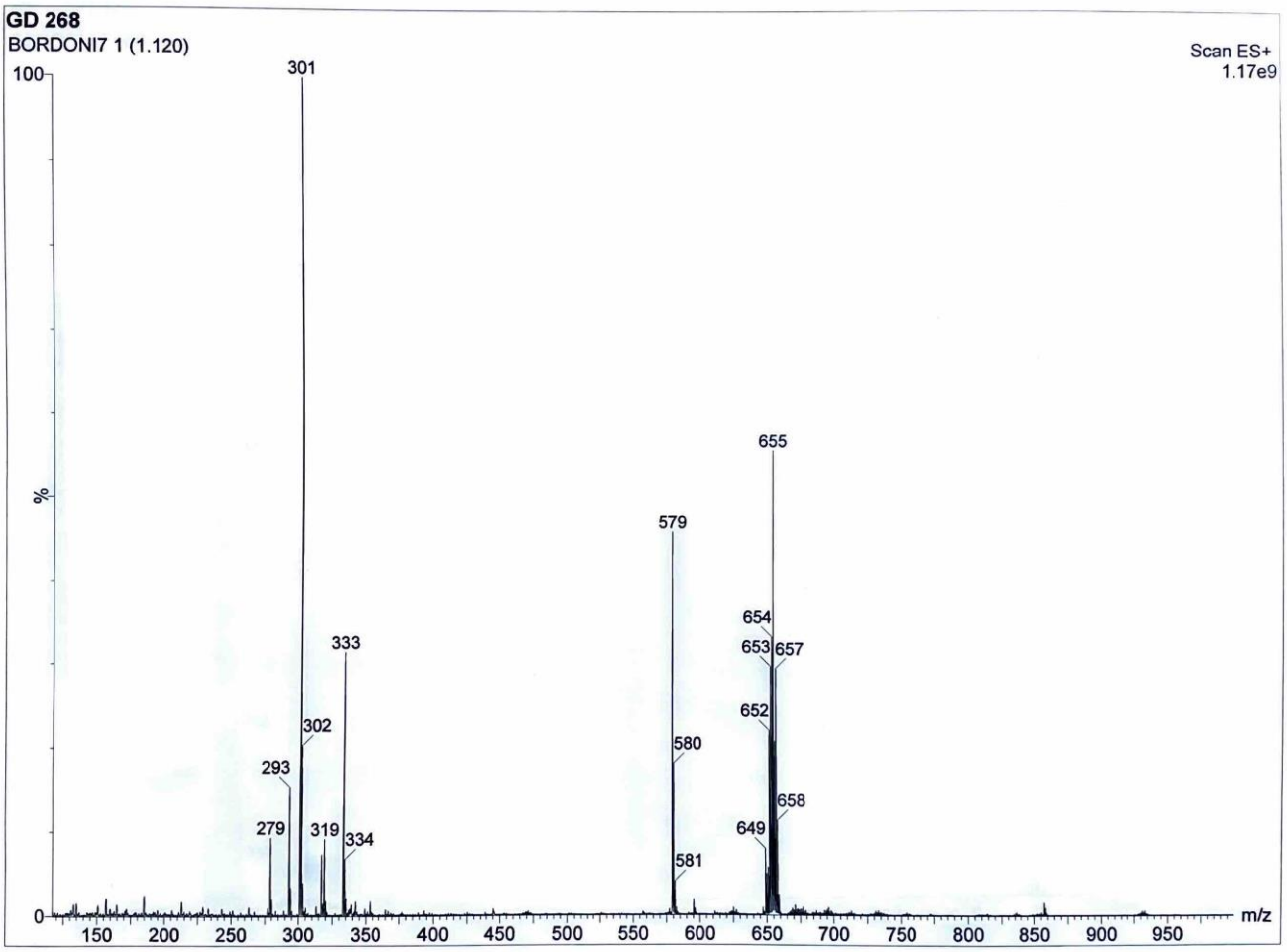
GD 268
BORDONI7 1 (1.120)
Scan ES+
1.17e9
100
%
0
301
579
655
654
653
657
333
652
302
580
293
658
649
279
319
334
581
150
200
250
300
350
400
450
500
550
600
650
700
750
800
850
900
950
m/z

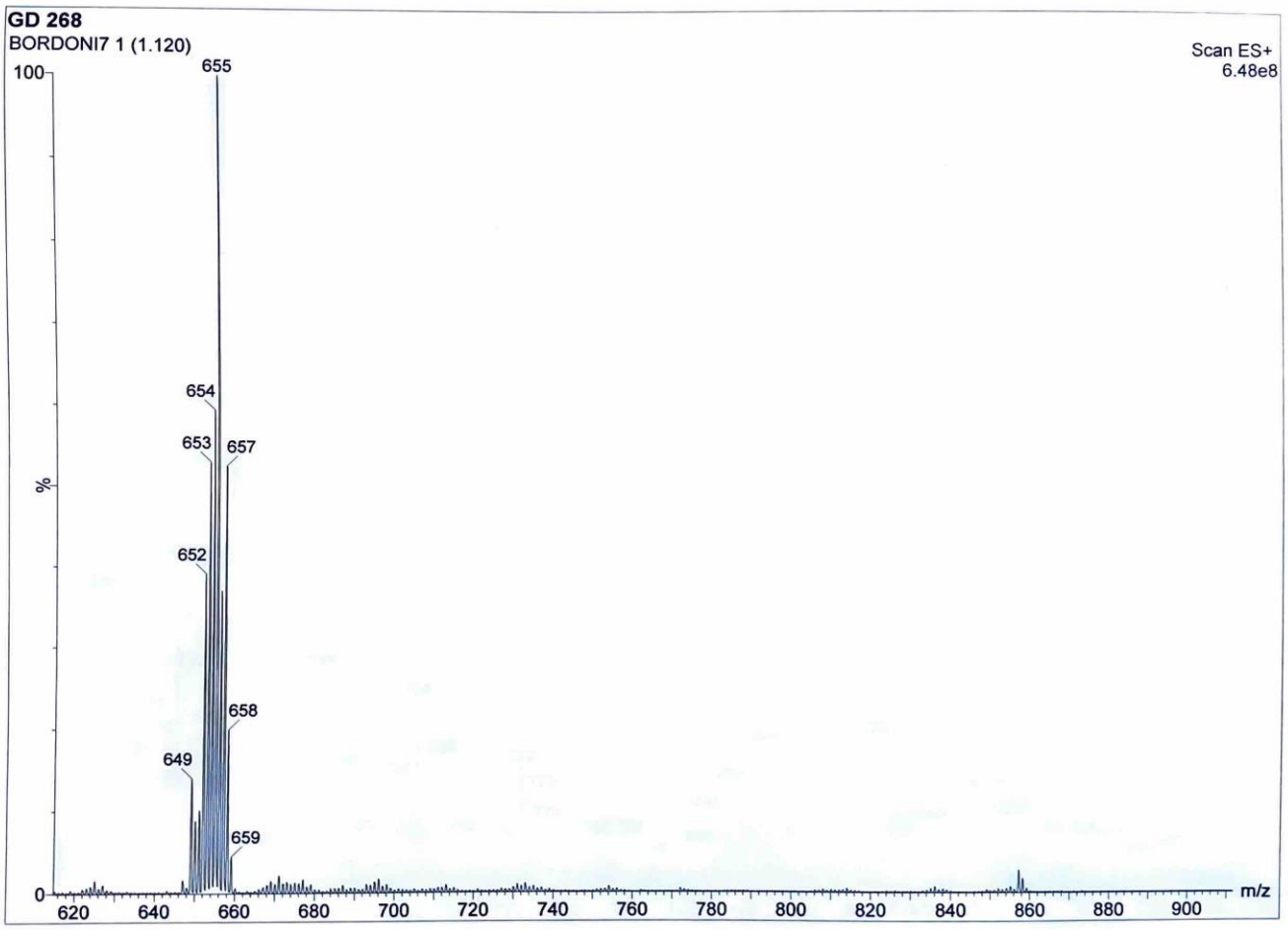
GD 268
BORDONI7 1 (1.120)
Scan ES+
6.48e8
100
%
0
655
654
653
657
652
658
649
659
620
640
660
680
700
720
740
760
780
800
820
840
860
880
900
m/z

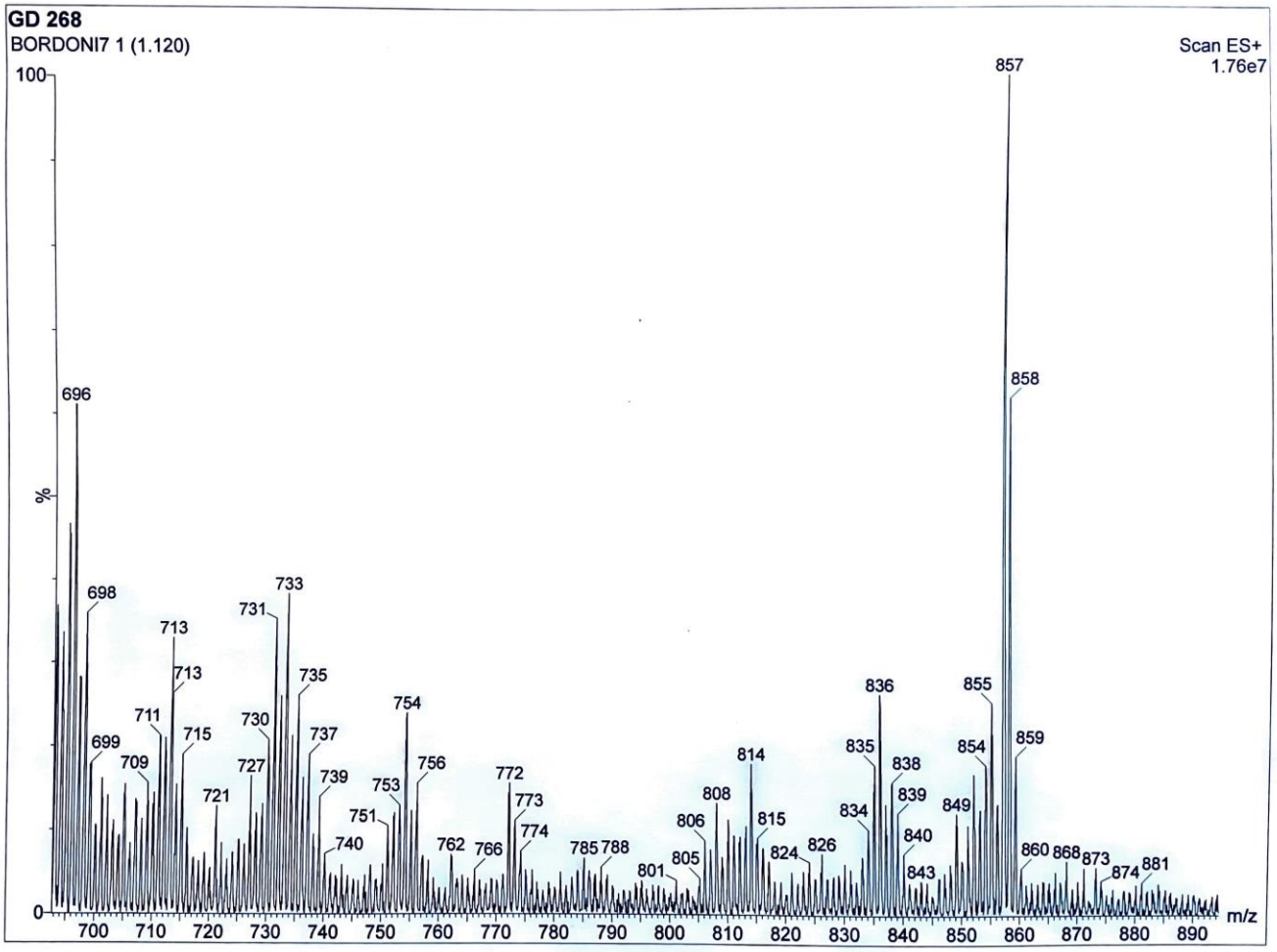

ESI-Mass of complex 6: [M+L]=815 (m/z), $[M-H]^+$ =814 (m/z), $[M-H+CH_3CN]^+$ =855(m/z), $[M-L+2CH_3CN]^+$ =737 (m/z), $[M-L+ CH_3CN]^+$ =696 (m/z), $[M-L]^+$ =655 (m/z).

The mass spectrum displays the expected signals for the loss of the Indole-2-carboxylate ligand, with a peak at m/z 655 $[M–L]^+$. Peaks at m/z 696 and 737 correspond to the subsequent incorporation of acetonitrile (MeCN). The peak at m/z 855 is attributed to the fragmentation of the hydride, accompanied by the addition of an acetonitrile molecule. Another peak at m/z 814 indicates the elimination of the hydride from the complex.

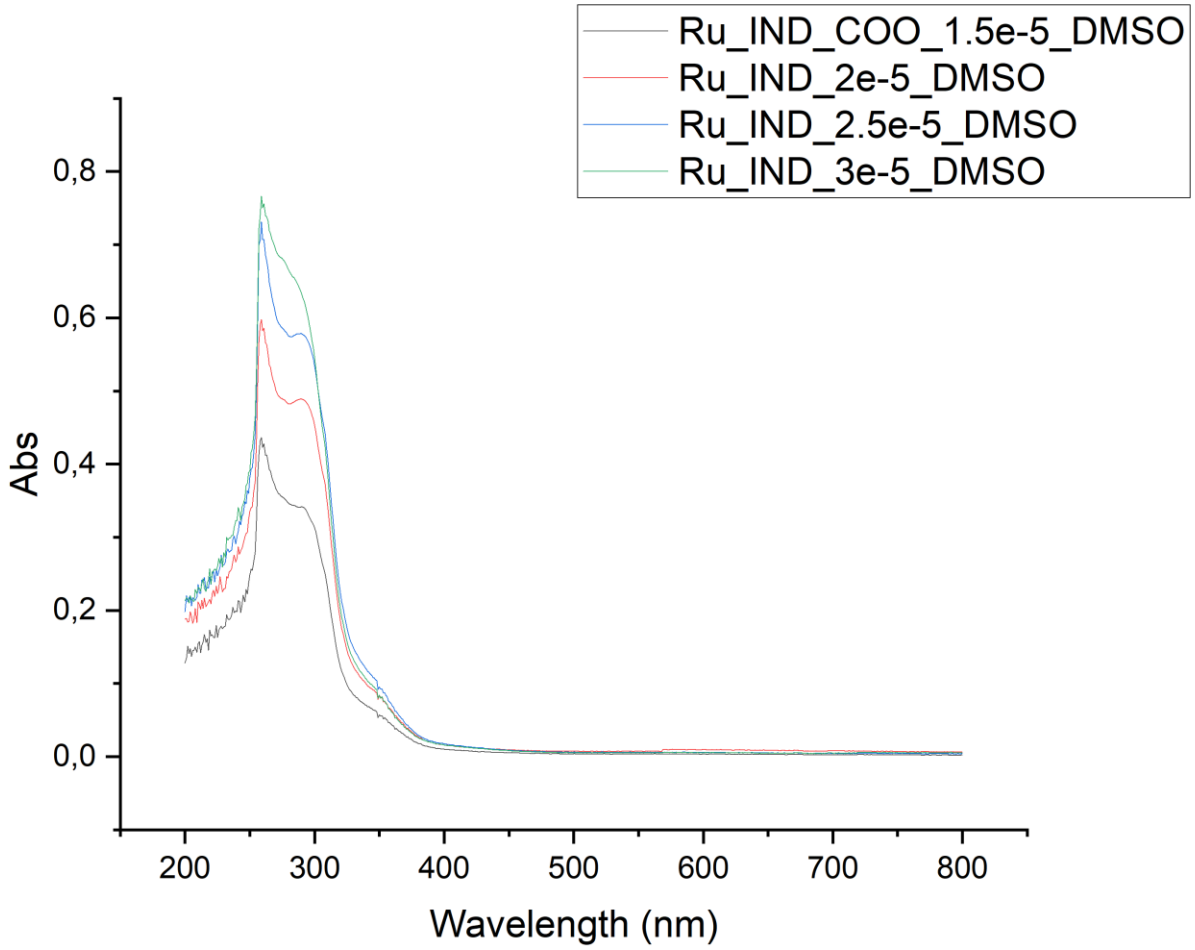

UV-Vis of complex 6: λ_{max}=259nm , Ɛ=11260

The absorption peak at 259 nm in the UV-Vis spectrum of complex **6** is attributed to a ligand-centered transition. To determine the molar extinction coefficient (Ɛ), four measurements were taken at varying concentrations of the complex in accordance with the Lambert-Beer law.

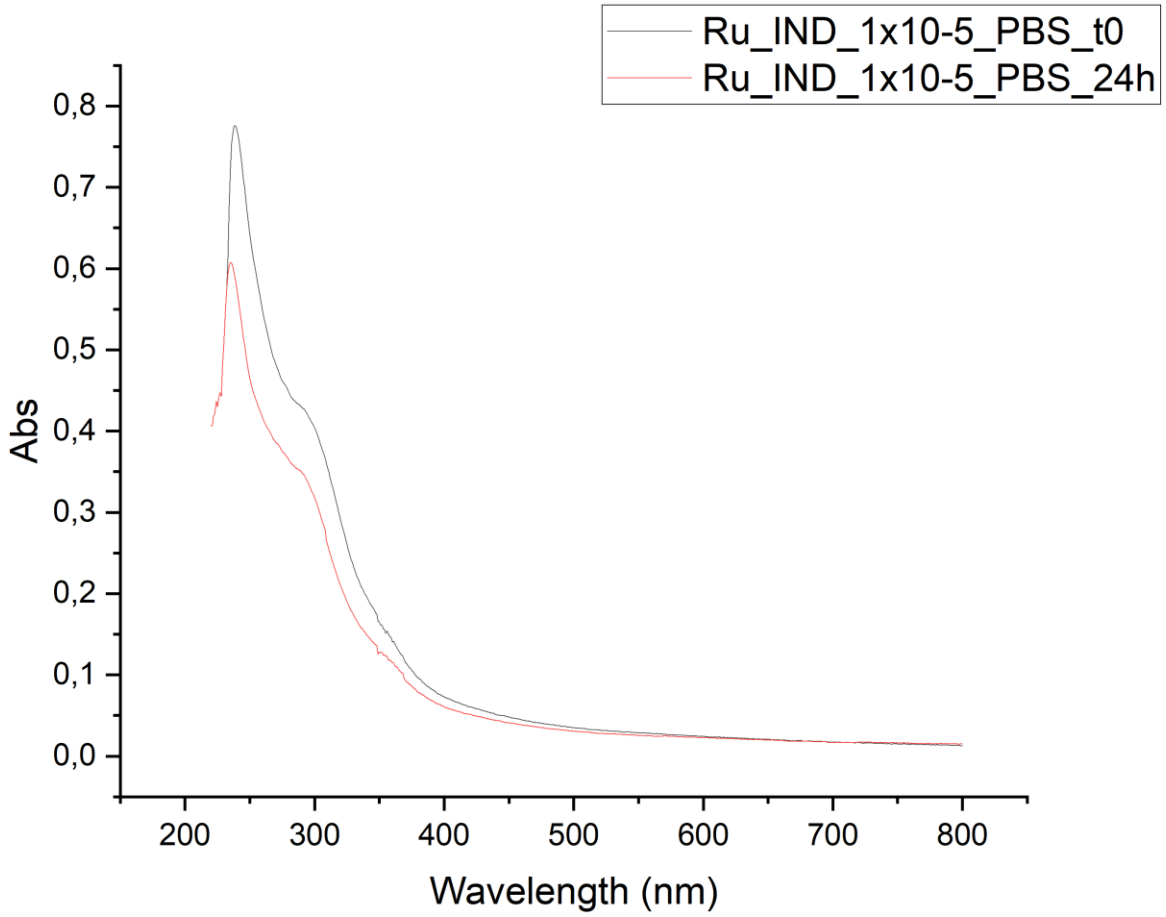

Stability of complex 6 for 24 h in PBS at 37 ˚C: To assess the stability of the complexes at physiological pH, UV-Vis spectra were recorded in a phosphate buffer solution (PBS-5% DMSO) over 24 hours. No wavelength shifts were observed, indicating the complexes retained their structural integrity during the experiment. However, a reduction in band intensity was noted after 24 hours, suggesting a decrease in complex concentration, potentially due to partial precipitation over time.

- **Characterization of Complex 7 [Ru(NCMe)(CO)(PPh_3)$_2$(K^2(N,O)-Carboxyindole)]**

Complex **7** is synthesized by refluxing Complex **6** in Acetonitrile under Argon atmosphere.

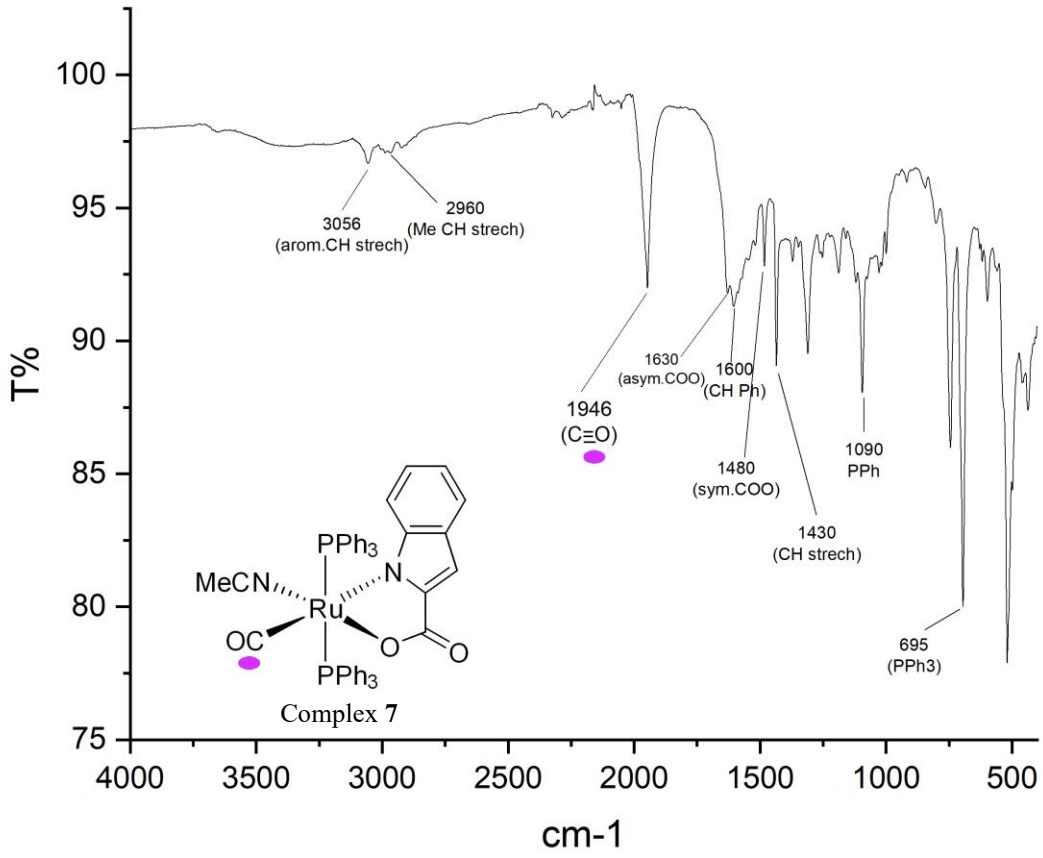

Complex **7**

IR of Complex 7: As indicated in the spectrum, the CH stretch of the methyl group in acetonitrile coordinated to Ruthenium appears at 2960 cm^{-1}, and the CO peak has shifted from 1931 cm^{-1} to 1946 cm^{-1}. Upon coordination of acetonitrile to Ruthenium, indole-2-carboxylate binds through N,O instead of O,O.

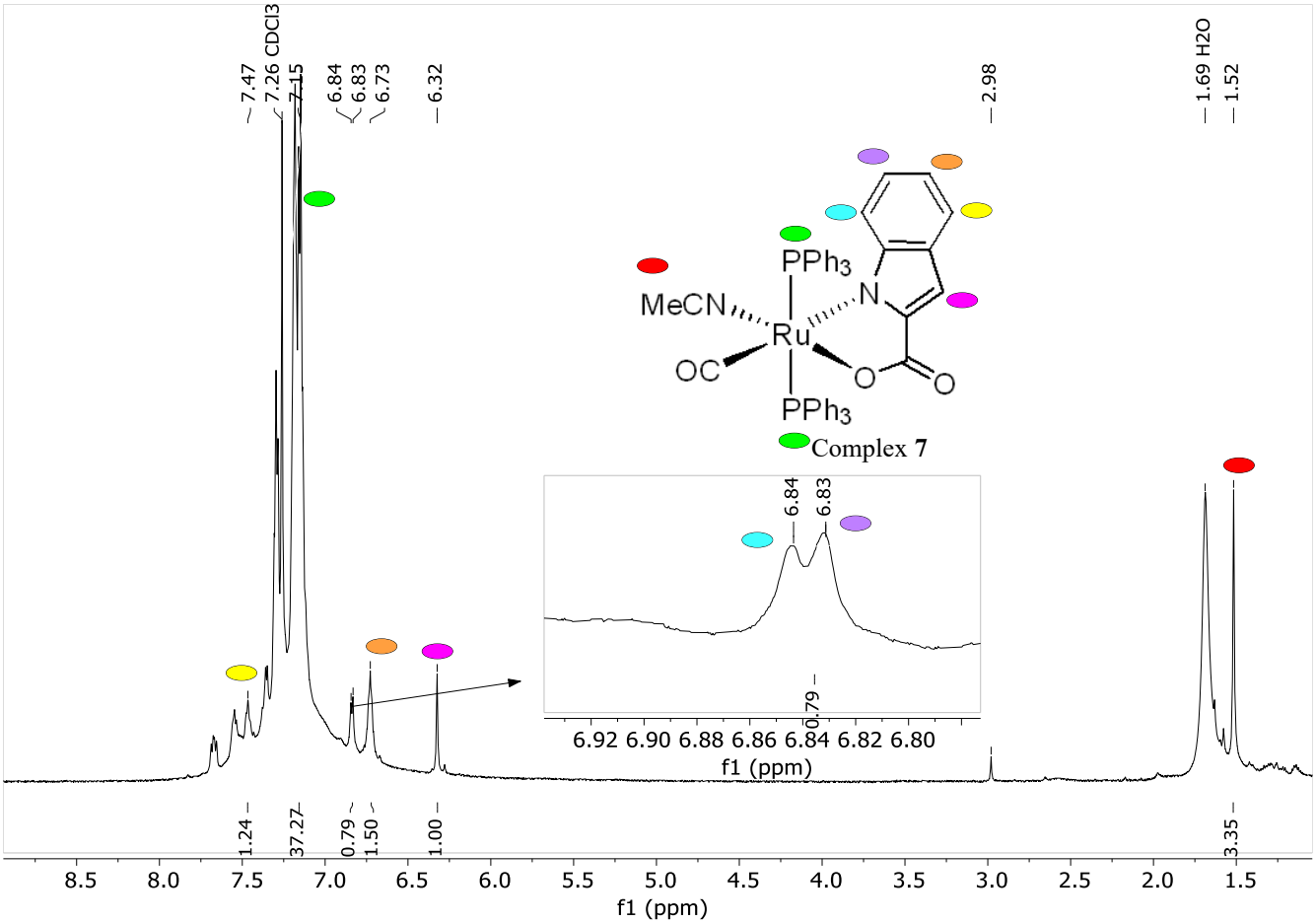

^{1}H-NMR of Complex 7: This spectrum illustrates the 5 distinct proton signals in indole-2-carboxylate coordinated to Ruthenium by N,O site, with their assignments based on nearby atoms. The signals of the hydride bonded to the nitrogen of the indole disappears after the coordination of MeCN.

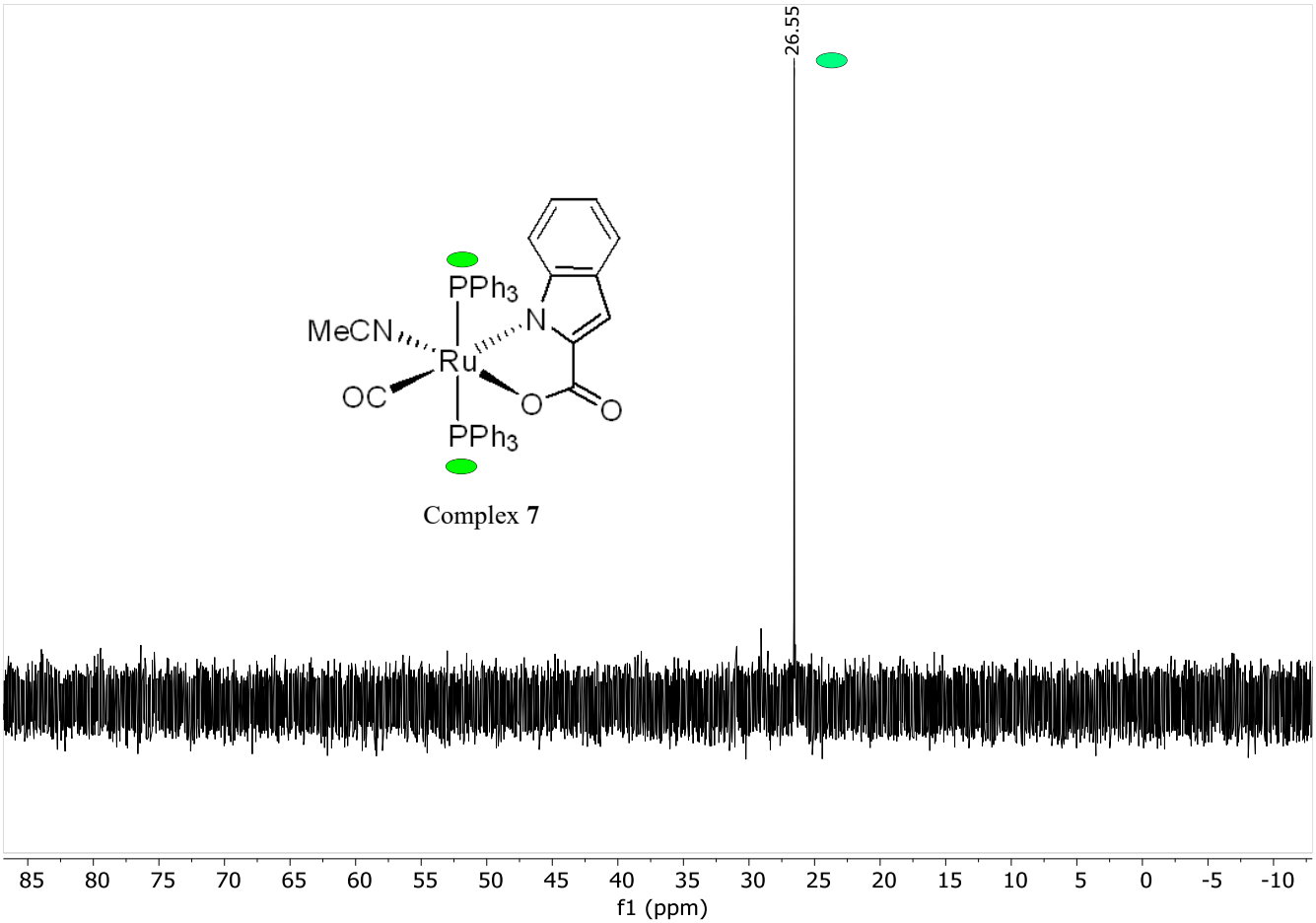

Complex **7**

^{31}P-NMR of complex 7: In the spectrum, a singlet peak is observed for the two phosphorus atoms, which are in the same chemical environment confirming the octahedral geometry of the complex.

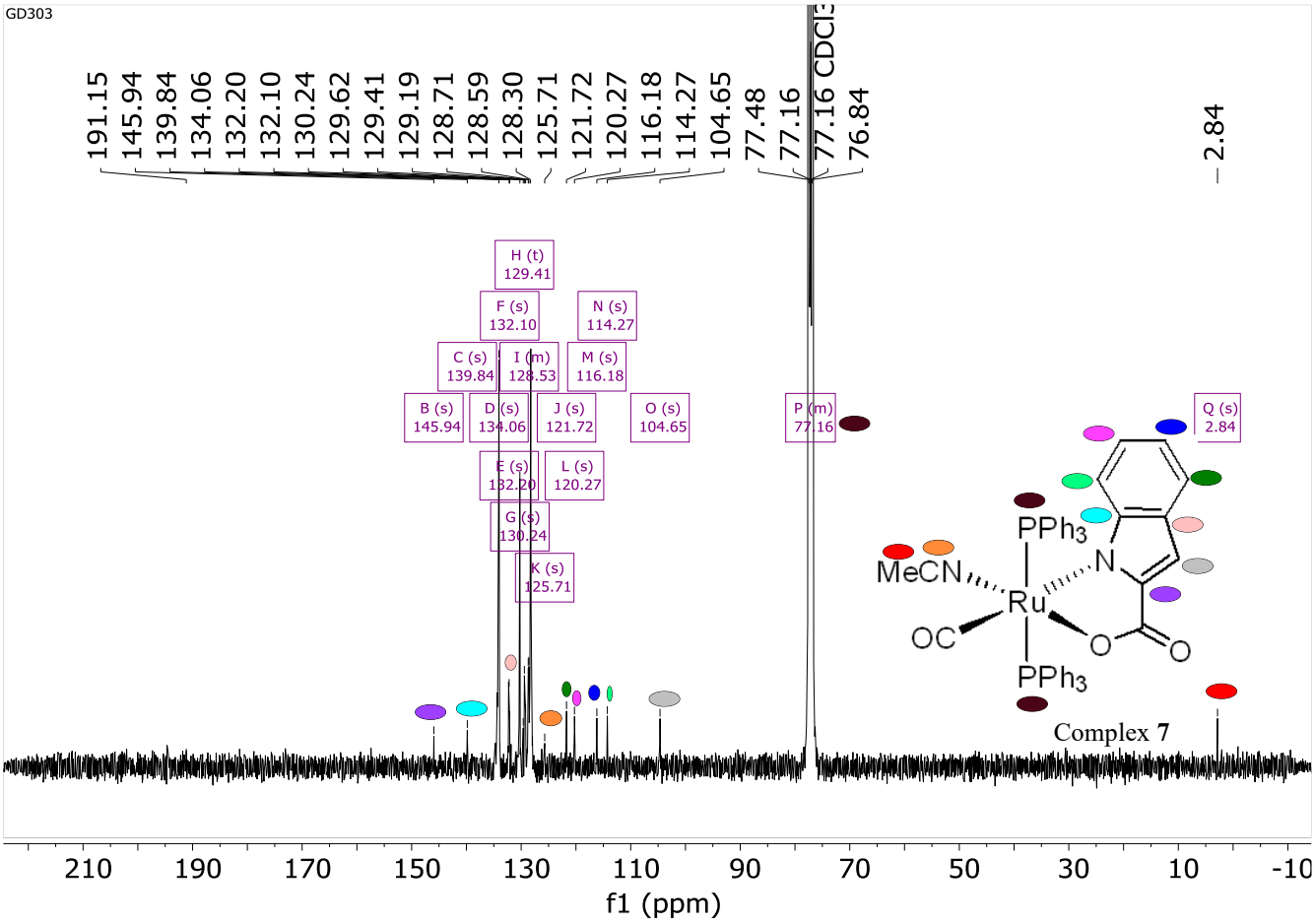

^{13}C-NMR of complex 7: As shown in this spectrum, the intensity of some peaks is very low, making it difficult to distinguish them from the noise. The different types of indole carbons have been assigned. The signals related to carbons of the methyl group in acetonitrile appearing downfield marked in red. The multiplet peaks marked in brown are attributed to the phenyl's carbons of triphenyl phosphine groups. The C≡O peak is not assigned here due to its low intensity, which causes it to be lost in the noise.

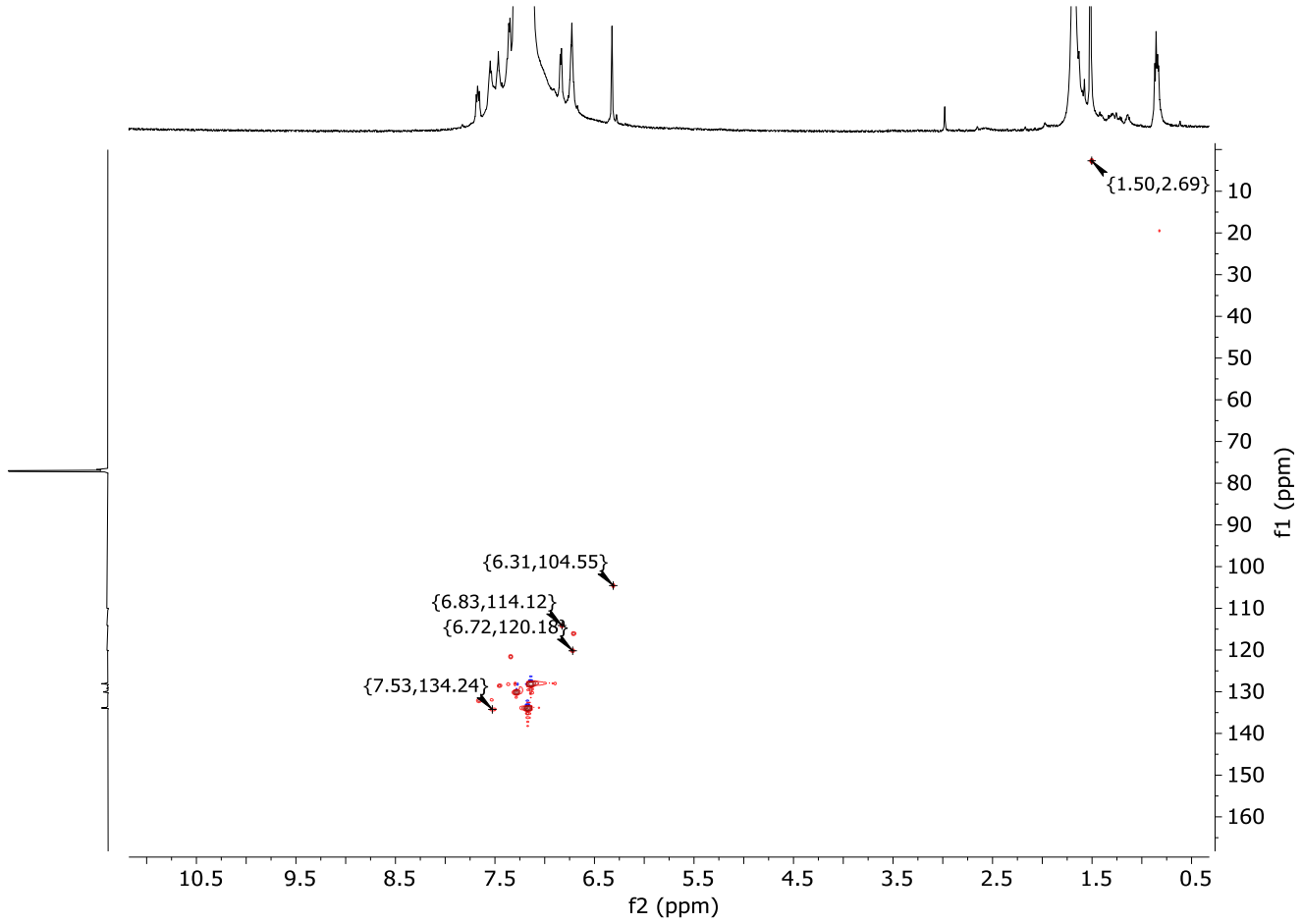

Heterocorrelated NMR spectrum {^{13}C,^{1}H} HSQC of complex 7

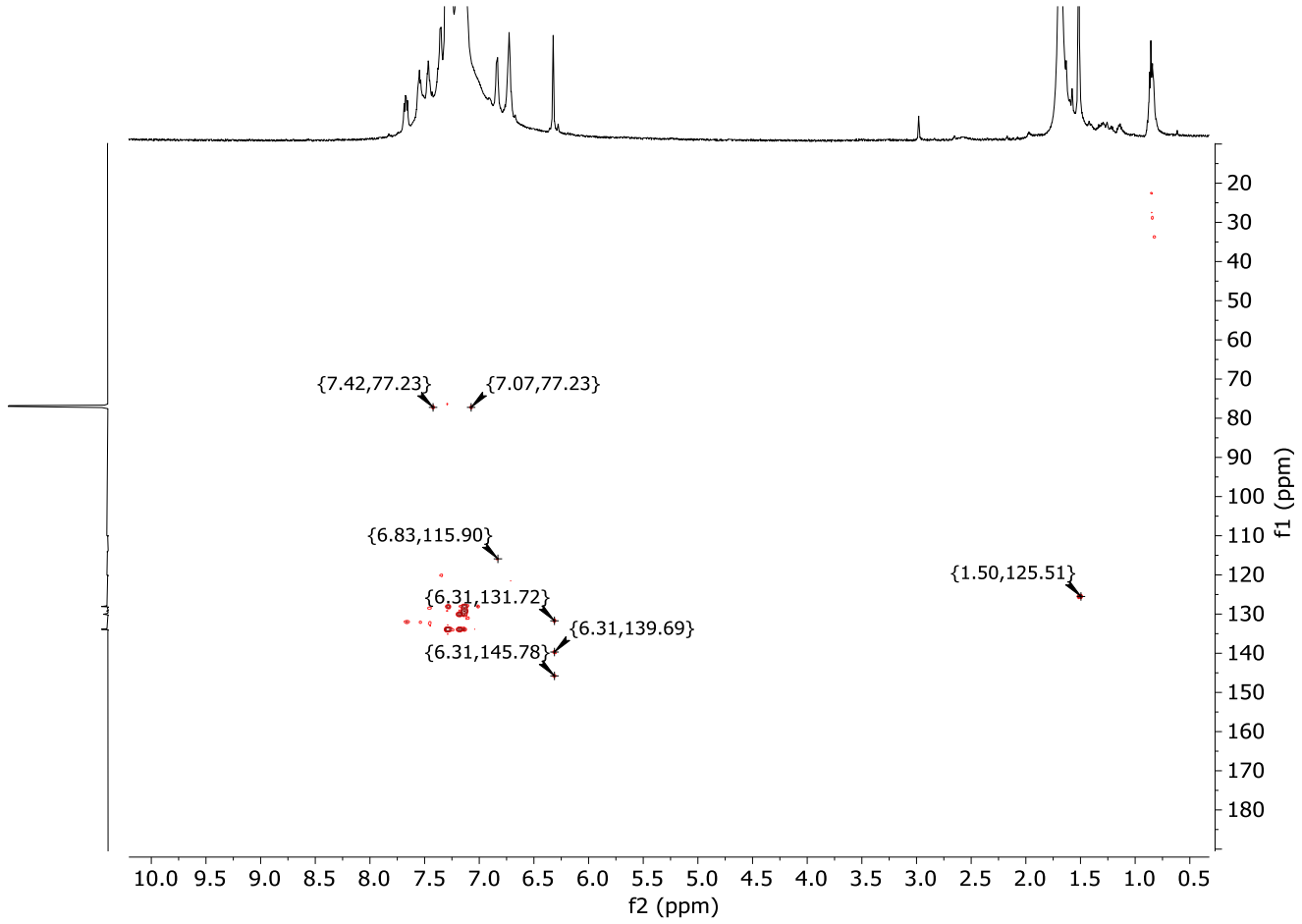

Heterocorrelated NMR spectrum {^{13}C,^{1}H} HMBC of complex 7

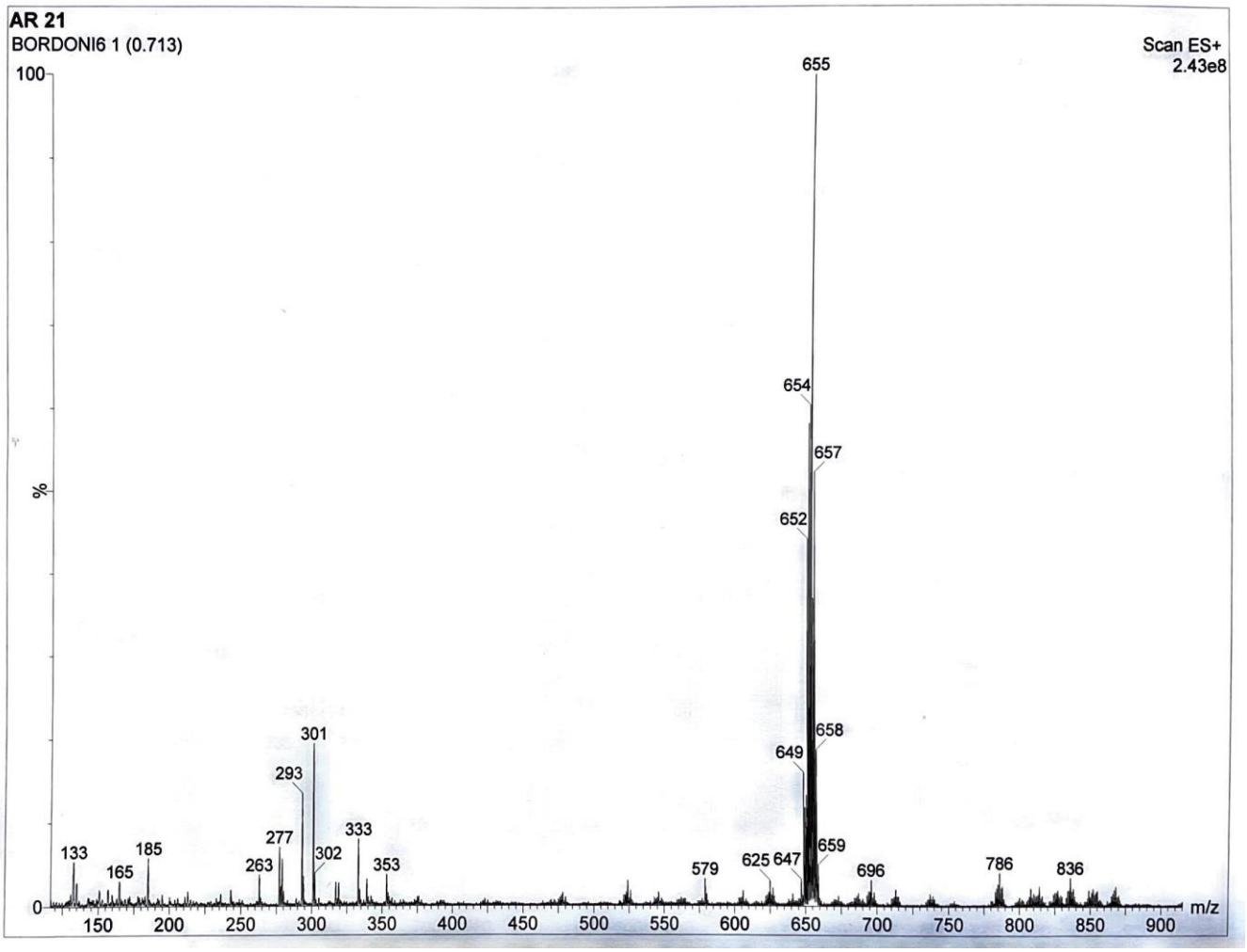
AR 21
BORDONI6 1 (0.713)
Scan ES+
2.43e8
100
%
0
655
654
657
652
658
649
301
293
333
277
302
263
353
133
185
165
579
625
647
659
696
786
836
150
200
250
300
350
400
450
500
550
600
650
700
750
800
850
900
m/z

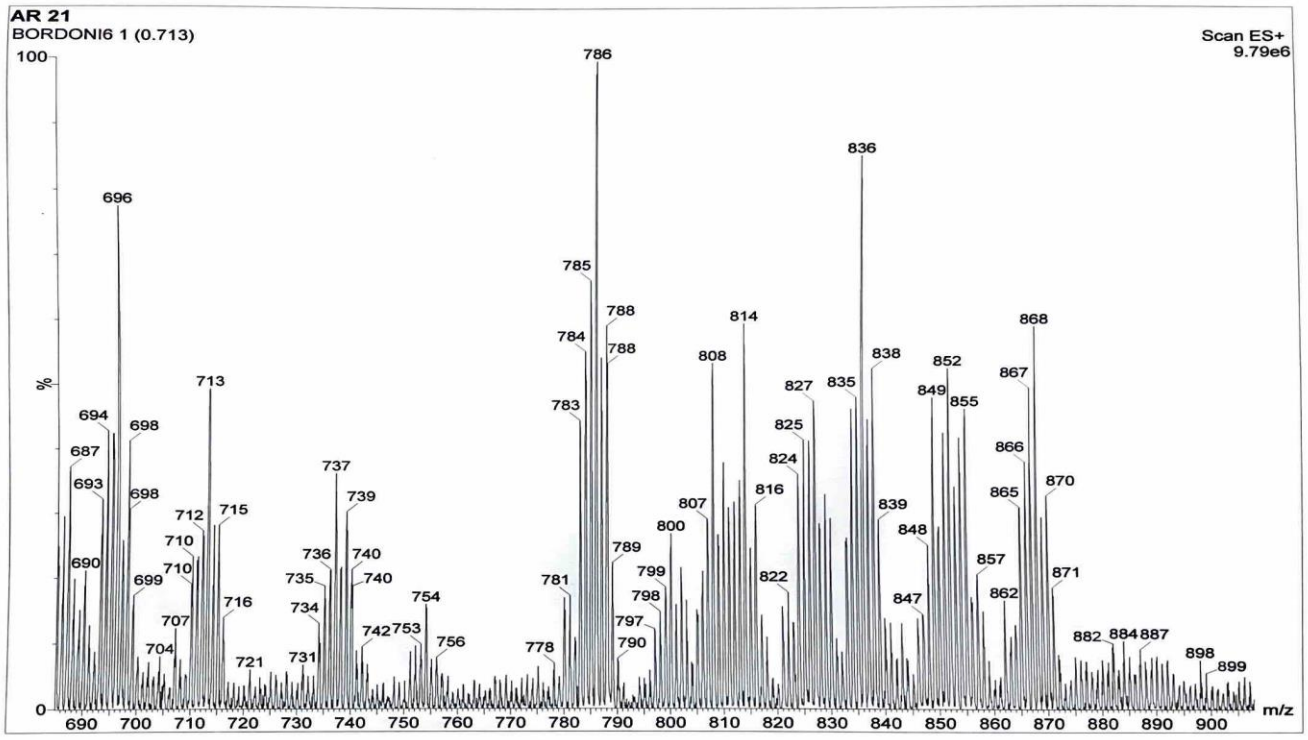

ESI-Mass of Complex 7: [M]=854 (m/z), $[M+H]^+$ =855(m/z), $[M-CH_3CN+H]^+$ =814 (m/z), $[M-L-CO+H]^+$ =786 (m/z), $[M-CO+H]^+$ =827 (m/z), $[M-L+H]^+$ =696 (m/z), $[M-L+CH_3CN+H]^+$ =737 (m/z), $[M-L-CH_3CN]$=655 (m/z).

The mass spectrum displays the expected signals for the loss of the Indole-2-carboxylate ligand, with a peak at m/z 655 [M–L–CH3CN]+. Peaks at m/z 696 and 737 correspond to the incorporation of acetonitrile (MeCN). The peak at m/z 827 is associated with the fragmentation of CO and the exchange for a hydride, while in addition to that dissociation of the inodole-2-carboxylate ligand results in a peak at m/z 786.

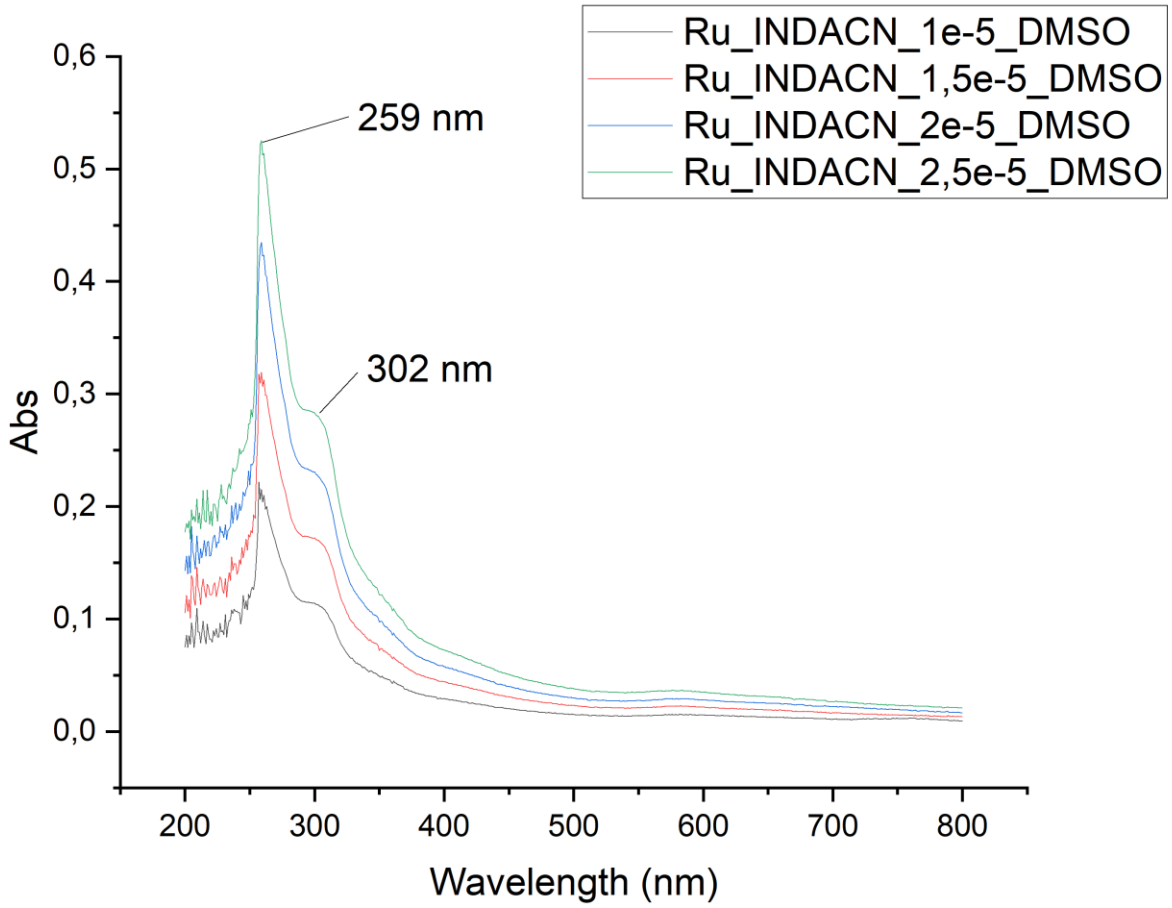

UV-Vis of complex 7: λ_{max}=259nm , Ɛ=20560

The absorption peaks at 259 nm and 302 nm in the UV-Vis spectrum of complex **7** are attributed to ligand-centered transitions. To calculate the molar extinction coefficient (Ɛ), four measurements were performed at different concentrations of the complex, following the Lambert-Beer law.

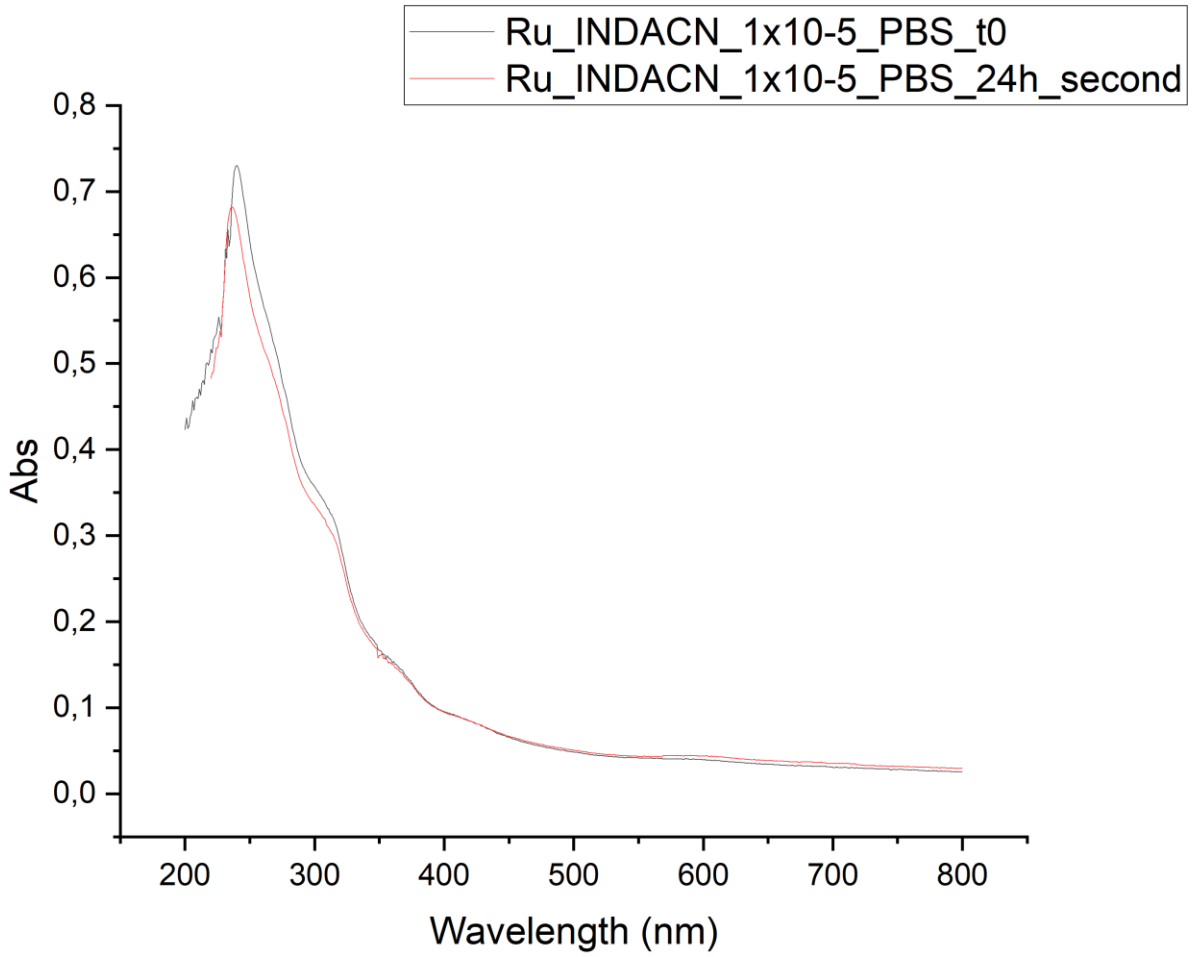

Stability of complex 7 for 24 h in PBS at 37 ˚C: To evaluate the stability of the complexes at physiological pH, UV-Vis spectra were recorded in a phosphate buffer solution (PBS-5% DMSO) over a 24-hour period. No shifts in wavelength were detected, indicating that the complexes maintained their structural integrity throughout the experiment. However, a decrease in band intensity was observed after 24 hours, implying a reduction in the concentration of the complex, likely caused by partial precipitation over time.

- **Characterization of Complex 9 [Ru(4-Aminopyridine)(CO)(PPh_3)$_2$(K^2(N,O)-Carboxyindole)] and Complex 5 [Ru(4-Aminopyridine)(CO)(PPh_3)$_2$(K^2(N,O)-Carboxypyrrole)]**

Complex **9** was synthesized by adding 4-Aminopyridine to Complex **7** and refluxing them in 1,4-Dimethoxyethane. Complex **5** is synthesized by refluxing Complex **3** and 4-Aminopyridine in 1,4-Dimethoxyethane.

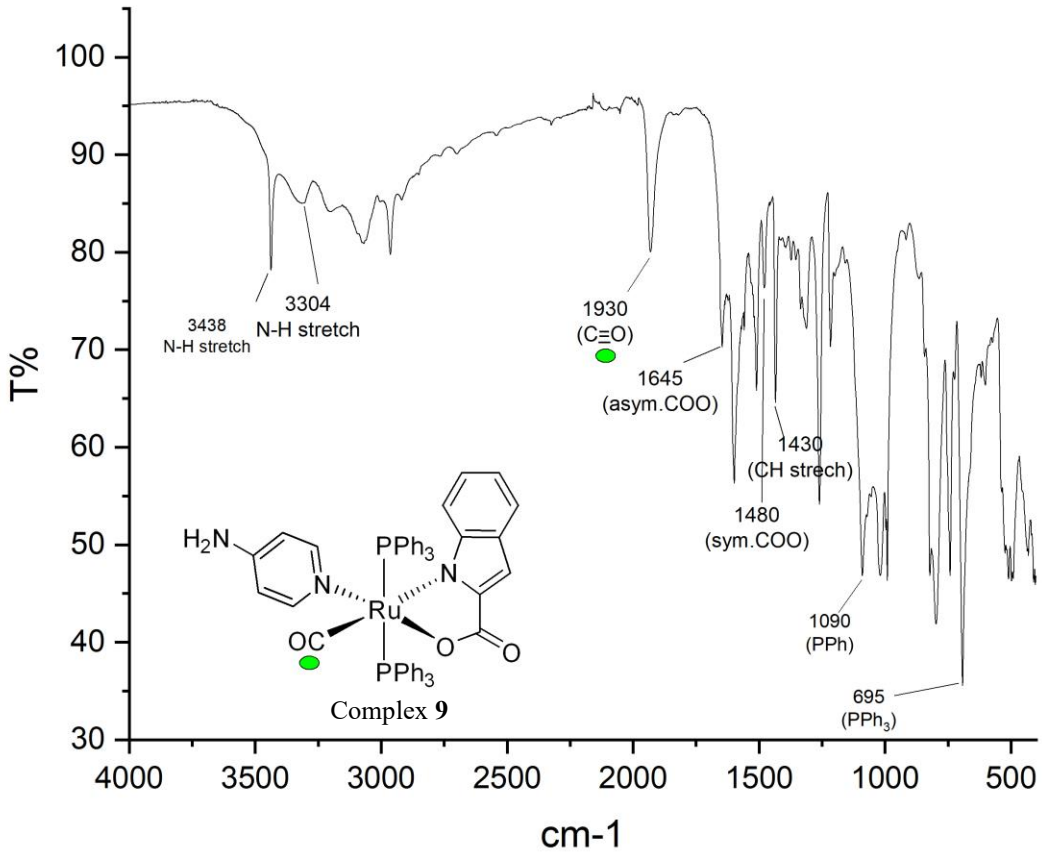

IR of Complex 9: The spectrum shows a sharp CO peak at 1930 cm^{-1}, representing a notable shift from the CO peak of the reactant (complex **7**) at 1944 cm^{-1}.

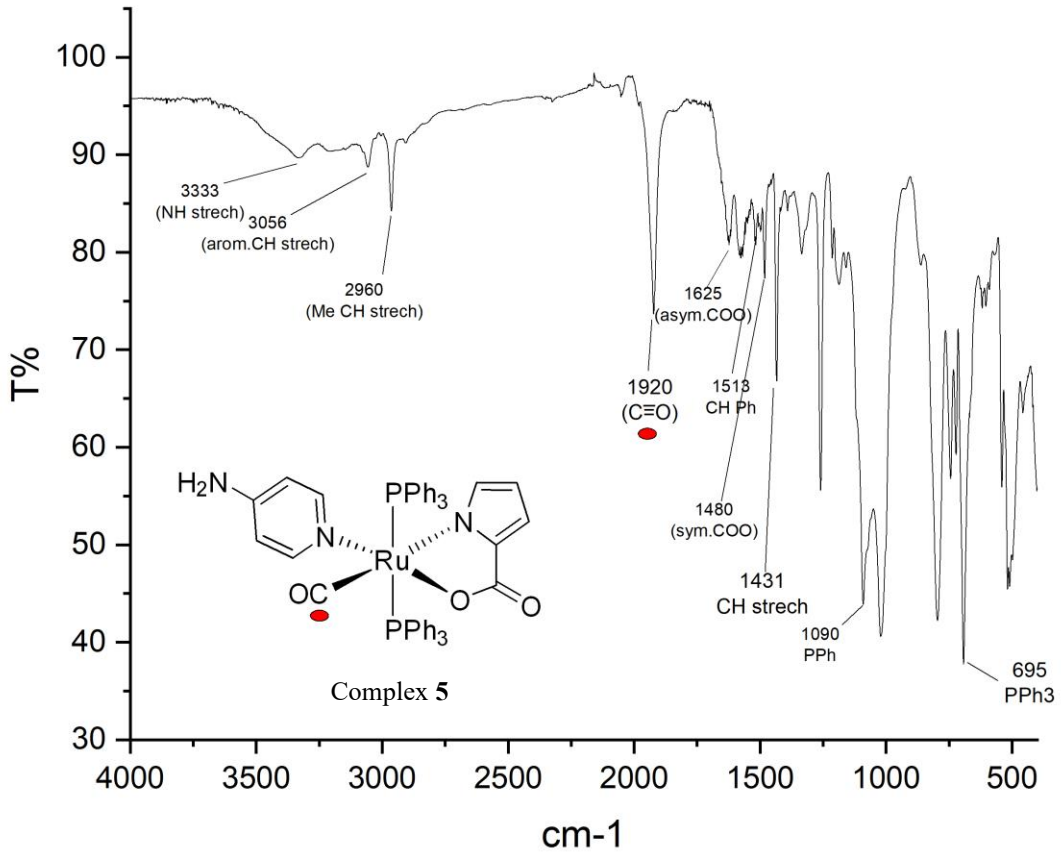

Complex **5**

IR of Complex 5: The spectrum shows a CO peak at 1920 cm^{-1}, representing a notable shift from the CO peak of the reactant (complex **3**), which is at 1944 cm^{-1}.

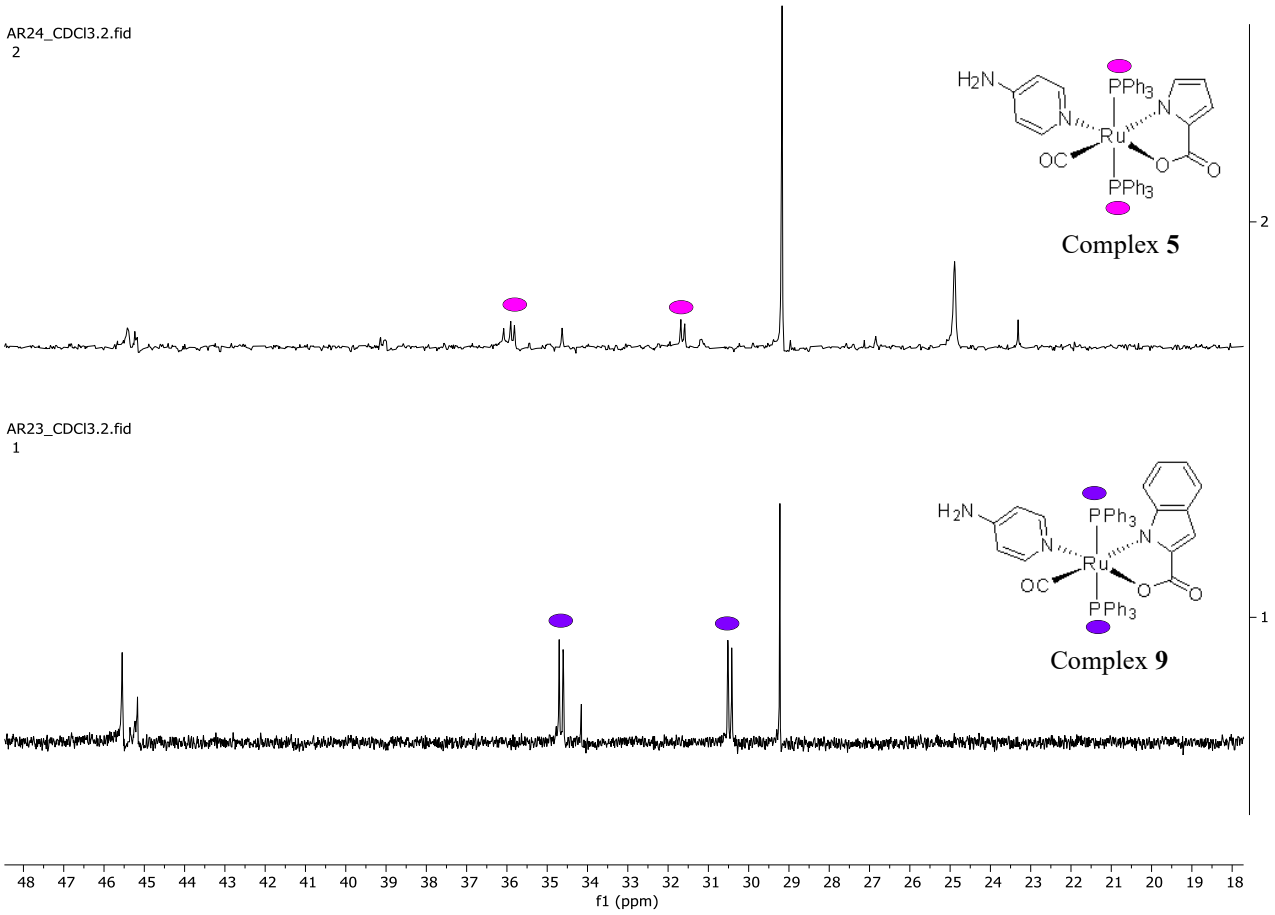

^{31}P-NMR of Complex 5 and Complex 9: In the spectrum of Complex **9** (bottom spectrum), the two doublet peaks correspond to the product. due to steric hindrance, the two phosphorus atoms experience different chemical environments. As a result, the two phosphorus atoms are coupled to each other and they appear as doublets. In the upper spectrum that is for complex **5**, product's peaks are two doublets, observed at 35.99 and 31.64 ppm which are different from the peaks of complex **9**. There are many other side products peaks but by comparison of two spectrums we can confirm the presence of pyrrole products. The peaks at 29.22 ppm in both spectrums are related to triphenylphosphine oxide.

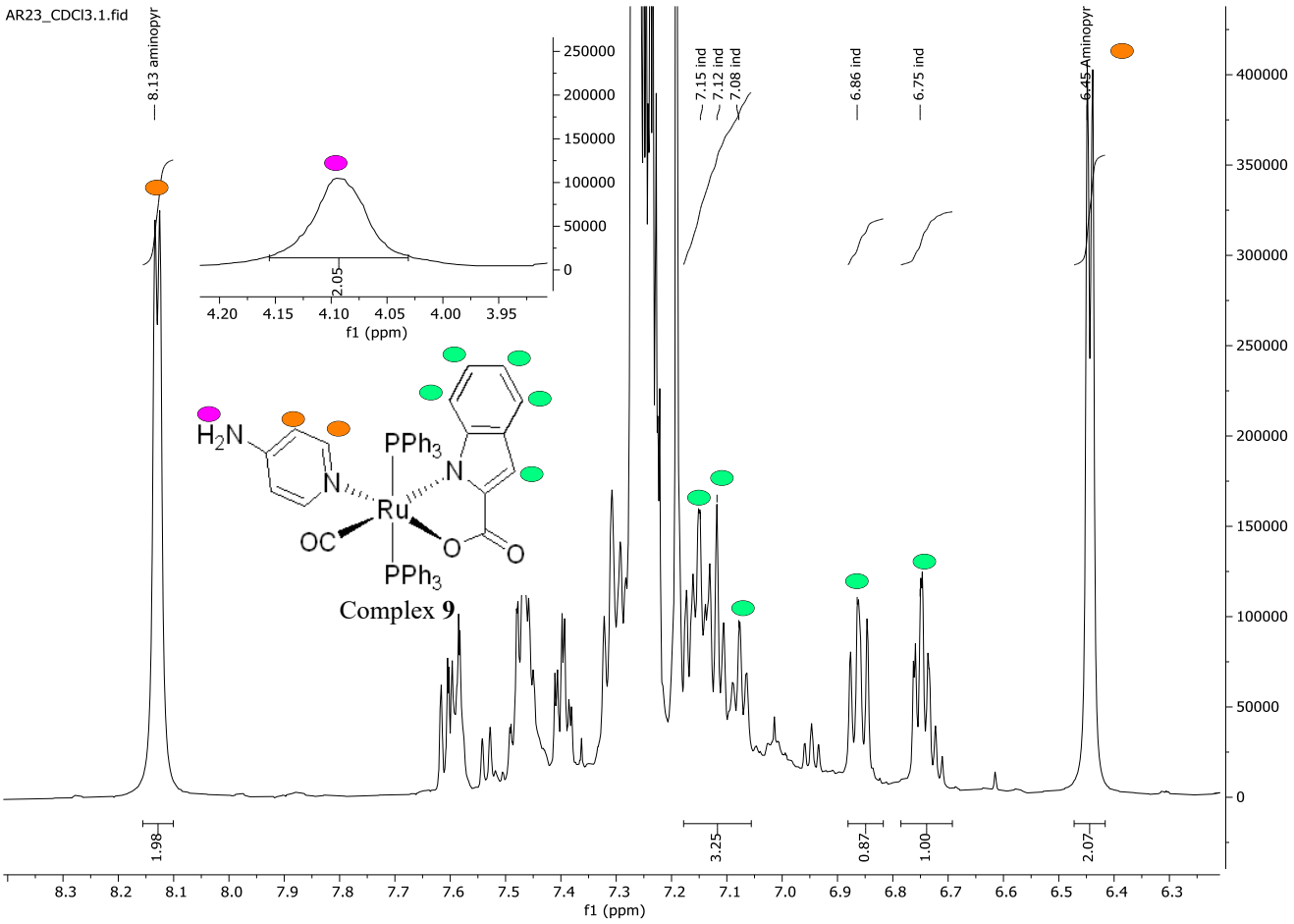

^{1}H-NMR of Complex 9: As seen in the spectrum, two doublets with an integration of 2 correspond to 4-aminopyridine successfully coordinated to the complex. The two hydrogens of the amine group, with an integration of 2, are marked in pink. The other peaks, marked in green, represent the five hydrogens of indole.

- **Characterization of Complex 10 [Ru(DMSO)(CO)(PPh_3)$_2$(K^2(N,O)-Carboxyindole)]**

Complex **10** was synthesized by adding 4-Aminopyridine to Complex **7** and refluxing them in toluene.

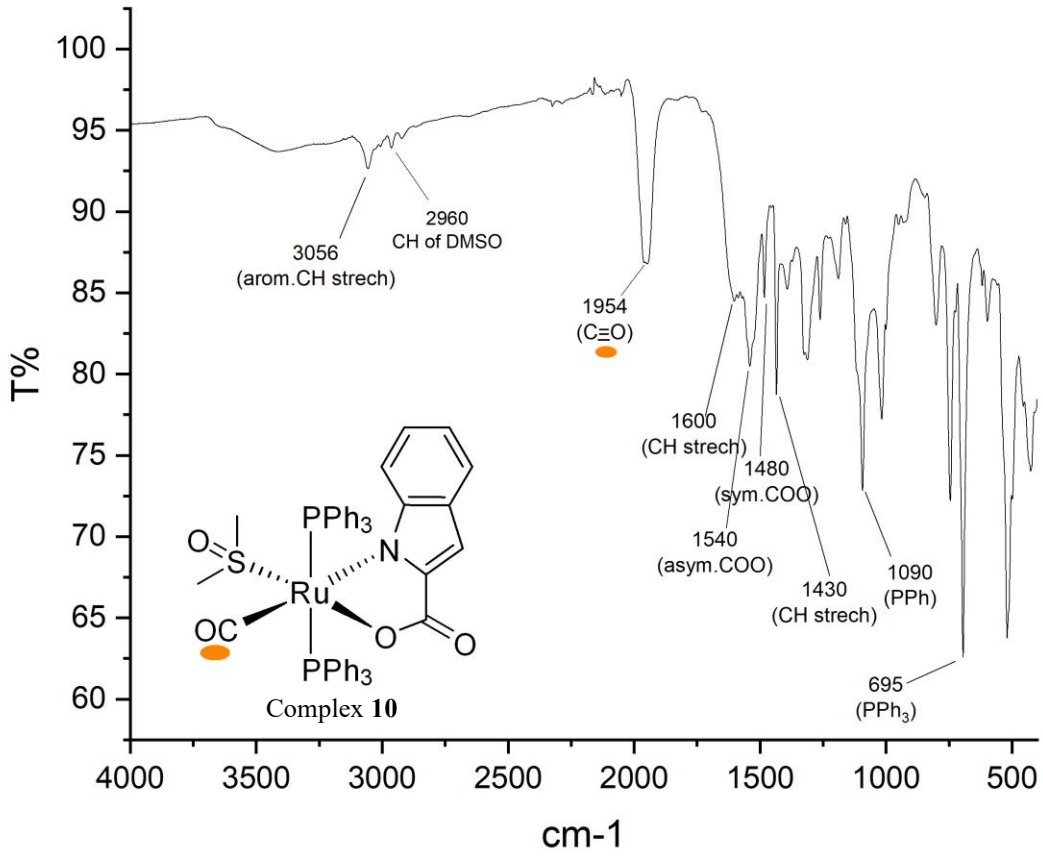

Complex **10**

IR of Complex 10: The spectrum reveals a CO peak at 1954 cm^{-1}, indicating a significant shift from the CO peak of the reactant (complex **7**), which appears at 1944 cm^{-1}. C-H stretching of aliphatic methyl groups of DMSO can be observed.

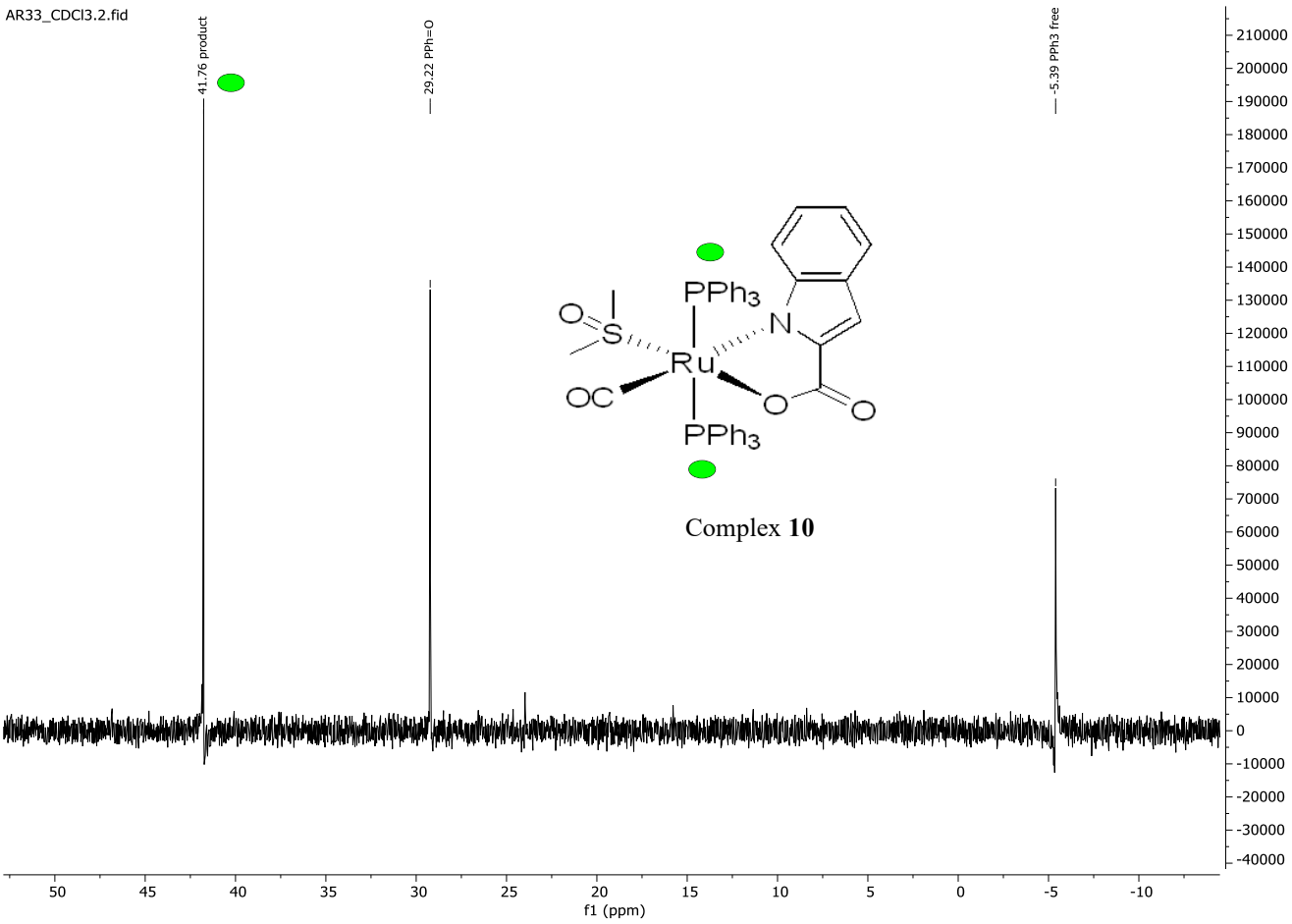

Complex **10**

^{31}P-NMR of Complex 10: The product peak is observed at 41.76 ppm, and since both phosphorus atoms share the same chemical environment, it appears as a single sharp peak. The other two peaks correspond to triphenylphosphine oxide and free triphenylphosphine.

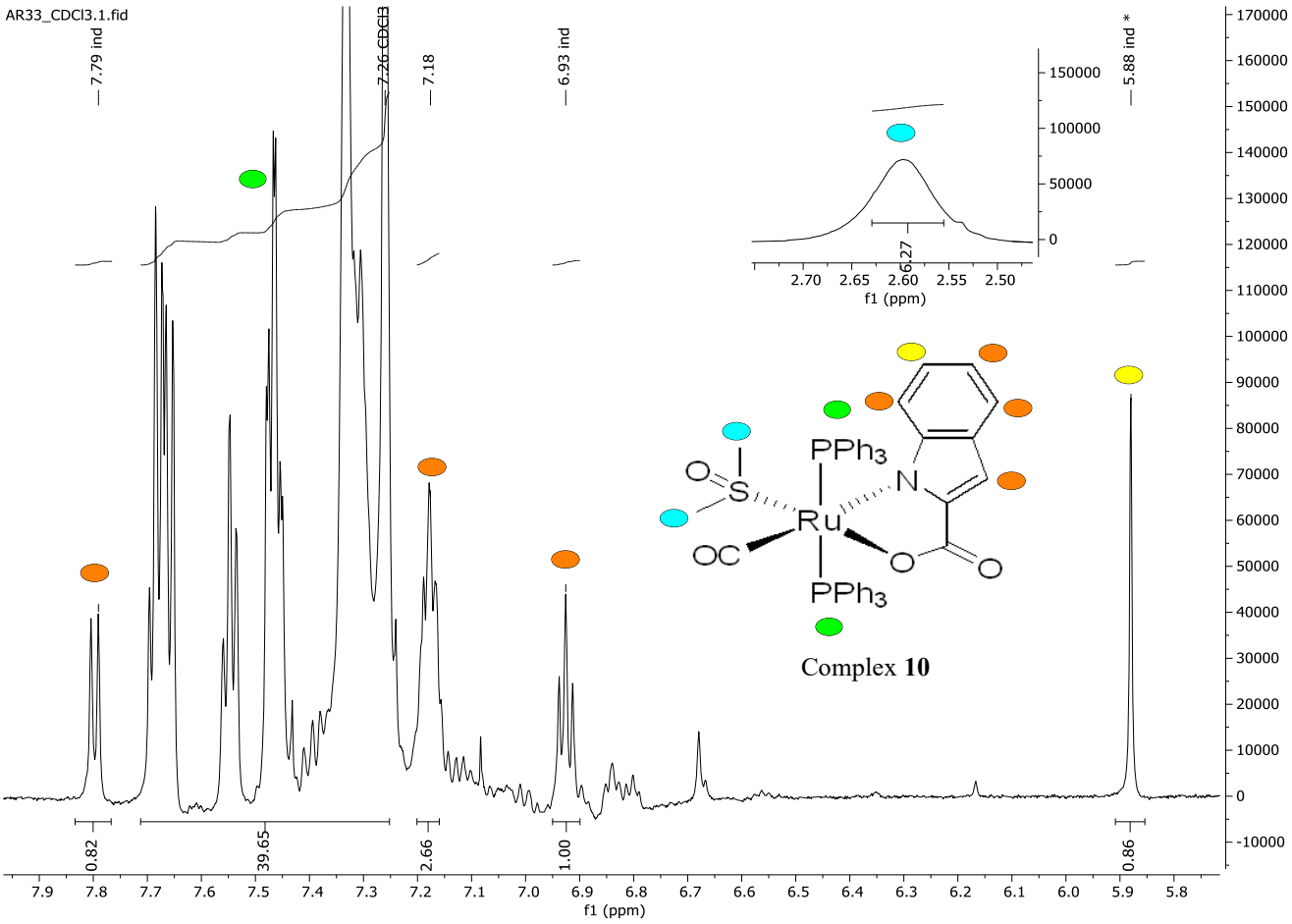

[1]H-NMR of Complex 10: The multiplet peak of the triphenylphosphines coordinated to Ruthenium is marked in green, with an integration of around 40. Peaks corresponding to the hydrogens of indole are marked in orange, while the peak at 5.88 ppm, marked in yellow, represents the least decoupled hydrogen. The peak at 7.18 ppm is believed to correspond to two superimposed indole hydrogens, with an integration of 2. The peak at 2.60 ppm, integrating about 6, is attributed to the six hydrogens of the coordinated DMSO.

Conclusion

The synthesized Ruthenium complexes presented in this work demonstrate the ability to form stable organometallic compounds with various ligands, including pyrrole, indole, and solvato species as coordinated acetonitrile and DMSO. The research highlights the conversion from K^2-(O,O) to K^2-(N,O) upon incorporating the acetonitrile solvent as ligand, which affects electronic properties and potential reactivity of the complexes.

By characterization through, including IR, NMR, UV-Vis spectroscopy, and ESI-mass spectrometry, the distinct structural differences between the synthesized complexes were elucidated. The coordination alterations due to the role of solvato ligands were explored, showing how they can influence the stability and the solubility of complexes, making them as viable candidates for further studies in medicinal chemistry, particularly for their potential anticancer and/or antibacterial properties.

Overall, this work provides insight into the structural versatility and reactivity of Ruthenium-based complexes, emphasizing their potential ability towards application in drug design.

Experimental part

- **Synthesis of Complex 1 [$Ru(H)_2(CO)(PPh_3)_3$] as precursor**

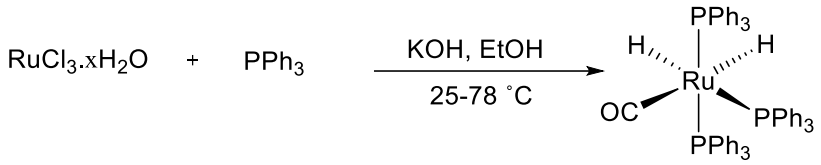

Complex **1**

	Molar Mass ($g.mol^{-1}$)	**Mass (mg)**	**Volume (mL)**	**mMol (mmol)**	**Yield (%)**
$RuCl_3.xH_2O$	**207.43**	**1000**	**-**	**4.821**	**-**
PPh_3	**262.29**	**4000**	**-**	**15.250**	**-**
KOH	**50.10**	**2140**	**-**	**42.714**	**-**
EtOH	**-**	**-**	**100**	**-**	**-**
[$Ru(H)_2(CO)(PPh_3)_3$]	**917.97**	**3766**	**-**	**4.102**	**85**

$RuCl_3.xH_2O$ is dissolved in absolute ethanol under argon atmosphere and is heated to reflux, then PPh_3 is added and the mixture remained under reflux for 1 hour. A dark brown suspension is achieved. It is cooled down to room temperature and then KOH is added. The mixture was initially agitated at room temperature for 1 hour, followed by heating at 50–60 °C for another hour, during which the dark brown reaction mixture changed first to dark green and then to yellow. It was then vigorously stirred under reflux for 10 hours. Once the mixture cooled to room temperature, the precipitate was filtered in air, washed with ethanol (2 × 20 mL), deionized water (3 × 20 mL), and ethanol again (3 × 20 mL), then dried under vacuum. obtained product is a pale yellowish microcrystalline solid.[84]

The product is characterized by:

^{1}H NMR (benzene-d6, 25 °C): δ 7.6-6.8 (m, 45H, PPh3), -6.5 (tdd, 1H, J = 31, 15, and 6 Hz, Ru-H trans to C), -8.3 (dtd, 1H, J = 74, 29, and 6 Hz, Ru-H trans to P);

^{31}P{^{1}H} NMR: δ 60.7 (d, 2P, J = 17 Hz), 48.6 (t, 1P, J = 17 Hz).[85]

- **Synthesis of Complex 2 [RuH(CO)(PPh$_3$)$_2$(K^2(O,O)-Carboxypyrrole)]**

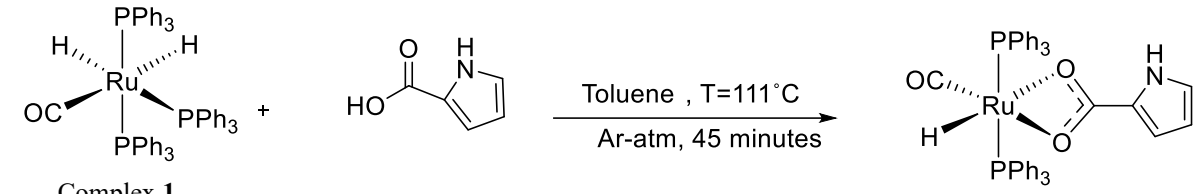

Complex **1**
M.W.: 917.97g.mol^{-1}

M.W.: 111.10g.mol^{-1}

Complex **2**
M.W.: 764.76g.mol^{-1}

	Molar Mass (g.mol^{-1})	**Mass (mg)**	**Volume (mL)**	**mMol (mmol)**	**Yield (%)**
[Ru(H)$_2$(CO)(PPh$_3$)$_3$]	**917.97**	**250**	**-**	**0.271**	**-**
Pyr−2−COO	**111.10**	**30**	**-**	**0.271**	**-**
Toluene	**-**	**-**	**12**	**-**	**-**
[RuH(CO)(PPh$_3$)$_2$(Pyr−2COO)]	**764.76**	**134**	**-**	**0.175**	**65**

Complex **1** and Pyrrole-2-carboxylic acid are dissolved in Toluene under Argon atmosphere. The mixture heated to reflux (111˚C) for 45 minutes. The reaction is cooled and the solvent is evaporated under vacuum. The precipitation is dissolved in Dichloromethane (2 ml) under Argon and then precipitated by Diethyl ether (30 ml). The precipitation is filtered and the solid product washed successively with Petroleum ether (3 x 10 ml), Diethyl ether (3 x 10 ml) and dried under vacuum for 10 minutes. The product is a gray powder.[86]

- **Synthesis of Complex 3 [Ru(NCMe)(CO)(PPh_3)$_2$(K^2(N,O)-Carboxypyrrole)]**

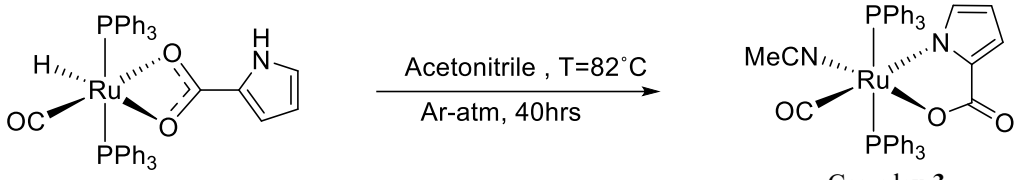

Complex **2**
M.W.: 764.76g.mol^{-1}

Complex **3**
M.W.: 803.80g.mol^{-1}

	Molar Mass (g.mol^{-1})	**Mass (mg)**	**Volume (mL)**	**mMol (mmol)**	**Yield (%)**
[RuH(CO)(PPh_3)$_2$(Pyr−2COO)]	**764.76**	**100**	**-**	**130**	**-**
Acetonitrile	**-**	**-**	**30**	**-**	**-**
[Ru(NCMe)(CO)(PPh_3)$_2$(Pyr−2COO)]	**803.80**	**97**	**-**	**120**	**92**

Complex **2** is dissolved in Acetonitrile under Argon atmosphere. The mixture is heated to reflux (82˚C) for 40 hours. The reaction is cooled and the solvent is evaporated under vacuum. The precipitation is dissolved in Dichloromethane (2 ml) under Argon and then precipitated by Petroleum ether (30 ml). The precipitation is filtered and the solid product washed with Petroleum ether (3 x 10 ml) and dried under vacuum for 10 minutes. The product is dark gray powder.[87]

- **Synthesis of Complex 4 [Ru(4-picoline)(CO)(PPh_3)$_2$(K^2(N,O)-Carboxypyrrole)]**

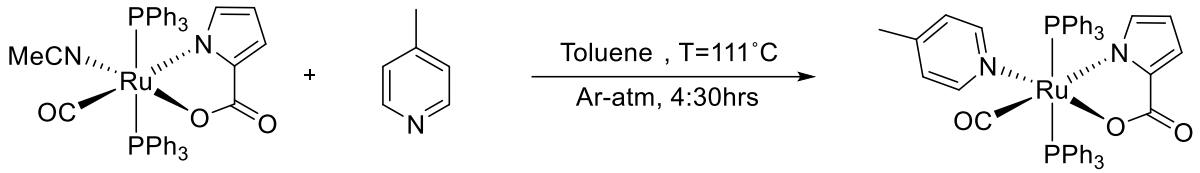

Complex **3**
M.W.: 803.80g.mol^{-1}

M.W.: 93.13g.mol^{-1}

Complex **4**
M.W.: 855.88g.mol^{-1}

	Molar Mass (g.mol^{-1})	**Mass (mg)**	**Volume (mL)**	**mMol (mmol)**	**Yield (%)**
[Ru(NCMe)(CO)(PPh_3)$_2$(Pyr−2COO)]	**803.80**	**24**	**-**	**0.029**	**-**
4-Picoline	**93.13**	**-**	**0.0035**	**0.029**	**-**
Toluene	**-**	**-**	**12**	**-**	**-**
[Ru(4-Picoline)(CO)(PPh_3)$_2$(Pyr−2COO)]	**855.88**	**12**	**-**	**0.014**	**48**

Complex **3** and 4-picoline are dissolved in Toluene under Argon atmosphere. The mixture heated to reflux (111˚C) for 4 hours and 30 minutes. The reaction is cooled to room temperature and the solvent is evaporated under vacuum. The precipitation is dissolved in Dichloromethane (1 ml) under Argon and then precipitated by petroleum ether (10 ml). The precipitation is filtered and the solid product washed with Petroleum ether (3 x 10 ml) and dried under vacuum for 10 minutes. The product is dark gray powder.

- **Synthesis of Complex 5 [Ru(4-Aminopyridine)(CO)(PPh_3)$_2$(K^2(N,O)-Carboxypyrrole)]**

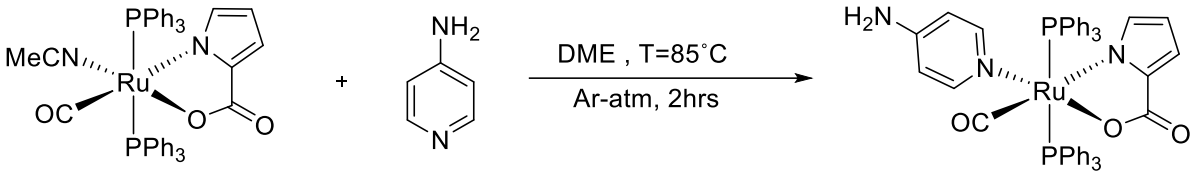

Complex **4**
M.W.: 803.80g.mol^{-1}

M.W.: 94.12g.mol^{-1}

Complex **5**
M.W.: 856.86g.mol^{-1}

	Molar Mass (g.mol^{-1})	**Mass (mg)**	**Volume (mL)**	**mMol (mmol)**	**Yield (%)**
[Ru(NCMe)(CO)(PPh_3)$_2$(K^2(N,O)-Carboxypyrrole)]	**803.80**	**40**	**-**	**0.050**	**-**
4-Aminopyridine	**94.12**	**4**	**-**	**0.042**	**-**
1,2-Dimethoxyethane	**-**	**-**	**10**	**-**	**-**
[Ru(4-Aminopyridine)(CO)(PPh_3)$_2$(K^2(N,O)-Carboxypyrrole)]	**856.86**	**32**	**-**	**0.037**	**88**

Complex **3** and 4-Aminopyride are dissolved in 1,2-Dimethoxyethane under an Argon atmosphere. The mixture is heated to reflux (85˚C) for 2hours. The reaction is cooled to room temperature and the solvent is evaporated under vacuum. The precipitation is dissolved in Dichloromethane (3 ml) and then filtered on celite column under Argon atmosphere. The precipitation in the column eluted by Dichloromethane (3 x 5 ml). Then Dichloromethane is evaporated under the vacuum. The product remaining is a black powder.

- **Synthesis of Complex 6 [RuH(CO)(PPh$_3$)$_2$(K^2(O,O)-Carboxyindole)]**

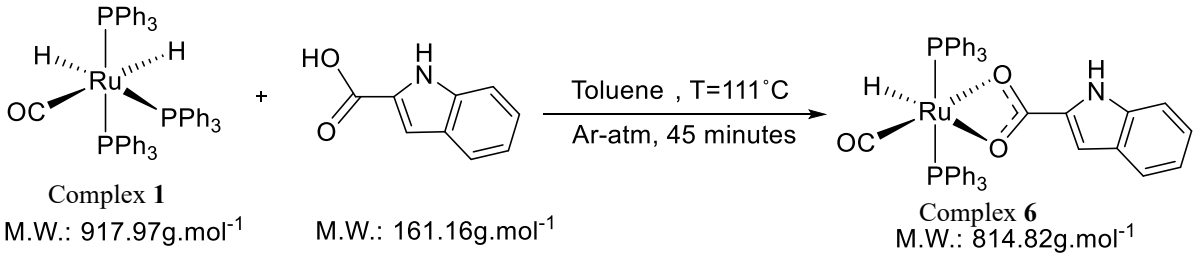

Complex **1**
M.W.: 917.97g.mol^{-1}

M.W.: 161.16g.mol^{-1}

Complex **6**
M.W.: 814.82g.mol^{-1}

	Molar Mass (g.mol^{-1})	**Mass (mg)**	**Volume (mL)**	**mMol (mmol)**	**Yield (%)**
[Ru(H)$_2$(CO)(PPh$_3$)$_3$]	**917.97**	**150**	**-**	**0.163**	**-**
Indole-2-carboxylic acid	**161.16**	**26**	**-**	**0.161**	**-**
Toluene	**-**	**-**	**8**	**-**	**-**
[RuH(CO)(PPh$_3$)$_2$(K^2(O,O)-Carboxyindole)]	**814.82**	**95**	**-**	**0.116**	**72**

Complex **1** and Indole-2-carboxylic acid are dissolved in Toluene under Argon atmosphere. The mixture heated to reflux (111˚C) for 45 minutes. The reaction is cooled and the solvent is evaporated under vacuum. The precipitation is dissolved in Dichloromethane (2 ml) under Argon and then precipitated by Diethyl ether (30 ml). The precipitation is filtered and the solid product washed successively with Petroleum ether (3 x 10 ml), Diethyl ether (3 x 10 ml) and dried under vacuum for 10 minutes. The product is a green powder.

- **Synthesis of Complex 7 [Ru(NCMe)(CO)(PPh$_3$)$_2$(K^2(N,O)-Carboxyindole)]**

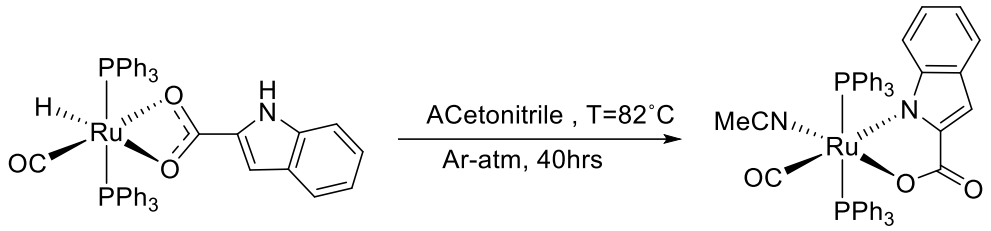

Complex **6**
M.W.: 814.82g.mol^{-1}

Complex **7**
M.W.: 853.86g.mol^{-1}

	Molar Mass (g.mol^{-1})	**Mass (mg)**	**Volume (mL)**	**mMol (mmol)**	**Yield (%)**
[RuH(CO)(PPh$_3$)$_2$(K^2(O,O)-Carboxyindole)]	**814.82**	**100**	**-**	**0.121**	**-**
Acetonitrile	**-**	**-**	**30**	**-**	**-**
[Ru(NCMe)(CO)(PPh$_3$)$_2$(K^2(N,O)-Carboxyindole)]	**853.86**	**61**	**-**	**0.071**	**59**

Complex **6** is dissolved in Acetonitrile under Argon atmosphere. The mixture is heated to reflux (82˚C) for 40 hours. The reaction is cooled to room temperature and the solvent is evaporated under vacuum. The precipitation is dissolved in Dichloromethane (2 ml) under Argon and then precipitated by Petroleum ether (30 ml). The precipitation is filtered and the solid product washed successively with Petroleum ether (3 x 10 ml), Diethyl ether (3 x 10 ml) and dried under vacuum for 10 minutes. The product is a green powder.

- **Synthesis of Complex 8 [Ru(4-Picoline)(CO)(PPh$_3$)$_2$(K^2(N,O)-Carboxyindole)]**

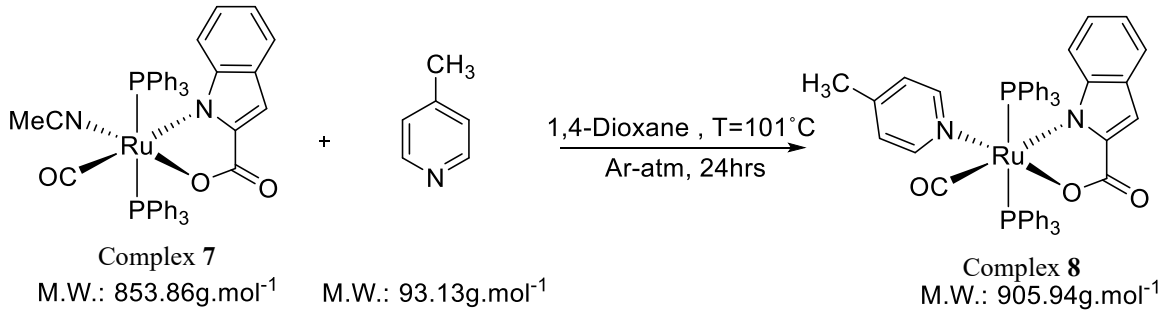

Complex **7**
M.W.: 853.86g.mol^{-1}

M.W.: 93.13g.mol^{-1}

Complex **8**
M.W.: 905.94g.mol^{-1}

	Molar Mass (g.mol^{-1})	**Mass (mg)**	**Volume (mL)**	**mMol (mmol)**	**Yield (%)**
[Ru(NCMe)(CO)(PPh$_3$)$_2$(K^2(N,O)-Carboxyindole)]	**853.86**	**58**	**-**	**0.068**	**-**
4-Picoline	**93.13**	**-**	**0.007**	**0.067**	**-**
1,2-Dioxane	**-**	**-**	**10**	**-**	**-**
[Ru(4-Picoline)(CO)(PPh$_3$)$_2$(K^2(N,O)-Carboxyindole)]	**905.94**	**45**	**-**	**0.050**	**74**

Complex **7** and 4-picoline are dissolved in 10 ml of 1,2-dioxane under an argon atmosphere. The mixture is heated to reflux at 101˚C for 24 hours, then cooled to room temperature, and the solvent is evaporated under vacuum. The resulting product is dissolved in 1 ml of dichloromethane and filtered through a celite column under an argon atmosphere, which was previously washed with 30 ml of petroleum ether. After adding the dissolved product in dichloromethane to the column, it is washed again with petroleum ether (3 x 10 ml), and the remaining product is eluted with dichloromethane. The dichloromethane is evaporated under vacuum. The product is redissolved in 1 ml of dichloromethane, and 20 ml of petroleum ether is added to precipitate it. The precipitate is filtered, washed successively with petroleum ether (3 x 10 ml) and diethyl ether (3 x 10 ml), and dried under vacuum for 10 minutes. The final product is a green powder.

- **Synthesis of Complex 9 [Ru(4-Aminopyridine)(CO)(PPh_3)$_2$(K^2(N,O)-Carboxyindole)]**

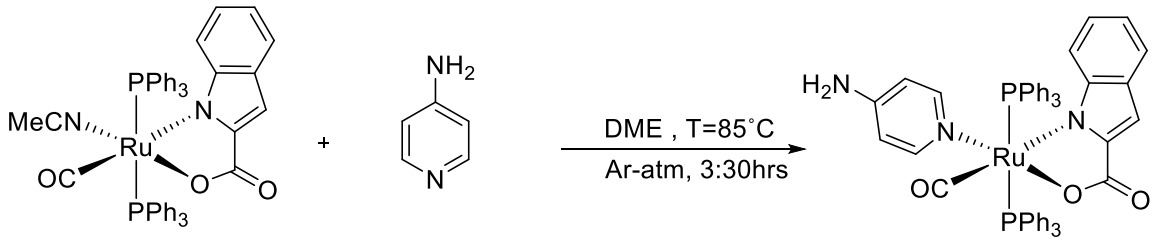

Complex **7**
M.W.: 853.86g.mol^{-1}

M.W.: 94.12g.mol^{-1}

Complex **9**
M.W.: 906.92g.mol^{-1}

	Molar Mass (g.mol^{-1})	**Mass (mg)**	**Volume (mL)**	**mMol (mmol)**	**Yield (%)**
[Ru(NCMe)(CO)(PPh_3)$_2$(K^2(N,O)-Carboxyindole)]	**853.86**	**60**	**-**	**0.070**	**-**
4-Aminopyridine	**94.12**	**6**	**-**	**0.063**	**-**
1,2-Dimethoxyethane	**-**	**-**	**10**	**-**	**-**
[Ru(4-Aminopyridine)(CO)(PPh_3)$_2$(K^2(N,O)-Carboxyindole)]	**906.92**	**25**	**-**	**0.027**	**43**

Complex **7** and 4-aminopyridine are dissolved in 10 ml of 1,2-dimethoxyethane under an argon atmosphere. The mixture is heated to reflux at 85˚C for 3 hours and 30 minutes, then cooled to room temperature, and the solvent is evaporated under vacuum. The resulting precipitate is dissolved in 1 ml of dichloromethane and filtered through a celite column under an argon atmosphere, which was previously washed with 30 ml of petroleum ether. After adding the dissolved product in dichloromethane to the column, it is first washed with petroleum ether (3 x 10 ml), followed by dichloromethane to elute the product. The solvent is then evaporated under vacuum. The product is redissolved in 1 ml of dichloromethane, and 20 ml of petroleum ether is added to precipitate it. The precipitate is filtered, washed successively with petroleum ether (3 x 10 ml) and diethyl ether (3 x 10 ml), and dried under vacuum for 10 minutes. The final product is a green powder.

- **Synthesis of Complex 10 [Ru(DMSO)(CO)(PPh_3)$_2$(K^2(N,O)-Carboxyindole)]**

Complex **7**

M.W.: 853.86g.mol^{-1}

Complex **10**

M.W.: 890.94g.mol^{-1}

	Molar Mass (g.mol^{-1})	**Mass (mg)**	**Volume (mL)**	**mMol (mmol)**	**Yield (%)**
[Ru(NCMe)(CO)(PPh_3)$_2$(K^2(N,O)-Carboxyindole)]	**853.86**	**50**	**-**	**0.060**	**-**
DMSO	**78.13**	**-**	**0.041**	**0.600**	**-**
Toluene	**-**	**-**	**10**	**-**	**-**
[Ru(DMSO)(CO)(PPh_3)$_2$(K^2(N,O)-Carboxyindole)]	**890.94**	**14**	**-**	**0.016**	**27**

Complex **7** and 10 equivalents of dimethyl sulfoxide are dissolved in toluene under an argon atmosphere. The mixture is heated to reflux at 111˚C for 9 hours, then cooled to room temperature, after which the solvent is evaporated under vacuum. The precipitate is dissolved in 1 ml of dichloromethane and filtered through a celite column, previously washed with 30 ml of hexane, under an argon atmosphere. After the dissolved product is loaded into the column, it is first eluted with hexane (3 x 10 ml), and the eluent is collected as the first fraction. The remaining product is then eluted with dichloromethane until the eluent runs clear, collected as the second fraction. The solvents from both fractions are evaporated under vacuum. The product is redissolved in 1 ml of dichloromethane, and 20 ml of hexane is added to precipitate it. The precipitate is filtered through a filter funnel, washed with hexane (3 x 5 ml), and dried under vacuum for 10 minutes. The product is gel-like and brown.

REFERENCES

[1] Irena Kostova, 'Ruthenium Complexes as Anticancer Agents', *Current Medicinal Chemistry*, 13.9 (2006), pp. 1085–1107, doi:10.2174/092986706776360941.
[2] Gilles Gasser and Nils Metzler-Nolte, 'The Potential of Organometallic Complexes in Medicinal Chemistry', *Current Opinion in Chemical Biology*, 16.1–2 (2012), pp. 84–91, doi:10.1016/j.cbpa.2012.01.013.
[3] H. Christine Lo and others, 'Regioselective Reduction of NAD+ Models with [Cp*Rh(Bpy)H]+ : Structure-Activity Relationships and Mechanistic Aspects in the Formation of the 1,4-NADH Derivatives', *Angewandte Chemie (International Ed. in English)*, 38.10 (1999), pp. 1429–32, doi:10.1002/(SICI)1521-3773(19990517)38:10<1429::AID-ANIE1429>3.0.CO;2-Q.
[4] Nicola J. Farrer and Peter J. Sadler, 'Medicinal Inorganic Chemistry: State of the Art, New Trends, and a Vision of the Future', in *Bioinorganic Medicinal Chemistry*, ed. by Enzo Alessio, 1st edn (Wiley, 2011), pp. 1–47, doi:10.1002/9783527633104.ch1.
[5] Richard D. Taylor, Malcolm MacCoss, and Alastair D. G. Lawson, 'Rings in Drugs', *Journal of Medicinal Chemistry*, 57.14 (2014), pp. 5845–59, doi:10.1021/jm4017625.
[6] Deepak Dalvie and others, 'Influence of Aromatic Rings on ADME Properties of Drugs', in *Metabolism, Pharmacokinetics and Toxicity of Functional Groups: Impact of the Building Blocks of Medicinal Chemistry on ADMET*, ed. by Dennis A Smith (The Royal Society of Chemistry, 2010), doi:10.1039/BK9781849730167-00275.
[7] Peter Ertl, 'Database of Bioactive Ring Systems with Calculated Properties and Its Use in Bioisosteric Design and Scaffold Hopping', *Bioorganic & Medicinal Chemistry*, Chemoinformatics in Drug Discovery, 20.18 (2012), pp. 5436–42, doi:10.1016/j.bmc.2012.02.058.
[8] Deepak Dalvie and others, 'Influence of Aromatic Rings on ADME Properties of Drugs', in *Metabolism, Pharmacokinetics and Toxicity of Functional Groups: Impact of the Building Blocks of Medicinal Chemistry on ADMET*, ed. by Dennis A Smith (The Royal Society of Chemistry, 2010), doi:10.1039/BK9781849730167-00275.
[9] Eric Meggers, 'Targeting Proteins with Metal Complexes', *Chemical Communications*, 9, 2009, p. 1001, doi:10.1039/b813568a.
[10] Sven Rottenberg, Carmen Disler, and Paola Perego, 'The Rediscovery of Platinum-Based Cancer Therapy', *Nature Reviews. Cancer*, 21.1 (2021), pp. 37–50, doi:10.1038/s41568-020-00308-y.
[11] Chunyu Zhang and others, 'Platinum-Based Drugs for Cancer Therapy and Anti-Tumor Strategies', *Theranostics*, 12.5 (2022), pp. 2115–32, doi:10.7150/thno.69424.
[12] Dospivova Dana and others, 'Catalytic Electrochemical Analysis of Platinum in Pt-DNA Adducts', *International Journal of Electrochemical Science*, 7 (2012), pp. 3072–88, doi:10.1016/S1452-3981(23)13936-8.
[13] Étienne Chatelut, 'Pharmacologie des dérivés du platine : différences entre les trois composés et les facteurs de variabilité entre patients', *Bulletin du Cancer*, 98.11 (2011), pp. 1253–61, doi:10.1684/bdc.2011.1464.
[14] Suzanne Hector and others, 'In Vitro Studies on the Mechanisms of Oxaliplatin Resistance', *Cancer Chemotherapy and Pharmacology*, 48.5 (2001), pp. 398–406, doi:10.1007/s002800100363.
[15] Ana-Maria Florea and Dietrich Büsselberg, 'Cisplatin as an Anti-Tumor Drug: Cellular Mechanisms of Activity, Drug Resistance and Induced Side Effects', *Cancers*, 3.1 (2011), pp. 1351–71, doi:10.3390/cancers3011351.
[16] Chunyu Zhang and others, 'Platinum-Based Drugs for Cancer Therapy and Anti-Tumor Strategies', *Theranostics*, 12.5 (2022), pp. 2115–32, doi:10.7150/thno.69424.
[17] Luyu Qi and others, 'Advances in Toxicological Research of the Anticancer Drug Cisplatin', *Chemical Research in Toxicology*, 32.8 (2019), pp. 1469–86, doi:10.1021/acs.chemrestox.9b00204.
[18] RobertA. Hazlitt, Jaeki Min, and Jian Zuo, 'Progress in the Development of Preventative Drugs for Cisplatin-Induced Hearing Loss', *Journal of Medicinal Chemistry*, 61.13 (2018), pp. 5512–24, doi:10.1021/acs.jmedchem.7b01653.
[19] Tatjana Lazarević, Ana Rilak, and Živadin D. Bugarčić, 'Platinum, Palladium, Gold and Ruthenium Complexes as Anticancer Agents: Current Clinical Uses, Cytotoxicity Studies and Future Perspectives', *European Journal of Medicinal Chemistry*, Current advances in cancer research: Therapeutics, Targets, and Chemical Biology, 142 (2017), pp. 8–31, doi:10.1016/j.ejmech.2017.04.007.
[20] Guillermo Moreno-Alcántar, Pierre Picchetti, and Angela Casini, 'Gold Complexes in Anticancer Therapy: From New Design Principles to Particle-Based Delivery Systems', *Angewandte Chemie International Edition*, 62.22 (2023), doi:10.1002/anie.202218000.
[21] Angela Casini and others, 'Biophysical Characterisation of Adducts Formed between Anticancer Metallodrugs and Selected Proteins: New Insights from X-Ray Diffraction and Mass Spectrometry Studies', *Journal of Inorganic Biochemistry*, 13th International Conference on Biological Inorganic Chemistry, 102.5 (2008), pp. 995–1006, doi:10.1016/j.jinorgbio.2007.12.022.
[22] 'Auranofin' <https://go.drugbank.com/drugs/DB00995> [accessed 26 August 2024].

[23] Angela Casini and Luigi Messori, 'Molecular Mechanisms and Proposed Targets for Selected Anticancer Gold Compounds', *Current Topics in Medicinal Chemistry*, 11.21 (2011), pp. 2647–60, doi:10.2174/156802611798040732.
[24] Chi-Ming Che and others, 'Gold(III) Porphyrins as a New Class of Anticancer Drugs: Cytotoxicity, DNA Binding and Induction of Apoptosis in Human Cervix Epitheloid Cancer cellsElectronic Supplementary Information (ESI) Available: Further Experimental and Crystallographic Details. See Http://Www.Rsc.Org/Suppdata/Cc/B3/B303294a/', *Chemical Communications*, 14, 2003, p. 1718, doi:10.1039/b303294a.
[25] Giordana Marcon and others, 'Gold(III) Complexes with Bipyridyl Ligands: Solution Chemistry, Cytotoxicity, and DNA Binding Properties', *Journal of Medicinal Chemistry*, 45.8 (2002), pp. 1672–77, doi:10.1021/jm010997w.
[26] Chi-Ming Che and others, 'Gold(III) Porphyrins as a New Class of Anticancer Drugs: Cytotoxicity, DNA Binding and Induction of Apoptosis in Human Cervix Epitheloid Cancer cellsElectronic Supplementary Information (ESI) Available: Further Experimental and Crystallographic Details. See Http://Www.Rsc.Org/Suppdata/Cc/B3/B303294a/', *Chemical Communications*, 14, 2003, p. 1718, doi:10.1039/b303294a.
[27] Giordana Marcon and others, 'Gold(III) Complexes with Bipyridyl Ligands: Solution Chemistry, Cytotoxicity, and DNA Binding Properties', *Journal of Medicinal Chemistry*, 45.8 (2002), pp. 1672–77, doi:10.1021/jm010997w.
[28] Luca Ronconi and Dolores Fregona, 'The Midas Touch in Cancer Chemotherapy: From Platinum- to Gold-Dithiocarbamato Complexes', *Dalton Transactions*, 48, 2009, p. 10670, doi:10.1039/b913597a.
[29] Luca Ronconi and Dolores Fregona, 'The Midas Touch in Cancer Chemotherapy: From Platinum- to Gold-Dithiocarbamato Complexes', *Dalton Transactions*, 48, 2009, p. 10670, doi:10.1039/b913597a.
[30] Rahul Kanaoujiya and others, 'Recent Advances and Application of Ruthenium Complexes in Tumor Malignancy', *Materials Today: Proceedings*, 2nd International Conference on Sustainable Materials, Manufacturing and Renewable Technologies 2022, 72 (2023), pp. 2822–27, doi:10.1016/j.matpr.2022.07.098.
[31] Olivier Lentzen, Cécile Moucheron, and Andrée Kirsch-De Mesmaeker, '$_{44}$ Ru Perspectives of Ruthenium Complexes in Cancer Therapy', in *Metallotherapeutic Drugs and Metal-Based Diagnostic Agents*, ed. by Marcel Gielen and Edward R.T. Tiekink, 1st edn (Wiley, 2005), pp. 359–78, doi:10.1002/0470864052.ch19.
[32] Michael J. Clarke and others, 'Biochemical Effects of Binding [(H2O)(NH3)5RuII]2+ to DNA and Oxidation to[(NH3)5RuIII]*n*—DNA.', *Inorganica Chimica Acta*, 124.1 (1986), pp. 13–28, doi:10.1016/S0020-1693(00)82080-0.
[33] Enzo Alessio and others, 'Cis- and Trans-Dihalotetrakis(Dimethyl Sulfoxide)Ruthenium(II) Complexes (RuX2(DMSO)4; X = Cl, Br): Synthesis, Structure, and Antitumor Activity', *Inorganic Chemistry*, 27.23 (1988), pp. 4099–4106, doi:10.1021/ic00296a006.
[34] Olga Novakova and others, 'Correlation between Cytotoxicity and DNA Binding of Polypyridyl Ruthenium Complexes', *Biochemistry*, 34.38 (1995), pp. 12369–78, doi:10.1021/bi00038a034.
[35] Haimei Chen and others, 'Highly Selective Binding of Organometallic Ruthenium Ethylenediamine Complexes to Nucleic Acids: Novel Recognition Mechanisms', *Journal of the American Chemical Society*, 125.1 (2003), pp. 173–86, doi:10.1021/ja027719m.
[36] Justin J. Wilson and Stephen J. Lippard, 'Synthetic Methods for the Preparation of Platinum Anticancer Complexes', *Chemical Reviews*, 114.8 (2014), pp. 4470–95, doi:10.1021/cr4004314.
[37] Gasser and Metzler-Nolte.
[38] 'RUTHENIUM', *Chemical & Engineering News Archive*, 81.36 (2003), p. 112, doi:10.1021/cen-v081n036.p112.
[39] Viktor Brabec and Olga Nováková, 'DNA Binding Mode of Ruthenium Complexes and Relationship to Tumor Cell Toxicity', *Drug Resistance Updates: Reviews and Commentaries in Antimicrobial and Anticancer Chemotherapy*, 9.3 (2006), pp. 111–22, doi:10.1016/j.drup.2006.05.002.
[40] K. C. Gatter and others, 'Transferrin Receptors in Human Tissues: Their Distribution and Possible Clinical Relevance', *Journal of Clinical Pathology*, 36.5 (1983), pp. 539–45, doi:10.1136/jcp.36.5.539.
[41] Alberta Bergamo and Gianni Sava, 'Linking the Future of Anticancer Metal-Complexes to the Therapy of Tumor Metastases', *Chemical Society Reviews*, 44 (2015), doi:10.1039/c5cs00134j.
[42] Robert H Crabtree, 'The Organometallic Chemistry of the Transition Metals'Yale University, New Haven, Connecticut, Published by John Wiley & Sons, Inc., Hoboken, New Jersey. Published simultaneously in Canada, sixth edition, 1948.
[43] Sang Yeul Lee, Chul Young Kim, and Tae-Gyu Nam, 'Ruthenium Complexes as Anticancer Agents: A Brief History and Perspectives', *Drug Design, Development and Therapy*, 14 (2020), pp. 5375–92, doi:10.2147/DDDT.S275007.
[44] Ileana Dragutan, Valerian Dragutan, and Albert Demonceau, 'Editorial of Special Issue Ruthenium Complex: The Expanding Chemistry of the Ruthenium Complexes', *Molecules (Basel, Switzerland)*, 20.9 (2015), pp. 17244–74, doi:10.3390/molecules200917244.
[45] Simone Strasser and others, 'On the Chloride Lability in Electron-Rich Second Generation Ruthenium Benzylidene Complexes', *Monatshefte Für Chemie - Chemical Monthly*, 146 (2015), pp. 1143–51, doi:10.1007/s00706-015-1484-x.
[46] Jeany M. Rademaker-Lakhai and others, 'A Phase I and Pharmacological Study with Imidazolium-Trans-DMSO-Imidazole-Tetrachlororuthenate, a Novel Ruthenium Anticancer Agent', *Clinical Cancer Research: An Official Journal of the American Association for Cancer Research*, 10.11 (2004), pp. 3717–27, doi:10.1158/1078-0432.CCR-03-0746.

[47] R. Gagliardi and others, 'Antimetastatic Action and Toxicity on Healthy Tissues of Na[Trans-RuCl4(DMSO)Im] in the Mouse', *Clinical & Experimental Metastasis*, 12.2 (1994), pp. 93–100, doi:10.1007/BF01753975.
[48] S. Zorzet and others, 'Lack of In Vitro Cytotoxicity, Associated to Increased G(2)-M Cell Fraction and Inhibition of Matrigel Invasion, May Predict In Vivo-Selective Antimetastasis Activity of Ruthenium Complexes', *The Journal of Pharmacology and Experimental Therapeutics*, 295.3 (2000), pp. 927–33.
[49] G. Sava, I. Capozzi, and others, 'Pharmacological Control of Lung Metastases of Solid Tumours by a Novel Ruthenium Complex', *Clinical & Experimental Metastasis*, 16.4 (1998), pp. 371–79, doi:10.1023/a:1006521715400.
[50] 'Vacca A, Bruno M, Boccarelli A, et al. Inhibition of Endothelial Cell Function and of Angiogenesis by the Metastasis Inhibitor NAMI-A. Br J Cancer 2002;86:993– 8.
[51] D. Pluim and others, '32P-Postlabeling Assay for the Quantification of the Major Platinum-DNA Adducts', *Analytical Biochemistry*, 275.1 (1999), pp. 30–38, doi:10.1006/abio.1999.4302.
[52] G. Mestroni and others, 'Water-Soluble Ruthenium(III)-Dimethyl Sulfoxide Complexes: Chemical Behaviour and Pharmaceutical Properties', *Metal-Based Drugs*, 1.1 (1994), p. 748960, doi:10.1155/MBD.1994.41.
[53] E. Alessio and others, 'Synthesis and Characterization of Two New Classes of Ruthenium(III)-Sulfoxide Complexes with Nitrogen Donor Ligands (L): Na[*Trans*-RuCl4(R2S*O*)(L)] and *Mer, Cis*-RuCl3(R2SO)(R2SO)(L). The Crystal Structure of Na[*Trans*-RuCl4(DMSO)(NH3)] · 2DMSO, Na[*Trans*-RuCl4(DMSO)(Im)] · H2O, Me2CO (Im = Imidazole) and *Mer, Cis*-RuCl3(DMSO)(DMS*O*)(NH3)', *Inorganica Chimica Acta*, 203.2 (1993), pp. 205–17, doi:10.1016/S0020-1693(00)81659-X.
[54] G. Sava, A. Bergamo, and others, 'Influence of Chemical Stability on the Activity of the Antimetastasis Ruthenium Compound NAMI-A', *European Journal of Cancer*, 38.3 (2002), pp. 427–35, doi:10.1016/S0959-8049(01)00389-6.
[55] G. Sava, S. Pacor, and others, 'Na[Trans-RuCl4(DMSO)Im], a Metal Complex of Ruthenium with Antimetastatic Properties', *Clinical & Experimental Metastasis*, 10.4 (1992), pp. 273–80, doi:10.1007/BF00133563.
[56] Orsolya Dömötör and others, 'Characterization of the Binding Sites of the Anticancer Ruthenium(III) Complexes KP1019 and KP1339 on Human Serum Albumin via Competition Studies', *Journal of Biological Inorganic Chemistry*, 18.1 (2013), pp. 9–17, doi:10.1007/s00775-012-0944-6.
[57] Temitayo Aiyelabola and others, 'Synthesis Characterization and Biological Activities of an Enamine Derivative and Its Coordination Compounds', *Advances in Biological Chemistry*, 10.6 (2020), pp. 172–89, doi:10.4236/abc.2020.106013.
[58] Christian G. Hartinger and others, 'KP1019, a New Redox-Active Anticancer Agent--Preclinical Development and Results of a Clinical Phase I Study in Tumor Patients', *Chemistry & Biodiversity*, 5.10 (2008), pp. 2140–55, doi:10.1002/cbdv.200890195.
[59] Shannon S. Stahl, 'Organotransition Metal Chemistry: From Bonding to Catalysis', *Journal of the American Chemical Society*, 132.24 (2010), pp. 8524–25, doi:10.1021/ja103695e.
[60] Robert H Crabtree, 'The Organometallic Chemistry of the Transition Metals'Yale University, New Haven, Connecticut, Published by John Wiley & Sons, Inc., Hoboken, New Jersey. Published simultaneously in Canada, sixth edition, 1948.
[61] E. Alessio and others.
[62] Gianni Sava, Sabrina Pacor, and others, 'Effects of Ruthenium Complexes on Experimental Tumors: Irrelevance of Cytotoxicity for Metastasis Inhibition', *Chemico-Biological Interactions*, 95.1 (1995), pp. 109–26, doi:10.1016/0009-2797(94)03350-1.
[63] Yun Qu and Nicholas Farrell, 'Synthesis and Chemical Properties of a Heterodinuclear (Pt,Ru) DNA-DNA and DNA-Protein Crosslinking Agent', *Inorganic Chemistry*, 34.13 (1995), pp. 3573–76, doi:10.1021/ic00117a033.
[64] Mohammed A. Abbas, Colin D. McMillen, and Julia L. Brumaghim, 'Synthesis, Characterization, and Structures of Ruthenium(II) Complexes with Multiple Solvato Ligands', *Inorganica Chimica Acta*, Special Volume: Protagonists in Chemistry Dedicated to Professor Luis Echegoyen, 468 (2017), pp. 308–15, doi:10.1016/j.ica.2017.07.003.
[65] Christopher C. Underwood and others, 'Synthesis and Electrochemical Characterization of [Ru(NCCH3)6]2+, Tris(Acetonitrile) Tris(Pyrazolyl)Borate, and Tris(Acetonitrile) Tris(Pyrazolyl)Methane Ruthenium(II) Complexes', *Inorganica Chimica Acta*, 405 (2013), pp. 470–76, doi:10.1016/j.ica.2013.02.027.
[66] Yi-Jung Tu and others, 'Selective Photodissociation of Acetonitrile Ligands in Ruthenium Polypyridyl Complexes Studied by Density Functional Theory', *Inorganic Chemistry*, 54.16 (2015), pp. 8003–11, doi:10.1021/acs.inorgchem.5b01202.
[67] R.R. Schrock, B.F.G. Johnson, and J. Lewis, 'Reactivity of Co-Ordinated Ligands. Part XVIII. Cationic Ruthenium(II) and Osmium(II) Complexes by Electrophilic Attack on a π-Allyl Ligand', *Journal of the Chemical Society, Dalton Transactions*, 9, 1974, pp. 951–59, doi:10.1039/DT9740000951.
[68] A. Anzellotti and A. Briceño, 'Hexakis-(Aceto-nitrile)-ruthenium(II) Tetra-chloro-zincate 2.55-Hydrate', *Acta Crystallographica Section E: Structure Reports Online*, 57.11 (2001), pp. m538–40, doi:10.1107/S1600536801017469.
[69] Albrecht Ludwig Harreus and others, '2-Pyrrolidone', in *Ullmann's Encyclopedia of Industrial Chemistry* (John Wiley & Sons, Ltd, 2011), doi:10.1002/14356007.a22_457.pub2.
[70] Nidhi Singh and others, 'Recent Progress in the Total Synthesis of Pyrrole-Containing Natural Products (2011–2020)', *Organic Chemistry Frontiers*, 8.19 (2021), pp. 5550–73, doi:10.1039/D0QO01574A.

[71] Verónica Estévez, Mercedes Villacampa, and J. Carlos Menéndez, 'Recent Advances in the Synthesis of Pyrroles by Multicomponent Reactions', *Chemical Society Reviews*, 43.13 (2014), pp. 4633–57, doi:10.1039/C3CS60015G.
[72] Yusuf Özkay and others, 'Synthesis of 2-Substituted-*N*-[4-(1-Methyl-4,5-Diphenyl-1*H*-Imidazole-2-Yl)Phenyl]Acetamide Derivatives and Evaluation of Their Anticancer Activity', *European Journal of Medicinal Chemistry*, 45.8 (2010), pp. 3320–28, doi:10.1016/j.ejmech.2010.04.015.
[73] Francisco Sánchez-Viesca, 'On the Baeyer- Emmerling Synthesis of Indigo', 2018, doi:10.12691/wjoc-6-1-2.
[74] F. Gowland Hopkins and Sydney W. Cole, 'A Contribution to the Chemistry of Proteids', *The Journal of Physiology*, 27.4–5 (1901), pp. 418–28, doi:10.1113/jphysiol.1901.sp000880.
[75] Navriti Chadha and Om Silakari, 'Indoles as Therapeutics of Interest in Medicinal Chemistry: Bird's Eye View', *European Journal of Medicinal Chemistry*, 134 (2017), pp. 159–84, doi:10.1016/j.ejmech.2017.04.003.
[76] José Barluenga and Carlos Valdés, 'Five-Membered Heterocycles: Indole and Related Systems', in *Modern Heterocyclic Chemistry* (John Wiley & Sons, Ltd, 2011), pp. 377–531, doi:10.1002/9783527637737.ch5.
[77] Hazrulrizawati A. Hamid, Aizi N. M. Ramli, and Mashitah M. Yusoff, 'Indole Alkaloids from Plants as Potential Leads for Antidepressant Drugs: A Mini Review', *Frontiers in Pharmacology*, 8 (2017), p. 96, doi:10.3389/fphar.2017.00096.
[78] S. J. Murch, S. KrishnaRaj, and P. K. Saxena, 'Tryptophan Is a Precursor for Melatonin and Serotonin Biosynthesis in in Vitro Regenerated St. John's Wort (Hypericum Perforatum L. Cv. Anthos) Plants', *Plant Cell Reports*, 19.7 (2000), pp. 698–704, doi:10.1007/s002990000206.
[79] Jose Barluenga and Carlos Valdes, 'ChemInform Abstract: Five-Membered Heterocycles: Indole and Related Systems', *ChemInform*, 43.7 (2012), doi:10.1002/chin.201207228.
[80] 'Essentials of Organic Chemistry: For Students of Pharmacy, Medicinal Chemistry and Biological Chemistry | Wiley' 2006.
[81] Emilio Mateev, Maya Georgieva, and Alexander Zlatkov, 'Pyrrole as an Important Scaffold of Anticancer Drugs: Recent Advances', *Journal of Pharmacy & Pharmaceutical Sciences*, 25 (2022), pp. 24–40, doi:10.18433/jpps32417.
[82] Dandan Chen, Qiong Xie, and Jun Zhu, 'Unconventional Aromaticity in Organometallics: The Power of Transition Metals', *Accounts of Chemical Research*, 52.5 (2019), pp. 1449–60, doi:10.1021/acs.accounts.9b00092.
[83] Luis Sanhueza and others, 'Effect on the Aromaticity of Heterocyclic Ligands by Coordination with Ruthenium Electron-Withdrawing Metal Centers', *International Journal of Quantum Chemistry*, 120.24 (2020), p. e26412, doi:10.1002/qua.26412.
[84] Hamidreza Samouei and Vladimir V. Grushin, 'New, Highly Efficient, Simple, Safe, and Scalable Synthesis of [(Ph3P)3Ru(CO)(H)2]', *Organometallics*, 32.15 (2013), pp. 4440–43, doi:10.1021/om400461w.
[85] Hamidreza Samouei and Vladimir V. Grushin, 'New, Highly Efficient, Simple, Safe, and Scalable Synthesis of [(Ph3P)3Ru(CO)(H)2]', *Organometallics*, 32.15 (2013), pp. 4440–43, doi:10.1021/om400461w.
[86] Giacomo Drius and others, 'Unpredictable Dynamic Behaviour of Ruthenium Chelate Pyrrole Derivatives', *Molecules*, 29 (2024), p. 3068, doi:10.3390/molecules29133068.
[87] Giacomo Drius and others, 'Unpredictable Dynamic Behaviour of Ruthenium Chelate Pyrrole Derivatives', *Molecules*, 29 (2024), p. 3068, doi:10.3390/molecules29133068.